DEPARTMENT OF THE INTERIOR

U.S. GEOLOGICAL SURVEY

On the graphical interpretation of paleoseismic data

by

Herbert R. Shaw[1]

and

Anne E. Gartner[1]

Open-File Report 86-394

[1] U.S. Geological Survey, Menlo Park, CA 94025

UNITED STATES DEPARTMENT OF THE INTERIOR
DONALD PAUL HODEL, Secretary
GEOLOGICAL SURVEY
Dallas L. Peck, Director

For additional information write to:

U.S. Geological Survey
IGP Branch, Room 2153A MS 910
345 Middlefield Road
Menlo Park, CA 94025

Copies of this report can be purchased from:
Open-File Report Section
U.S. Geological Survey
Box 25425, Federal Center
Denver, CA 80225

Call (303) 236-7476

TABLE OF CONTENTS

LIST OF ILLUSTRATIONS

LIST OF TABLES

Abstract

Frequency-magnitude data for earthquake activity in Japan, as interpreted by Wesnousky and others (1983) relative to Quaternary faulting, are compared with the data of faulting in the conterminous U.S., as interpreted by Shaw and others (1981) in terms of a generalized branching distribution of faults of all lengths measured at a scale of 1:5,000,000 (map compilation by Howard and others, 1978). The Japanese data plot as a zigzag trend (raw data as well as points based on the maximum moment model of Wesnousky and others) on the so-called seismic parallelogram of Shaw and others (renamed a fractogram to acknowledge formal relationships to the systematics of Mandelbrot's fractal geometry). The trend alternates between intervals roughly parallel to one or the other end-member modes of the fractogram. Interpreted in terms of the maximum moment model, this pattern suggests that each branch-length order defines a maximum earthquake and recurrence time each of which increases at the next lower order (longer fault branches of fewer number) according to a step-wise hierarchy. Activation of a given length-set engages longer and longer portions of segments (or complete segments having a scatter of lengths about the mean length for that order) in successive events, with a corresponding increase in recurrence time, until that subset attains a characteristic moment and magnitude for that order; activity is then expressed in terms of a shift, at a constant "buildup time", to a longer length-set order containing fewer segments. In each step the maximum earthquake increases, but the frequency decreases relative to what it would have been if the shorter length-set orders had not reached their characteristic maximum moment. This "maximum moment" is not necessarily the theoretical saturation maximum (in terms of potential fault length) for a given order; the latter is termed the SATURATION limit, representing activation of the longest fault segments in that order. In the case of Japanese earthquakes, the characteristic maxima seem to vary from 10 to nearly 100 percent of this SATURATION limit. Dynamically, these relations imply a quasi-steady, if piecemeal and seemingly haphazard, spatial and chronological flow of energy from the shorter to longer branch-length orders. Complex behavior of large fault systems relates to different regimes of a general progression in which aseismic creep, regular intermittent earthquakes, and large unpredictable earthquakes (including concepts of seismic gaps and locked and unlocked portions of long faults) represent fractally different subsets of the same systematic seismic cycle; the possibility is explored that such cycles may represent invariant fractal structures in space and time relative to the maximum topological dimension 4. Relative to 3 spatial dimensions, fractally self-similar subsets exist over small frequency-magnitude ranges, but, in general, the fractal dimension fluctuates from a nearly volume-filling mode during transitions from shorter to longer length-set orders to "less-than-linear" during the approach to maximum events at the longest length orders (as the number, N, of segments per order decreases to N = 1). These descriptions have also been modified to take account of the moment-magnitude correlations of Hanks and Boore (1984). On this basis, a theoretical "Ultimate Event" emerges as a natural limit of fractal dimensions calculated from slopes in frequency-magnitude, and moment-magnitude diagrams. Comparisons of paths in spatial and temporal fractal space suggest a concept of macroscopic uncertainty analogous to the Uncertainty Principle of quantum dynamics. Similar implications exist concerning simultaneous predictions of location and time for earthquakes. Paradoxically, this uncertainty may analogously increase our abilities to predict the dynamical characteristics of the earthquake process in space and time.

Introduction.

The "b-value problem" in seismology concerns the slope, -b, in a plot of the logarithm of frequency vs. magnitude for some class of earthquake events, as originally employed by Ishimoto and Iida (1939) and by Gutenberg and Richter (1944). The problem is one of interpreting how the events that make up this descriptive relation have evolved in time and space, and how this spatiotemporal pattern of earthquakes correlates with spatiotemporal patterns of tectonic deformations (and associated patterns of fault ruptures in space and time) which are either known or are assumed to have a causative relationship with a specific class of earthquakes. Although the problem is conceptually simple it has been notably recalcitrant to any general interpretation because of the large numbers of possible sequences and conceivable faulting events that may be implicit in a frequency-magnitude diagram. Regional boundaries and the spatial and chronological ordering of earthquake and faulting events are often either vague or unknown. Therefore, there is considerable ambiguity, and possible redundancy, concerning the matching up of earthquake and faulting events when there are no on-the-spot documentations of the correlative motions and shocks.

Wesnousky and others (1983) contributed significantly to a clarification of these problems by comparing the implications of certain simple limiting models of fault activation with what is probably the most completely documented combined sets of observations on faulting and earthquakes in the world; this is the catalog of Quaternary faulting and the 400-year record of seismicity in Japan (see Wesnousky and others, 1982, for documentation of data and sources). No similarly complete systematic set of data exists in the U.S.; however, a general compilation of young faults in the U.S. is given by Howard and others (1978), and a general compilation of seismicity is given by Algermissen and Perkins (1976) and Algermissen and others (1982). Shaw and others (1981) and Shaw and Gartner (1981, 1984) drew on these data sources to begin a tentative comparison of faulting and seismicity at the continental scale. The present paper attempts to bring these respective efforts into an alignment leading toward a unification of concepts with a common perspective that satisfies the requirements imposed by both the Japanese and the U.S. data.

Figure 1 shows a hypothetical set of mappable faults of different lengths at two magnifications. At the larger scale there is an essentially three-fold

Figure 1 near here

hierarchy of lengths in which there are fewer faults at the longer lengths. The smaller scale shows this set as a subinterval or subset of a more regional distribution which, in turn, may only be a subset of an even smaller-scale distribution. A map scale is not specified, so these general relations may apply to the outcrop scale or to the scale of tectonic plate boundaries; e.g., the smaller scale is not unlike a subinterval of a strike slip fault such as the San Andreas Fault, CA. A priori, without invoking any theoretical constraints, there could be several simple alternative sequences by which all fault segments would be eventually activated along their total mapped lengths.

In the discussion given by Shaw and others (1981, p 270 ff.), the term segment refers to a specified mapped fault that is a member of a given length-set order and is capable of producing an earthquake event associated with that length. A subinterval of a specific segment length (i.e., a subinterval of a single mappable fault of that total length) is referred to by the modifier partial segment length. The idealized branching model assumes that every branching-order of a characteristic length is composed of a fixed

number of faults of the same exact length; this distribution is approximated in Figure 1 where, at the larger scale, there are two longest segments, four segments of intermediate length, and ten of the shortest length. Within a specified total population of measured faults considered to represent a set, for whatever reason, there is a cumulative total length that represents the summation of all counted segment lengths. Use of the descriptive term total length refers to the complete set under consideration, unless it is specifically identified as referring to a different reference length (e.g., total length in the conterminous U.S. viewed as a set; total length within a Faulting Region viewed as a set; total length of faults outcropping within the boundary of a specified seismic zone viewed as a subset or as a combination of other subsets; total length within a given number/length-order viewed as a subset, and so on). The terms fractional length, fractional activation, or fractional rupture length rate (FRLR) normally will refer to the subset of total fault length represented by a unique number/length-order relative to the total length for a stipulated complete set of all number/length-orders, unless fraction is specifically identified in a different context. The fractional length of each number/length-order in Figure 1, at the larger scale, is roughly one-third; in the actual populations of faults measured by Shaw and others (1981), however, the fraction typically increases with decreasing segment length (and increasing numbers of segments per order).

In reality, the simplistic relation described above, and shown schematically in Figure 1, is likely to be violated in two important ways related to resolution and to changes of scale: (1) there may be a hierarchy of number/length sets each of which is distinguishably separable from longer or shorter number/length sets but which contains a range of segment lengths within each set (in the limit there could be a continuum of lengths subdivided by a specified ordering progression between a single-valued longest segment and a given population of shortest segments; this progression might conceivably be carried down to the scale of microcracks if the documentation warranted, but it is often limited in practice to documentation at a particular map scale where groupings of length populations are often discontinuous), and (2) segment lengths at one scale may lose their identities under a change in scale (e.g., the distribution of shorter lengths in Figure 1 may be lost as the map scale is made smaller, or the resolution of associated earthquake events is made larger; i.e., the entire interval may be counted as only two or three segments at a smaller scale where the smallest segments are unresolved and their associated slip events are included in generalized foreshock and/or aftershock sequences).

Thus, in general, it may not always be possible to distinguish between partial activations of segment lengths and the total activation of each segment length within a suite of variable lengths, in the absence of a one-to-one documentation of a correlative rupture length for each earthquake event. The Japanese data considered by Wesnousky and others (1983) apparently is of sufficient quality to justify the statement that the historic record of seismicity can in most cases be associated with mappable faults that are activated along their total segment lengths. Alternatively, this is another way of saying that the mappable scales of resolution are made sufficiently detailed to be compatible with the resolution of seismic events. Even there, however, there may be some ambiguity about distinguishing complete rupture events from what might be regarded as foreshock and/or aftershock sequences at a different spatiotemporal scale of observation. This point is raised because the observed frequency-magnitude relations, as expressed by Wesnousky and others (1983) in terms of the maximum moment model, imply either a range of segment lengths within characteristic classes of branching-order or a

progression of partial activations of each segment length. These alternative interpretational viewpoints will be used to illustrate the possible applications of paleoseismic fractograms; in the case of the Japanese earthquakes the data favor the former viewpoint, but they also illustrate both possibilities when major changes of tectonic scale are contemplated.

Figure 2 represents the explanation by Wesnousky and others (1983) of the maximum moment (and magnitude) model. It differs from what they call the

Figure 2 near here

"b-value" model in that each fault has only one event (the "maximum" event) per recurrence time for that fault; other smaller events are interpreted as being associated with foreshock/aftershock sequences. They felt that such a model is indicated by the absences of earthquake events between the maximum event and the smaller events on a given fault; a more or less continuous range would be predicted by the application of a generalized b-value plot. From the standpoint of deformation states and the total potential energy available for seismic radiation, the maximum moment model says that all the energy avaiable to a mappable fault segment is released in specific quanta at intervals given by the recurrence time (except for the relatively negligible moments associated with foreshocks and aftershocks of much smaller magnitudes). The b-value model, by contrast, implies that for every earthquake of a given moment equal to that of an event in the maximum moment model there is a substantial amount of energy associated with other events that are almost as large (i.e., the events that would fill the gap in the distribution of Figure 2b). This means either that the total energy available to that fault per unit time is greater for the b-value model, or the recurrence time for the same magnitude earthquake is larger than that given by the maximum moment model (it takes longer to build up an equivalent moment in the b-value mode, because part of the energy is being released in earthquakes that are almost as large). This also means that in a frequency-magnitude diagram, large-magnitude earthquakes (greater than a certain equivalence magnitude) will plot at a higher frequency if the maximum moment model describes the mechanism of energy release better than the b-value model. The equivalence point is a crossover at the centroid of the over-represented events in the b-value model. The b-value model, therefore, also overestimates the numbers of earthquakes smaller than the equivalence magnitude, because it assumes the existence of events that did not occur.

As pointed out by Wesnousky and others (1983, Figures 5 and 7), the difference in interpretation can amount to a factor of two in the forecast of earthquake recurrence for a given magnitude. Thus, the possible modes of activation of a coeval distribution of fault populations, or the sequence of activations in a hierarchy of genetically related fault branches, is of paramount importance to concepts of earthquake forecasting.

The fact that hierarchical branching patterns of fault evolution exist is substantiated by field studies of ground rupture before and after modern earthquakes. A well-studied example is the Dasht-e Bayaz earthquake of 31 August 1968 in Iran (see, Tchalenko and Ambraseys, 1970; Tchalenko and Berberian, 1975). Laboratory studies of fracture patterns during progressive deformations show similar patterns (e.g., Tchalenko, 1968). These examples are used later to illustrate concepts of self-similarity.

Some Alternative Modes Of Fault Activation In A Branching Hierarchy.

Figure 3 shows alternatives for activating fault segments in the distribution of Figure 1 according to modes that resemble either the b-value or maximum moment models. In example (a) one event is shown that activates

Figure 3 near here

the total length of one fault segment; example (b) shows a cummulative length that represents the same value of moment but which engages subintervals of several different fault segments at different times. Obviously, the largest magnitude event in Figure 3b is somewhat smaller than the maximum event in Figure 3a (this is one of a series of maximum events not indicated; no sequential correspondences between events in a and b are implied, nor are they deducible from the length distribution). If the overall rate at which the potential earthquake moment builds up is the same in the two cases, then an event in (b) that matches the maximum event in (a) will have a longer repeat time between occurrences. Besides the fact that in some specific cases the record of repetitive events on a given fault is not in accord with a distribution of partial activation events as in Figure 3b (see discussion of California earthquakes by Wesnousky and others, 1983), the assumption that each event is correlative with a specific fault segment makes the accounting of a sequence of events testable against data and/or hypotheses concerning the distribution of mappable faults. Therefore, we will examine the implications of this idea against the data and procedure used by Shaw and others (1981) to construct paleoseismic alternatives derived on the basis of mapped faults in the conterminous U. S. that have shown evidence of activity younger than about 15 m.y.

Figure 4 summarizes the data in the form of histograms showing the overall distribution of measured lengths vs. the counts of their occurrences; a subset for a well-documented map of fault distributions in the Los Angeles vicinity (Ziony and others, 1974) is shown to illustrate the approximate invariance with changes of map scale. The same data are shown in the form of log-log

Figure 4 near here

plots in Figure 5. Regression equations for these data, and for subsets of

Figure 5 near here

data for thirty different Faulting Regions, as well as the data for the Los Angeles vicinity, typically conform to a power-law distribution: $N = kL^m$, where k is a constant charateristic of the region and map scale, and m is an exponent that usually has a value of -2 ± 0.5 for distributions based on constant linear increments (Shaw and others, 1981, Table 2.2.1-1, p 91). Although the compilations of histograms and log-log plots were initially all carried out in terms of a constant linear increment of length, the data are also expressed in terms of a convention designated by Shaw and others (1981) DELX = X; this was done because the data sets for constant length increments have gaps, particularly at the longest lengths, whereas the geometrically progressing length scale results in sets with nearly continuous distributions of lengths. This convention also simplifies the manipulation of length/number orders, although any detailed analysis of subsets should refer to the linear distribution and to cummulative distributions derived from it (see Shaw and others 1981, Figures 4.1.1-1,-2,-3 p 214-216).

Shaw and others (1981) used the convention DELX=X to illustrate the

construction of a parallelogram that summarizes the relationships between assumed length distributions, rates of length activation (rates of buildup of seismic moment), and the consequent proportionalities between corresponding frequencies and magnitudes of events that would be associated with particular combinations of numbers of fault segments vs. their lengths. They used the following relation between length and magnitude:

$$M = 1.235 + 1.243 \log L; \quad L \text{ in meters}, \tag{1}$$

based on a range of possibilities from regression analyses of lengths and magnitudes for different classes of faults discussed by Mark (1977) and Mark and Bonilla (1977). This is retained as the reference equation for consistency and because it is reasonably compatible with relations described by Wesnousky and others (1983) between length, moment (M_0) and magnitude. Wesnousky and others (1983, Figure 6) give a regression equation for seismic moment vs. length for large intraplate earthquakes in Japan, and a relation between moment and magnitude (see Hanks and Kanamori, 1979), as follows:

$$\log M_0 = 23.50 + 1.94 \log L; \quad M_0 \text{ in dyne-cm, for } L \text{ in km}, \tag{2}$$

and

$$\log M_0 = 16.1 + 1.5 M. \tag{3}$$

Substituting the latter equation in the M vs. log L relation used by Shaw and others (1981) gives the equivalent relation between length and moment,

$$\log M_0 = 23.57 + 1.87 \log L, \tag{4}$$

which is reasonably close to the relation used by Wesnousky and others in Eq. 2. Thus, we can directly convert their data plotted in terms of numbers of events vs. moment (Wesnousky and others, 1983, Figure 7) to our graphs based on length and calculated magnitude with little comparative error. Although we use simple linear functions in log-log plots to represent the fractogram, later we also examine some of the implications of nonlinear moment-magnitude relations of the form discussed by Hanks and Boore (1984).

The DELX = X convention overestimates the numbers of faults at lengths below about 100 km, whereas the regressions of log N vs. log L based on constant linear increments of length underestimates the numbers of faults at lengths greater than about 200 km. In the absence of sufficient information to unequivocally resolve limiting distributions of both short and long faults, we derive an example for both distributions; however, the distribution of fault lengths in Japan does not have as wide a range as the U. S. data set, and the linear increment statistics will be used as the general basis for comparison.

Figure 6 shows frequency-magnitude diagrams on which we have delineated the areas (the fractograms of specified limits in log f and M) implied by the length distributions, based on an assumed overall rate of length activation; this has the value 10 km/yr of length activated (not to be confused with fault slip) as derived by Shaw and others (1981) based on extrapolations of lengths of faults vs. ages of activation (see p 269, and Figures 3.2-4, and 3.2-6 in that reference). The overall

Figure 6 near here

average of frequency-magnitude data for historic earthquakes in the U. S. as compiled by Algermissen (1969) is shown for reference; later we comment on the contrasts in slopes of different sets of frequency-magnitude data and on the adjustments of activation rates needed to bring the seismic and faulting data into alignment. Preliminary to that discussion, however, the method of constructing Figure 6 is derived with the aid of step-by-step tabulations based on number-length relations. In general, we assume a stationary (time-independent) distribution; the implications of transient deviations will be discussed in a later section.

Table 1 summarizes the calculations used to construct Figure 6. Part A gives the equations for number vs. length in terms of constant linear increments (1) and DELX = X (2); entries in subsequent sections are numbered (1) and (2) to indicate these conventions. Note that the equations are given in terms of measurements at the map scale in A (1 cm = 50 km); lengths in other parts of Table 1 have been converted to meters or kilometers depending on the context in which the data were used in the original sources. Part B shows the distribution of lengths ordered according to a 4-fold hierarchy to base 10. This arbitrary base was used to give a concise representation of a wide range of length-number relations for the composite statistics of U. S. faulting; in cases of specific fault sets there may be a nonarbitrary distribution that approximates a different geometric progression or which deviates in some way from an idealized mathematical set, as in Figure 1. Such deviations, however, should reveal themselves in terms of disproportionate lengths and slopes relative to any particular idealized distribution in a frequency-magnitude diagram. The numbers of fault segments, the segment lengths, total length per order, and the fraction of the cumulative length per order are tabulated. The length fraction, X (not to be confused with the general symbol DELX = X above), is used to proportion an aggregate rupture length over the range of length orders.

In part C of Table 1 the maximum event per segment length representative of each order (average or uniformly constant segments) is calculated for an assumed overall value of fault activation rate that includes all orders. This is the ultimate possible maximum moment model under an assumption that overall strain is steady and uniformly proportioned between the different orders; each fault segment ruptures when strain buildup reaches that appropriate length in each class. The segment recurrence time is the time between each maximum event, defining the frequency-magnitude distribution for this set of assumptions. Shaw and others (1981) referred to this distribution as the steady-state SATURATION mode of activation. That is, in order that the length-number distribution of activations shall be preserved over time, this is the limiting distribution (on average) of the frequencies of events in each length and magnitude, or moment, class. The value of overall rupture length rate, RLR, used in Table 1 is 10 km/yr, sudivided as described, which is the value used by Shaw and others (1981); they noted, however, that this was a conservative estimate of the overall rate of activation and suggested that the true rate was probably between 10 km/yr and 100 km/yr. Their nominal rate is used in the tabulation of example calculations for purposes of cross-reference, but we later adjust the value to about 40 km/yr to illustrate comparisons with overall U. S. seismicity.

If rupture according to some program of overall strain accumulation is not able to build up to the SATURATION limit, then ruptures must occur over partial segment lengths to preserve the steady state assumption. This may constitute a distribution like the b-value model or many other kinds of nonmaximized distributions. A simple way to inspect the range of possibilities, and to block out the region of frequency-magnitude space within

which specialized paths may occur, is to assume that strain buildup is sampled uniformly after different intervals of time on all partial segment lengths of all faults in every order. For example, Table 1 D shows that in one year there would be a buildup of 320 meters (1), or 160 meters (2), of potential length activation on the single fault in number-order N = 1 of total length 219 km (1) or 933 km (2); maximum segment lengths are from Table 1 C. If that buildup is relieved by earthquakes, there are partial events of magnitude 4.35 (1) or 3.97 (2). In order N = 1000, however, the buildup of total potential activation length is much larger because of the larger fractional representation according to the length distributions in section B of Table 1; accordingly, the partial activations now total 6.5 km (1) and 7.2 km (2), respectively. But this total is distributed equally over all the 1000 segments, so the average partial length of activation per segment is only 6.5 m (1) and 7.2 m (2), respectively; the equivalent magnitudes are now only 2.24 (1) and 2.30 (2), respectively. Thus, yearly seismic release of strain buildup uniformly over the entire network of fault branches would result in over a thousand earthquakes with magnitudes ranging from about 2 to 4. Other calculations of this sort are listed in part D of Table 1.

The distributed mode of calculation above defines the perimeter of the effective area in frequency-magnitude space that Shaw and others (1981) called the "paleoseismic parallelogram", which we abreviate to fractogram in the present paper. The reference area of the fractogram is determined by the range of number/length orders defined by a given branching distribution and by the range of times considered for fault activation; the position in frequency-magnitude space is determined by these relations and by the Rupture Length Rate, RLR, proportioned according to length fractions, X. The choice of potential Buildup Times, BT, from 1 to 1000 years is arbitrarily chosen to span the range of interest for practical hazards assessments, but the range can be extended to consider implications of branching distributions for the largest conceivable earthquakes on time-scales of 10,000 years or longer, consistent with the statistics of measured fault lengths (cf., Figure 6b).

The concept of SATURATION length is useful because longer lengths of activation, and Buildup Times, would not be expected at the predicted frequencies. For example, as BT is made larger and larger, a given distribution reaches its suite of SATURATION lengths within a specific time. This time is 684 yearsfor distribution (1), but it is 5831 years for distribution (2), at which times the maximum earthquakes are, respectively, 7.87 and 8.66 (Table 1 C). Prior to these limits the two different distributions give roughly the same sorts of predictions for partial potential events, generally differing by less than half a magnitude unit (Table 1 D). Distribution (1) "terminates" at 684 years where distribution (2) is still far from its SATURATION limit. Thus, for BT smaller than a thousand years, distribution (1) gives the more "cautious" suite of possibilities in that it predicts a larger magnitude at a given frequency of potential partial events. For BT greater than a thousand years, however, distribution (2) gives a crude estimate of potential events that might relate to faults lacking evidence of historic seismicity (both are subject to the general limitations discussed by Hanks and Boore, 1984). These are not predictions because they only represent possible suites of partial activations. More specific statements require knowledge or assumptions about the number/length orders activated and whether they represent partial or total activations of segment lengths. Therefore, comparisons of Figure 6, and the calculations of Table 1, with the analysis of Japanese earthquakes by Wesnousky and others (1983) suggest additional aspects of patterning in the possible sequences of fault activations.

Interpretation of Historic Seismicity by Use of the Simplified Fractogram With Constant Slopes.

Figure 7a compares the fractogram from Figure 6a with the 400-year record of Japanese seismicity, recalculated in terms of magnitude and frequency from Figure 7 of Wesnousky and others (1983); Figure 7b shows the adjusted position of this fractogram on the assumption that the limit of the seismic frequency-magnitude range for the U. S. defines a point on the SATURATION line for order N = 1. By this assumption, the longest segment length is about 300 km, a value consistent with the largest historic events on the San Andreas fault. If, on the other hand, the total mapped length of the essentially continuous portion of the San Andreas system is taken to define the maximum segment length at N = 1, then the SATURATION length is nearly 1000 km. SATURATION defined on the former basis implies that the San Andreas is considered to be made up of more than one characteristic branching distribution of genetically related faults (from the viewpoint of activation sequences). The SATURATION limit on the basis L = 1000 km at N = 1 is shown by the heavy dashed line in Figure 7b; apparently, the observed record of seismicity is characterized by events with maximum moments smaller than this single-valued maximum SATURATION event. We return to this point in later discussion of seismic zones in California.

Figure 7 near here

In Figure 7, the lines representing historic seismicity in the U. S. are based on data compiled by Algermissen (1969) and Algermissen and Perkins (1976). These sources expressed regression lines in terms of Modified Mercalli intensities. The corresponding magnitude scale is given by following relation :

$$M_c = 1.3 + 0.6\ I_o, \qquad (5)$$

where M_c is the "corresponding magnitude" and I_o is the Modified Mercalli intensity (Algermissen and Perkins (1976, p 16).

Although the time frames of the historic records are about the same, the Japanese data are more completely documented in terms of associated faulting. This is shown by the correspondences between observed zigzag offsets and those predicted by application of the maximum moment model in Figure 7. Similar behavior seems likely for the relation between faulting and earthquakes in the U. S., judging from the general parallelism of the overall distribution and the fact that frequency-magnitude compilations for individual seismic zones (Algermissen and Perkins, 1976) generally show flatter distributions than the composite. The distribution of seismic zones in California will be shown in a later graph; comparisons for all seismic zones and all faulting regions based on the distribution DELX = X as reference parallelogram are illustrated in Shaw and others (1981). Note that the U. S. data are for incremental frequencies, while the Japanese data are cumulative. Thus, the frequencies of the distribution of Japanese earthquakes would be reduced by about a factor of two for direct comparisons with the U. S. data. The comparisons of interest here, however, concern the general magnitudes and slopes of the respective patterns.

Referring to Figure 6 and Table 1 for proportionalities, two hypothetical alternative interpretations of the Japanese data illustrate application of the fractogram to a set of earthquake faults on the assumption that they belong to a generally systematic and cogenetic branching distribution of faults: (1) if it is assumed that the scaling of the fractogram in Figure 7a is correct, then

the implication is that the largest event, and fault length, portrayed represents SATURATION on the line N = 10; if so, events are not recorded for the longest branch N = 1 (i.e., M = 8 events would be expected only for recurrence times of the order 10^3 years), (2) if, on the other hand, it is assumed, or is known, that the largest event shown can definitely be correlated with a single fault of the maximum possible length in the set, then the fractogram would be shifted up and to the left so that the line N = 1 is at M = 7.4 (length of order 10^2 km), in which case the data span orders N = 1 to N= 100. In either case, at the lowest two orders (smaller N, larger L)the trend is close to the SATURATION line, which is consistent with the idea that the maximum moment model correlates well with the mapped lengths. In detail, however, the diagram suggests that there is a range of partial length activations spanning about 10 to 100 percent of the segment lengths at the shorter lengths (alternatively, this could be interpreted as a spread of lengths within an order that has a characteristic average length). These partial lengths could be interpreted as maximum moment events which occur at less than the ultimate SATURATION limit in the fractogram. Later we will examine the implications of similar step-like distributions for seismicity in California.

Figure 8 sketches some alternative schematic paths of relative fault activation in the fractogram. Example (a) signifies a "diffusive" activation

Figure 8 near here

of all number/length orders with time. Small earthquake events occur frequently, and the buildup of length activation never exceeds some small percentage of the possible SATURATION length. In the limit of smaller and smaller lengths per order (i.e., with a shift of the fractogram to lower magnitudes and higher frequencies) this mode merges with distributions more characteristic of aftershock sequences and ultimately with uniformly steady aseismic creep. The dashed line shows the corresponding record of composite seismic frequencies in the absence of information on number-length distributions; i.e., there is a trend alternately paralleling lines of constant N and BT, because the distribution is assumed to be homogeneous (lines of constant N parallel lines of constant Rupture Length Rate, RLR).

Example (b) in Figure 8 shows the activation of each number/length order in a series of epochs. That is to say, at some arbitrary starting time, the subset order N = 1000 begins to be activated over longer and longer times until the maximum segment lengths for that order are activated at the SATURATION limit. No other number/length orders experience any earthquake events during this time, which in this case is about a thousand years. Therefore, the line at N = 1000, over the range BT = 1 to 1000, directly represents the record of seismicity during this time. At BT = 1000, the activity shifts to the next larger number/length order, N = 100 (i.e., order N = 1000 has experienced sufficient local strain relaxation so that this subset becomes dormant to small fault activity). The subset N = 100 is now progressively activated over the next thousand years until it, too, reaches the SATURATION limit. This hierarchical series of sequential order activations proceeds until the longest single-valued fault length is activated. Then the sequence may become dormant for some period or may repeat in a series of seismic cycles. Obviously, the seismic record depends on the time frame of observation; the total time of the idealized cycle is 4000 years in this example. Thus, if observations are made early in the first epoch, the record consists of numerous small events, whereas observation late in the fourth epoch will show infrequent large magnitude events. A variety of

frequency magnitude slopes are possible depending on how the distribution is sampled. Also, the entire set could be viewed as an extreme case of the diffusive mode in (a) in which all orders are sampled uniformly over times long compared to the cycle time. If so, however, the record would have to be at least four thousand years long to display the full spectrum of activation rates.

Figure 8 (c) represents a stepwise composite cycle resembling (b), except that the transitions between orders proceed at proportional intervals of time and length in each order. Two obvious modes are possible: In mode (1) order N = 1000 becomes dormant after 10 years, order N = 100 after 100 years, and so on. Each transition represents a temporary period of activation of the same charateristic lengths in the two adjacent orders. If these lengths are characteristic of the cycle, then they represent the maximum moment condition for that order. The larger number/length orders (large N, small L) do not reach the SATURATION condition, presumably because partial strain relaxation is sufficient to cause the shift to smaller number/length orders (small N, large L). In mode (2) each order has a characteristic interval of partial segment lengths that are simultaneously being activated over characteristic ranges of BT for each order. In the steady state this implies a rather high degree of coordination among the respective ranges of mechanical properties for the set as a whole. It also implies, as in the uniform "diffusive" mode in (b), that the seismic record has to be very long to document the full suite of activation rates. The dashed line indicates the average trend of the composite seismic record. Notice that the smaller event sequences occupy smaller intervals of time, thus the average slope will be sensitive to the time window of observation. Some intervals of observation would give trends subparallel to the lines of constant BT, while others would be subparallel to lines of constant N (and RLR). Like (b), the mode (1) cycle in (c) may be repetitive; in this case the cycle time is longer than about a thousand years.

Example (d) in Figure 8 represents the uniform SATURATION condition. It might be termed the penultimate maximum moment model in that no events occur until the maximum available fault length can be totally activated. Episodes of activations could happen uniformly, as in (a), sequentially as in (b) and (c), or in swarms of activity separated by times of about a thousand years. In this latter case the limiting trend identifies only the average frequency-magnitude relation over multiple cycles. For example, at N = 1000, if the first event does not occur until all segments can be potentially activated, then the total time is BT = 1000. Then, however, if all segments are activated in rapid-fire sequence, there are 1000 events. Thus, the average rate of activation over many cycles is the same as activating one maximum event at the frequency corresponding to that segment length for the given value of FRLR (see Table 1).

The pattern of the record of seismicity and fault activation in Japan, as shown in Figure 7a, most closely resembles example (c) in Figure 8. Although it is beyond the scope of this report, it should be interesting to examine the data for either chronological sequences or uniformly haphazard activations of coordinated length sets. That is, does mode (1) or mode (2) in (c) more closely describe the history? Mode (1) is deterministically progressive in time, while mode (2) is stochastically homogeneous and haphazard in time. Since the record is 400-years long and the maximum recurrence times are of the order 10^2 years, mode (2) might be approximated. If so, the implication would be that the overall behavior is stationary in time, with corresponding implications for the mechanics of faulting relative to tectonic work rates.

Comparison of Seismic Zones in California With Patterns of Composite U. S. and Japan Seismicity: Dimensional Scaling of Fractograms With Constant Slopes.

Figure 9 summarizes frequency-magnitude data from Algermissen and Perkins (1976) for several seismic zones which encompass the faulting regions in California (modified from the suites of diagrams in Shaw and others, 1981, for all seismic zones and faulting regions of the conterminous U. S.). Figure 10 shows the delineation of seismic zones as given by Algermissen and Perkins (1976). Seismic zone 2 essentially encompasses the San Andreas fault zone

Figures 9 and 10 near here

between the Salton trough and its intersection with the northern California coastline (a distance of about a thousand kilometers). Notably, the frequency-magnitude position of the largest event in this zone is close to the magnitude limit as shown for the composite U. S. data (circled cross in Figure 9). This is the approximate magnitude limit of the linear regression line in Algermissen (1969); it is taken to represent the SATURATION limit consistent with one interpretation of faulting rates (the shift required for 1000 km as the SATURATION limit is indicated in Figure 7b), but the seismic record is not long enough to substantiate a general limit. In fact, an attempt to fit the frequency-magnitude data for all the seismic zones in California into the same fractogram, or a simple sequence of fractograms, meets with some difficulties relative to the varieties of possible paths outlined in Figure 8.

Hypothetically, if we were to consider the composite seismic record of the U. S. as being related to a single hierarchy of branching faults, then the San Andreas system would represent the first order or trunk fault, N = 1, which is associated with the longest total length activations and highest possible maximum moment and magnitude. Up to a point, despite the continent-scale implications concerning distributions of strain energy, this interpretation is grossly consistent with both the faulting and earthquake data, and with the similar interpretation of large scale faulting and earthquake distributions in Japan.

Although the San Andreas system seems to fit well into the Plate Tectonics scheme, there are many contradictory aspects at the regional scale of seismic zones in California. Comparing Figure 9 with the broad regional coverage of zones in Figure 10, there is a conspicuous paucity of frequency-magnitude trends that fall inside the same self-consistent fractogram, as delineated by the hierarchy of number/length sets and the general consistency of both the length-scaling and the magnitude scaling of the San Andreas system. At face value, there are three obvious possibilities for the "missing" information: (a) the San Andreas is in fact a higher order (N greater than 1) number/length order than was assumed by the coincidence of the length, magnitude and frequency agreement with the composite U. S. distribution (in this regard, Wesnousky and others, 1983, suggested that long strike-slip faults might be viewed as a system of chain-like and distinctly different fault segments each with a characteristic maximum moment; in the present context, however, this idea does not help with the problem of self-consistency of more general branch-length sets with different frequency-magnitude signatures), (b) the San Andreas is in fact an N = 1, single-valued, maximum fault with partial activations spanning the entire range of partial segment lengths from those consistent with short buildup times to SATURATION at L = 300 km and N = 1 (i.e., this maximum event is smaller than the SATURATION value for L = 1000 km at N = 1); the set of observations used to establish the seismic regression line 2 in Figure 9 represents a time interval within the culminating epoch of activity in a seismic cycle something like the one shown in Figure 8b (i.e.,

we are in the "fourth millenium" relative to the cyclical version of that scaling model), and (c) a cyclical model resembling the step-like distribution in Japan (and Figure 8c) actually exists but the sampling of seismic events in the historic catalog does not adequately represent the smaller higher frequency events in California (i.e., there have been episodes of events in the magnitude range 4 to 7 with frequencies exceeding one per year which are not adequately represented in Figure 9; if a maximum length of 1000 km were taken to be representative, there are also missing events at the largest magnitudes with recurrence times close to 10^3 years).

Each of the above interpretations, and probably others, has interesting and testable implications in the light of possible paths through a fractogram as sketched in Figure 8. We do not attempt to make a case for any single interpretation in this paper, but some comments are offered concerning those aspects which seem most likely to us relative to composite records such as those we have studied in the U. S. The San Andreas seems more reasonably interpreted as a system of first-order partial activations than as an "elongate hierarchy" of chain-like branch lengths of different orders along the same fault line. We therefore favor a combination of possiblities (b) and (c) above as an explanation for the lack of frequency-magnitude trends within the limits of the composite parallelogram in Figure 9. If a step-like distribution resembling Figure 8c is envisioned, the smaller-magnitude, higher-frequency episodes are of relatively short durations and could easily be underrepresented in the historic catalog. Some suggestion of this kind of effect may be represented by the frequency-magnitude trends in seismic zones 1, 7, 17, and 19 which have distributions near that of zone 2 but with steeper slopes and smaller maximum magnitudes; zones 1 and 17, in particular, represent more diffusely distributed systems of faults along the general trend of the San Andreas system.

If we now consider the other seismic zones in California in terms of the above interpretation, analogous conclusions might be drawn for the other frequency-magnitude trends in Figure 9 (namely, zones 3, 4, 5, 6, 8, 12, 13, 16, and 18). In view of the geographic discontinuities, the simplest recourse might be to construct several different fractograms each represented by one of the trends as order N = 1. In order to do so, each fractogram would be constructed on the basis of a characteristic rupture length rate, RLR, which is small compared with the composite summation of 40 km/yr. For example, if we were to construct such a parallelogram for zone 6 in the San Francisco Bay region east of the San Andreas system, we might use an effective RLR of the order 1 km/yr. Because of overlap, some of the higher-frequency events in such a distribution would be confused with those in zone 2; similar arguments might also apply to zone 5 in the region of complex faulting to the northwest of the Bay Area.

If such constructions are performed for each seismic zone, the distribution of N = 1 orders would be consistent with a series of maximum events smaller than that of the San Andreas system but also with lower net frequencies and longer cycle times. The interpretation of general behavior would otherwise be similar (notably, however, the behavior of zone 12 resembles that of the San Andreas system at somewhat lower frequencies, suggesting an N = 1 fault length exceeding the zone length; Shaw and others, 1981, Figure 4.3.2.2.-1, p 304, interpreted this as order N = 1 in the fault distribution of the Walker Lane faulting region and included with it the zones 9, 10 , 11, and part of 7).

If one attempts to combine several zones into a single number/length hierarchy, the self-consistent fractogram imposes certain constraints on the implied distribution. For example, the hypothesis might be entertained that

the coastal and offshore faults of southern California west of the San Andreas system might be lumped together into a single system (zones 3, 4, and 18). If so, zone 18 might be viewed as a portion of the first-order fault. By that interpretation, however, the potential maximum event is offscale in Figure 9 at a magnitude near 9 (linear extrapolation; see Hanks and Boore, 1984) and frequency of the order 10^{-5} yr^{-1}; the implied fault length would be of the order 10^{3} km activated at a partial rate of about 10^{-2} km/yr (this is shown in Figure 9 as the partially delineated dotted fractogram at the lower right). Although such an interpretation seems less likely than more piecemeal constructions, it is shrouded in the uncertainties of recognizing major offshore faults with very long recursion times near the margin of the continental shelf.

Figure 11 schematically summarizes the style of faulting and seismicity in California. The simplest pattern consistent with both faulting and seismic

Figure 11 near here

data is that the historic catalog reflects partial activations at constant N with short to long Buildup Times on systems of faults described by different, partially overlapping, fractograms (the Inset shows an example referred only to the vicinity of the San Andreas system). The higher frequency events are underrepresented because of their shorter durations in a generalized seismic cycle resembling Figure 8c and, to some extent, the pattern in Japan. We can not rule out, however, the possibility of composite systems of megafaulting with potential events larger than the known maximum event on the San Andreas fault; the diagrammatic magnitudes of such hypothetical events would range from 8.5 to 9 with recurrence times of 10^{3} to 10^{5} years, or longer (these events would be adjusted to lower magnitudes using the moment-magnitude scale of Hanks and Boore, 1984).

Paleoseismic Length Scales and Nested Hierarchies of Branching Fault Sets.

Figure 12 summarizes selected sets of of age data for comparative trends in the relation between numbers of faults (log N) and their distributions of length (log L) for the U. S. and Japan. Of particular interest are the

Figure 12 near here

numbers of faults of different activation ages in the U. S., relative to the composite distribution for all ages in the U. S. Faults categorized as "young" on the map of Howard and others (1978) are faults which have shown evidence of activation within several different age groups in the latest 15 m.y. (see Shaw and others, 1981). The crosses and associated regression line represent the conversion of moments to lengths for inferred historic faulting in Japan, using the earlier equation and data in Wesnousky and others (1983, Figure 7). We wish to illustrate two points with this diagram: (1) there is a general agreement between the total number/length distribution and the composite distribution of historic seismicity in the records of the U. S. and Japan (Figure 7 of the present paper), and (2) by contrast, the indicated record of documented historic fault activations in the U. S., or even those younger than 10,000 years, have a count much lower than in Japan, and too low to account for the historic seismicity in the U. S.

The most obvious interpretation of this discrepancy is that the overall fault count in the U. S. is roughly consistent with U. S. seismicity, but that, therefore, the recognitions of fault activations at ages less than 10,000 years are grossly underestimated. Some of the recent announcements of evidence of young faulting in midwestern and southeastern states are consistent with this interpretation (see Obermeier and others, 1985; Kerr, 1985); Shaw and others (1981, Sec. 5, p 344) made a generalized "prediction" of the discovery of expectable faulting events in several Faulting Regions across the U. S. on the basis of similar comparisons of fault activation lengths vis a vis historic seismicity.

Inspection of the 1:5,000,000 scale map of young faults in the U. S. (Howard and others, 1978; Shaw and others, 1981), or maps and catalogs of faulting in Japan (see Wesnousky and others, 1982, Figure 4), indicates that within given scales of observation faults tend to be distributed in subgroups having several different and discontinuous length-scales (as in Figure 1). When a large sample of such populations is plotted together, as in the composite data for the U. S. in Figure 4, however, the population resembles a continuum of lengths. Such a relativity is characteristic of branching distributions having a range of number/length hierarchies each with different coefficients of slope and/or length proportionalities. Perhaps the most familiar example of such distributions is the ordering of stream populations in different drainage networks. A local stream system often has a distinct hierarchy of well-defined and discontinuous segment lengths (characteristic values of length per order) as measured from points of bifurcation. If, on the other hand, all stream segments were compiled for the conterminous U. S., there would be a continuum of lengths up to that of the "maximum stream" represented by the Mississippi system.

Although stream systems are distributed on a more or less planar surface and fault systems are distributed within large volumetric domains, there is some resemblance between the respective concepts of branching hierarchies. Because of the dimensionality, and the preservation of overprinting, fault systems are much more complex. Nonetheless, it seems useful to explore characteristic proportionalities within different scales and domains of fault branching hierarchies. A system that displays characteristic

proportionalities among number/length orders is said to be self-similar or scale invariant, in that the pattern is predictable at different scales on the basis of the same ordering rules. There may be, and usually are, different rules for different sets, as is the case for stream networks of different types in different settings. Even so, however, there may also be a general rule of self-similarity that describes the average behavior of composite sets of subsystems at different scales. For example, there are predictable numbers of streams in the U. S. of a given average length even though those numbers are not correct for a specific subsystem (i.e., the upper Missouri River subsystem is likely to have a different kind of scale invariance than the Ohio River subsystem).

The above distinctions resemble the problem of distinguishing different characteristic first-order faults in Figure 9. The descriptive numbering of fault orders, however, is the inverse of the convention for stream orders (see Shaw and Gartner, 1984). That is, we use the term first-order to refer to the set $N = 1$, whatever the range of numbers and lengths may be. This is because information defining a characteristic "shortest" length and number for faults is usually not available (stream order 1 is the shortest distinguishable tributary stream). Each of the different possible scale relations discussed for fractograms in Figure 9 is analogous to a different stream system with differing scale ratios of self-similarity and different transport properties. In this crude analogy, the value of RLR associated with the construction of a given fractogram takes the place of the discharge variable in a stream system. Qualitatively, a fractogram based on a small RLR is analogous to a stream in an arid or semiarid climate zone. That is to say, the distribution of numbers and lengths of stream channels may be consistent with a large potential rate of discharge, but the actual rate may be very small,....or, more importantly, the average rate may be very small but the intermittent flood may be transiently even larger than that of the stream with high average discharge rate. This would be the analogous case in the discussion of a fractogram that would simultaneously accomodate possible long-term behavior for seismic zones 3, 4, and 18 in Figure 9. Stated another way, confusion in the correlations of seismic data with fractograms in Figure 9 reflects the fact that analogous systems of tectonic "drainage networks" have not yet been established relative to the definitions of Seismic Zones (Note: In a later section we attempt to relate such "dendritic models" to more rigorous discussions of strain energy, as exemplified by Andrews, 1978).

These analogies lead naturally to an exploration of some relevant geometric properties of self-similar sets which may eventually prove useful in more quantitative evaluations of the relations between fault activation rates and the volumetric rates of tectonic energy transport in the earth (more specific attempts to compare principles of ordering are outlined in Shaw and Gartner, 1984). This approach may also aid in resolving some of the problems of missing information that have been mentioned in the contexts of compatible frequency-magnitude and number-length correlations, as in the comparisons of Figure 12.

A pictorial demonstration of the problems of correlations between possible self-similar patterns and energy transport rates is indicated in Figure 13. This diagram shows plan views of actual faulting and fracture

Figure 13 near here

patterns, lacking detailed information on the specific chronologies of individual segments, at four different scales spanning a range of almost 10^8 in length ratios. The ratios of formative time scales are yet larger and more

discontinuous between the different sets. The smallest two scales, (c) and (d), represent the deformation of a clay material in the laboratory within a time scale of hours and an energy scale that is very small compared with the larger two systems, (a) and (b). Pattern (b) shows the approximate distribution of ground breakage mapped after the Dasht-e Bayaz (Iran) earthquake of 1968 (Tchalenko, 1970; Tchalenko and Ambraseys, 1970; Tchalenko and Berberian, 1975), and pattern (a) is a sketch map of some of the larger faults in California showing evidence of movement in the latest 15 m.y. (the solid circles in this sketch are the points in Figure 10 roughly demarking the mappably continuous portion of the San Andreas system). According to the earlier discussions of Figures 9 and 12, many more fault segments exist, and some of the larger faults shown probably were activated much more recently than is indicated by the age groupings documented by Howard and others (1978).

Except for angular relationships, there is a crude visual self-similarity to these distributions. If no scales were indicated they would categorically look much alike in terms of the distributions of lengths. This similarity can be quantified by measurement, and even if these patterns are not from the same system of deformations the result represents a test of parameters defining the extent of general scale invariance in faulting patterns. In the absence of a compilation of data at all map scales for pattern (a) in California, it is nonetheless evident that patterns like those in Figure 13 exist (Sieh, 1981; Wallace, 1981). We might therefore ask, in general, how the energy of shear deformation might be distributed across the larger system on the assumption that it contains a self-similar distribution of smaller shears of the sort portrayed in the figure. It will aid that investigation if we can first identify some of the implications of self-similarity relative to the paths already discussed in the construction of fractograms.

Some Properties of Fractal Sets Relative to Questions of Self-Similarity in Fault Systems.

The term fractal was coined by Mandelbrot (1975, 1977, 1982) by analogy with problems of characterizing surfaces in metal fractography (see Mandelbrot and others, 1984). Our use of the term fractogram was chosen to acknowledge the relations between studies of fractography, on the one hand, and fractal geometry on the other. At the time of this writing many other investigators have made similar observations about the application of fractal geometry to earthquake problems. Because this is not a review, we cite only those papers which directly illustrate a point we wish to emphasize relative to the more obvious possible interpretations of fractograms.

The definition of a fractal dimension, as applied to physical problems, has been illustrated in diverse ways in the literature. We will discuss concrete examples in which the dimension is derived from measurements involving fracture surfaces, fault-segment distributions, numerical "dissection sets", and fingering flow of viscous fluids. First, however, some derivative remarks may clarify the context of a fractal (read fractional) dimension.

If we define a line, whether straight or curved, as a locus of points, then a plane is a locus of a locus of points, and so on. Any spatial measure, viewed in this way, can therefore be considered to represent topological loci of point sets (i.e., sets with elements of near-zero dimension; "granular" domains, which also may have properties of shape, as in clouds, and so on). Higher order constructions of planes from lines and volumes from planes, according to Euclidean geometry, assume that there is continuity at lower dimensions. If we allow the idea, however, that all descriptions of form are essentially measurements of the relative distributions of point densities, then the concept of material dimensions has elements of differing relative sharpness, or relative fuzziness, of resolution. Described in this way, any quantitative measurement of resolution depends on an assumed relation between the measuring device and the object being measured.

If a distribution of points is defined by measurements with a linear measuring tool (i.e., another sort of point set defined as a ruler) which is capable of a limited resolution relatve to the material points of interest, then the dimension assigned to the measurement depends on the point spacing in the material relative to the ruler length. Given a standard ruler, a standard topological description results. This is essentially a paraphrase of the common rules of map scale: given a standard scale (such as the 1:5,000,000 scale for portraying fault lengths in this paper), a standardized range of geometric structures results. Dimensional descrimination, then, can be expressed in terms of a range of length multiples of a standard length.

Thus, it could be said with some truth that the study of fractal geometry is very little different from the traditional studies of geology, geophysics, and seismology in which the challenge at hand concerns an ability to relate measurements on one scale of description to those at other (often vastly different) scales of description. As an example, we can witness the advances in our understanding of tectonic processes in the continents once the patterns of Plate Tectonics were established on the basis of scale relations for the kinematics of the ocean basins. A common goal of geology (including astrogeology) and fractal geometry, is to discover and describe techniques for classifying, illustrating, and correlating patterns which possess internally consistent types of fabrics by means of simple rules. In one way or another,this goal invokes concepts of relative similarity or, in geometrical terms, concepts of self-similarity.

Avoiding mathematical definitions, a self-similar geometry is one in which

the intrinsic dimensional character of a fabric, no matter how complex, is preserved and described by means of simple constants of proportionality which are invariant when the pattern is scrutinized at arbitrary magnifications and/or reductions. The value of fractal concepts stems from the systematic demonstration that such criteria of self-similarity exist even when there are no fixed proportionalities of topological dimensions in Euclidean space (or even higher order spaces). One may in some cases prefer to descriminate between fractally self-similar and topologically self-similar structures, but the former is rooted in the context of scientific measurement applied to the natural world, whereas the latter is an idealization, or sometimes even a corruption, of natural geometries. The fractal dimension provides proportionality constants for descriptions of such nontopological sets; they can exist in unlimited variety, because the fractal dimension can take on any fractional value from zero to the maximum topological dimension under consideration. These "fractal objects" represent those point-sets, or loci, mentioned above which can not be described in terms of constructions involving lines, planes or topological volumes. That is to say, they apply to geometries that consist of some potentially characteristic granularity (or segmented linearity) where the geometry can not be assigned universally to any single Euclidean dimension; for example, there are collective geometric forms as seen in a map view like Figure 13 that can't be described in terms of unique lines, or planar areas.

These "in-between" objects, if they are self-similar, are characterized by a constant, but generally noninteger, dimension. That dimension, which remains to be demonstrated for any class of fractal object, defines the spatial distribution, specifically (as in numerical dissection sets illustrated later) or statistically (as in fault distributions), for any change of scale within an appropriate domain of physical properties. The example used most often to illustrate fractal dimensions is the map-scale-dependent coastline length of any irregular landmass which increases as the ruler used for its measurement is made smaller and smaller (down to the scales of irregularities in sand and rock granularities). It is easy to see, in this case, that the tortuosities of the coastline (and other types of geological contacts) define a complex geometric form that does not preserve the constant proportional relation between perimeter and area for a regular geometric object bounded by elements of integer Euclidean dimensions. The fractal dimension of such a contact, in map view, is larger than one and smaller than two; in the same sense, the fractal dimension for an intricately curved planar surface, such as the brain, is between two and three (actually close to the latter because of the compactness of the involute-convolute complexity). We carry this kind of observation to the general conclusion that the description of any object will be found to involve fractional dimensions when it is examined over a wide enough range of magnifications, within stipulated topological limits. Stated differently, fractal geometry is the descriptive study in which we are engaged as geologists and geophysicists.

Rather than beginning with a description of bounded geometric sets, it seems more appropriate to the problems of faulting, fracture and earthquakes to start from the more general viewpoint of point sets. This is because, even though faults are represented as linear features on maps, they are notably imbricate and discontinuous over many different length scales (as in Figure 13). Even if we consider them to be linearly continuous over some range of minimum lengths, they can still be thought of as "elongated" point sets or dissected line sets. The point-set analogy reflects the fact that it is rarely possible to uniquely define a fault as a single continuous line on the ground, or as a single continuous plane in excavation. In the geometric

description of laboratory fracture experiments with metals, this problem has been circumvented by Mandelbrot and others (1984) by what they call "slit island" analysis. This technique involves sectioning and impregnating the fractured fabric, so that the description of its irregularities can be defined in terms of area/perimeter relations of the "lakes" and "islands" of contrasting materials in a manner parallel to that for coastlines. The fractal dimension documented in that study, relative to the surface of section, is about 1.28, which is similar to the fractal dimension of rugged coastlines like that of Great Britain (such measurements and equations of fractional proportionality were quantified by L. F. Richardson as an appendix to his remarkable work The Statistics of Deadly Quarrels long before the concept of fractals was systematized; see Mandelbrot, 1977, p 30-32, Plate 32). Because the same technique is not practicable at the scale of faulting, we appeal to less direct methods. Depending on assumptions about the accuracy of map data, our measurements give a similar fractal dimension for the map distribution in Figure 13 (see comparisons in Figure 14, described below).

Figure 14 illustrates one approach to the determination of fractal dimensions for fault-fracture sets. We start by assuming that the data in

Figure 14 near here

Figure 13 hypothetically form a characteristic set, even though they are from different sources, scales and types of fracture systems (both field and laboratory); we later describe a different approach that is confined to the California-scale set in Figure 13 that produces a similar value (see Figure 16). Although the values we find seem to be typical for these kinds of dissected complexity (as will also be demonstrated with a more formal set theory analogous to the dissected "cutout" set called the Cantor set; see Mandelbrot, 1977, p 99), Figure 14 also demonstrates the conditions under which an almost "area-filling" set can occur in plan view, or a "volume-filling" set over a depth interval that is compatibly self-similar.

In Figure 14a, the map data of Figure 13 were measured and portrayed in the same manner as the faulting data in Shaw and others (1981). The segments fall into natural groupings of four or five orders (representing characteristic, if subjectively chosen, ranges of segment lengths) all of which are distributed in the log N vs log L plot around a trend with slope slightly larger than one; Shaw and others (1981, Table 2.2.1.1, p 91) give the regression slope for the Fault Region "California Coast" as -1.28; Figure 13, however, is more extensive and somewhat generalized relative to that determination. Thus, all these data are statistically somewhat similar in terms of a self-consistent distribution of lengths. Figure 14b shows the same suite of data concatenated according to the changes of scale plotted versus the range of characteristic "ruler-lengths", R, used for the measurements at each scale. The resulting regression trend has a slope of about -.25, which is equivalent to a fractal dimension of 1.25 based on the following formula relating map length to changing ruler length, as in the coastline problem:

$$L = \text{Const.} \times R^{(1-D)}, \qquad (6)$$

or

$$\log L = \text{Const.} + (1-D) \log R, \qquad (7)$$

where D is the fractal dimension. Thus the slope in plots such as Figure 14b defines the coefficient (1-D).

The way in which the concatenation was carried out identifies how the fractal dimension would be changed by modifying the assumptions concerning the packing density of fault segments relative to the map data taken at face

value. The cumulative length of fractures was summed for each map scale in Figure 13, and the ratio of that length to the map width was determined at each scale. This ratio was used to multiply the total length of segments at the next smaller map scale (larger fracture system) on the assumption that every larger fracture also implies a suite of smaller fractures that were not mappable at that scale. This procedure was carried through from scale (d) to scale (a) in a sequence of multiplications of the total length of all fractures from the smallest in (d) to the largest in (a). In other words, a network of fracture sets was hypothetically added to (a) on the assumption that all lengths down to the pattern of fractures in (d) are actually present in the vicinities of the major faults, even though the fractures can't be seen at the map scale of (a).

The above procedure defines the values of log L vs log R in Figure 14b (two values are shown based on different assumptions concerning the slope of log N vs. log L). In Figure 14c, on the other hand, the lengths at each scale were multiplied by a factor determined from the ratio of the area at scale (a) in Figure 13 to the areas in each of the other map scales, normalized to the length scale in (a); i.e., the overall area of the California system in km^2 was divided by the areas of each of the smaller fracture systems expressed in units of km^2, and the total lengths were multiplied by that ratio at each scale. In other words, this normalization represents an assumption that the entire area between the major fault systems at scale (a) contains fractures at each of the smaller sizes with a density distribution proportional to the areas. This assumption is equivalent to saying that young fracture systems with lengths of the order 1 km and less are likely to exist at any random location in California, even at large distances from the mapped faults.

The length distribution in Figure 14c represents this maximum packing density model. This is confirmed by the fact that the slope is approximately -1, which gives a fractal dimension of D = 2 according to the previous relation. That is, this dimension implies that the space is essentially "filled" with smaller and smaller fractures as it is examined at higher and higher magnifications. If the same proportionalities held in arbitrary cross section throughout the depth range of hypocenters, the fractal dimension would be nearly volume-filling, or D = 3. The more dendritic, or "fuzzy", distribution conforming to D = 1.25 in Figure 14b, would imply a fractal dimension of about 2.25 if the vertical distribution is similar to the horizontal distribution (see Figure 14e). If, on the other hand, the fractures are restricted in vertical distribution, the overall fractal dimension can be even smaller than 2.

The slope of the number-length distribution in Figure 14a is less steep than the distribution for other Fault Regions in the U. S. Figure 14d indicates the approximate effect of increasing the slope and counts to conform to the equation log N = 2 - 2 log L ; the corresponding fractal dimension would increase to between about 1.4 and 1.5 for the concatenated dendrite model. The densest-packing limit model, however, would remain about 2 because the proportionalities remain the same (the area-filling, and potentially volume-filling, set).

Figure 15 investigates the question of what kind of mathematical set of dissected line lengths might resemble the fractal dimension of fault sets in plan view. The general set theory for dissected lines is described by

Figure 15 near here

Mandelbrot (1977, p 98 ff.) in terms of "cutouts", for which the usually cited example is the Cantor set. In the Cantor set (Figure 15a), the central 1/3 of

the line segment is cut out, then the central third of each smaller segment, and so on. Such dissections are possible in general with any ratio of the "empty" to "solid" segment lengths. The relation between these ratios and the fractal dimension is given by the function:

$$D = \log N / \log (1/r), \qquad (8)$$

where N is the number of "solid" segments in the unit length (2 of 3 in the case of the Cantor set), and r is the ratio of the cutout length to the unit length (1/3 in the Cantor set). Thus, the fractal dimension of the Cantor set is about .6309, in keeping with the "less than linear" character of the progressive sequence of cutouts in producing the set.

Figure 15b investigates the inverse of the Cantor set. We ask the question: is there a simple form of dissection in which the total line length is increased rather than decreased? This is a growth model something like the replication of partial lengths in DNA splicing, in that when the central third is cut out, it is allowed to duplicate and remain part of the set. The general physical argument would be that during the initial growth history (whenever that was) short segments spawned shorter segments while the overall unit length increased. To make the distribution somewhat more fault-like the dashed portions of the growing system would also be preserved. Such a model symbolizes the pristine growth of fractures from the smallest state of incipient microfractures in a previously unfractured material. Fault activation, as envisioned in terms of the fractogram for a previously formed set, however, essentially represents the reverse process, in that sets of smaller to larger existing fault segments are progressively activated according to paths in the fractogram as described earlier (Figure 8). The fractal dimension of the simple "inverse Cantor set" is 1.26, as determined both by the above formula and by the summation of numbers and lengths (Figure 15c); the fractal dimension including inherited lengths, as shown in that same figure, is about 1.47. Thus, the inverse Cantor set is essentially the same sort of fractal object as the systems of measured faults (relative to a maximum topological dimension of 2; it would be 2.26 to 2.47 relative to the limit 3, if there were linear similarity in depth). The direct Cantor set, itself, may describe some systems of highly disperse activations, as discussed later.

One more illustration of spatial fractal dimensions (temporal fractals are considered subsequently) is considered, because it bridges the gap between the viewpoints of discontinuous branching sets (dissected dendrites) and finger-like distributions analogous to stream dendrites and bifurcating modes of continuous fluid flow. Figure 16 compares the results of an experimental demonstration of the fractal dimension of fingering flow in a Hele-Shaw cell with a fractal dimension for the system of California faults, treated as though the faults represent the ghost traces of stream beds in an old river system (e.g., like an ancestral Mississippi). The method of analysis is

Figure 16 near here

highly subjective in terms of the ways in which ends of faults might be linked together to outline the overall "basin" of influence, but the generally elongated irregularity is preserved by a variety of delineations. The fractal dimension for the viscous fingers in Figure 16a is about 1.38, and for the fault system, using the same procedure, it is roughly 1.4. Qualitatively, it can be seen that the fingering mode of description tends to increase the fractal dimension for the same regional aspect ratio, relative to that of

dissected branch sets, because it encloses more area (i.e., it represents a packing distribution somewhere between the concatenated and area-filling modes of Figure 14). These various modes of description, however, are consistent with the variety of branching distributions described by Shaw and others (1981), and by Shaw and Gartner (1984), for different Faulting Regions of the U. S.

Trends in the Fractogram and Fractal Distributions of Energy Potentials.

Aki (1981) pointed out that concepts of fractal geometry should be useful in interpretations of frequency-magnitude data. Smalley and others (1985) and Turcotte and others (1985) have also applied the fractal concept to the discussion of asperity models of failure on a fault surface. We will now attempt to reconcile the interpretation of fractal dimensions with paths in the fractogram and with the above viewpoints concerning fault failure. Using the relation given previously for numbers vs segment lengths of dissected sets (Eq. 8), $D = \log N / \log (1/r)$, and the fact that the seismic moment is generally defined in terms of a volume of rock with topological dimension 3 (i.e., M_o proportional to the product $L_{sz} \times W_{sz} \times d_{sz}$, where the subscripts refer to a seismic zone of prescribed volume), Aki (1981) showed that the fractal dimension is related to slopes in frequency-magnitude plots (the b-value of earlier diagrams) and moment-magnitude plots (the c-value, where a constant value of 1.5, as in Eq. 3, has been assumed in the comparisons of fractograms with the models of Wesnousky and others, 1983). According to the ratio derived by Aki (1981), $D = 3 (b/c)$. Therefore, we can compare such determinations of fractal dimensions with the measurements of the preceding section, and with the earlier discussions of slopes in the fractogram.

Aki's generalization essentially reflects the fact that characteristic trends in the fractogram define fractally self-similar sets of relations among fault segment lengths, numbers, magnitudes, moments (and strain energies), and time. Time adds to the dimensionality, but we initially restrict the discussion to a maximum spatial topological dimension of 3; later we explore time as an additional fractal dimension. Evidently, the traditional frequency-magnitude scaling laws, from their inception, have represented a documentation of fractal geometries (many examples of fractal geometry exist in the literature, such as the measurements of coastline lengths mentioned earlier, prior to the development of a systematic nomenclature by Mandelbrot, 1975, 1977, 1982).

Aki (1981) founded his reasoning on the general idea of fractal asperity models of a fault surface, and on the numbers of ways the fault length is subdivided. Thus, there is a strong resemblance between his model and that of the fractogram, except that we have generalized the distributions of segment lengths to sets of branching distributions consisting of a hierarchy of number/length orders. Fractal dimensions based on the relation $D = 3b/c$ essentially represent tests of internal consistency of the earlier parameters. That is to say, the direct estimates of fractal dimensions, and the various slope regimes of log N vs log L, can be compared with the values based on the idealized proportionalities calculated using Aki's method.

Figure 17a illustrates the ranges of slopes and fractal dimensions based on the data of this paper and the c-value consistent with the construction of the fractogram ($c = 1.5$, as in Eq. 3). This is the value usually cited

Figure 17 near here

in the literature, but Hanks and Boore (1984) have given arguments in favor of nonlinearly varying c-values in their development of a modified scale of moment-generated magnitudes: simplistically, below about M = 3 on their scale (their Figure 2) the slope is in the vicinity of $c = 1$, increasing to a value of about $c = 3$ at the highest recorded magnitudes. The value $c = 1.5$ seems to be a reasonable average for intermediate to moderately large earthquakes. For the sake of direct comparisons with Wesnousky and others (1983), and other sources of earthquake data, we have not modified our earlier correlations to

take these variations into account, which should be done for comparisons of our results with the highest possible magnitudes, interpreted according to the Hanks-Boore correlations.

If we allow c-values to vary, it would appear that c-value regimes might represent progressively changing types of fractal geometries of fault activations. Using the relation D = 3b/c, some characteristic limits can be delineated depending on what information is considered primary. For example, if we were to limit D to the topological maximum of 3, then b = c, meaning that the frequency-magnitude relations would plot near the steepest limb of Figure 17a for a c-value of about 1.5 (Note: The DELX = X convention of Figure 6b has a steepest b-value of about 1.7, giving D = 3.4 for c = 1.5; since this exceeds the topological limit, this convention would be allowed only if the larger lengths and magnitudes also have larger c-values according to the Hanks-Boore relations. Such an interpretation is consistent with our remarks about the respective ranges of validity of the Constant Increment and DELX = X conventions of Figures 4 and 5). If c = 3 for the largest earthquakes, however, then b = 3 for D = 3. Hence, the conditions under which fault activations can be volume-filling are more complicated than is indicated by our linearized fractograms.

As discussed earlier, a broad and steeply oriented fractogram is consistent with a steep slope in the log N vs. log L relation (e.g., compare Table 1, Figures 6a and 6b, and Figure 14). Such fractograms represent a fractal space in which the distributions of earthquake faults could fill the topological volume of the seismic zone along the trends of constant Buildup Time, BT; i.e., depending on the modes of activation as outlined in Figure 8. Slopes in plots of log N vs log L for all Fault Regions in the U. S. (from Shaw and others, 1981, Table 2.2.1-1, p 91) range from about -1 to -2.5 for the raw data based on constant linear increments. The upper limit resembles Figure 6b, but the lower limit resembles the relation illustrated in Figure 14, log N = 1 - log L. As we will show, this lower limit constitutes a degenerate condition in which the fractogram is of minimum slope and virtually zero width. It is also the condition for which the fault activations would be least volume-filling in the linearized models, other things being equal.

Stated another way, if b = 1.5 were assumed to be an effective upper limit for the composite data of faulting and earthquakes in the U. S. and Japan, as in Figures 6a and 7a, then the range of c-values for D = 3 would reduce to the invariant value c = 1.5. While this is self-consistent with our analysis, it disagrees with the magnitude limits implied by the analysis of Hanks and Boore (1984). To be consistent with both analyses, the earlier fractographic models would apply only to the intermediate magnitudes, where the value c = 1.5 is approximately satisfied. This might suggest that volume-filling fractal modes would be consistent only with the small to intermediate range of magnitudes (i.e., larger magnitudes would imply either smaller fractal dimensions, or larger b-values). A list of fractal dimensions for three different c-value regimes is shown in Table 2.

Table 2 near here

Table 2 summarizes many of the conclusions we have already drawn from earlier discussions. In general, the fractal dimension increases with increasing b-value (and implicitly with absolute value of slope in log N vs log L). Volume-filling fractal modes are most likely for suites of small to intermediate earthquakes in systems of strongly varying numbers of fault-length segments. The largest earthquakes have fractal dimensions near D = 1.2 $\pm$ .3 for the typical ranges of b-values we have discussed, in keeping

with the various kinds of direct measurements we have shown for branching geometries. These values of D also resemble those of inverse Cantor sets (Figure 15b), implying that earthquake faults with lower bifurcation numbers are more like linear fractal objects rather than topologically continuous planes. In some cases, the limiting form of the fractogram, as shown in Figure 17b for the distribution log N = 1 - log L, collapses to a line (parallelogram with zero width). This implies that all activations would correspond to fractally "planar" to "less-than-linear" sets for the entire range of small to large earthquakes (top row of numbers in Table 2), unless the fractogram becomes nonlinear and b-values are considerably larger than those we have shown based on seismic data. The fact that the California system of faults, as sketched in Figure 13, approximates such a number-length distribution suggests that the largest earthquake events for very long strike-slip faults, under these assumptions, might be fractally "less-than-linear", chainlike Cantor sets (see Figure 15a), even in three dimensions (see Wesnousky and others, 1983).

This, possibly surprising, conclusion is qualitatively consistent with earlier discussions of the problems of reconciling the various scales of partial activations in California. That is, the system behaves in a generally coordinated manner but with a piecemeal distribution of activations over the ranges of potential values of the composite fractogram which tend to be "condensed" along a single trend parallel to the base of the fractogram. Thus, event sequences for the larger number/length orders (large N, small L) are collapsed onto the same frequency-magnitude trend as the hypothetical single-valued trend (N = 1, L greater than 100 km). In a sense, this agrees with the suggestion of Wesnousky and others (1983) that long faults might be viewed as a linear system of distinctly different chain-like fault segments each with a characteristic set of maximum moment events. The implication of the collapsed trend in Figure 17b, however, differs from this interpretation in a rather subtle way, in that characteristic suborders of distinct number-length activations, for both the partial and SATURATION modes, occupy specific intervals of the trend (e.g., the open circles in Figure 17b represent the left-hand side of the collapsed parallelogram at the shortest Buildup Times, and the solid circles represent the range of SATURATION values). The so-called "locked" and "unlocked" portions of the San Andreas system portrayed in Figure 11 would represent this "collapsing" of the different number/length orders of the same systematic distribution onto the same frequency-magnitude trend. The branching distribution of faults, however, is still distributed, geographically and in depth, rather than being restricted to a single chain-like topology having segments with differing mechanical properties (Note: This is the distinction between Euclidean and fractal objects that is central to interpretations of natural fabrics; e.g., the Euclidean dimension 1 implies a continuously connected linear object, whereas D = 1 implies a complex fabric that may be highly discontinuous and distributed within planar or volumetric Euclidean domains). Therefore, the buildup to large events (and interpretations of seismic gaps, etc.) might be evaluated in the same way as in the more general fractograms, by identifying the distributions of segment lengths with specific intervals along the trend. This differs from other interpretations in the implication that different portions of the system may appear to be locked or unlocked depending on the sequencing of activations in a seismic cycle much longer than the historic record, meaning that characteristic fractal subsets of earthquake events are rather "scattered" within large domains of topological volume.

Figure 17c schematically indicates how the fractogram would be modified to incorporate large c-values for the limits of large magnitudes according to the

analysis of Hanks and Boore (1984). Ignoring the low-magnitude end, the essential effect at high magnitudes is to nonlinearly distort and foreshorten the "parallelogram" and therefore to progressively increase the b-values, both along the curves at constant N and constant BT. If this modification is carried to the extreme where both b = 3 and c = 3, then everything converges to an invariant fractal condition where the ultimate event also can be volume-filling (lower right entry in Table 2). Now, however, there is "nowhere to go" at lower orders of larger faults. If the moment-magnitude relation derived by Hanks and Boore (1984) is valid, then two simple alternatives suggest themselves: (1) this condition may in fact reflect the convergence to the absolutely "ultimate" earthquake, barring global changes to an entirely different tectonic regime, or (2) it represents a growth transition where an entirely new first order fault is generated so that the fractogram essentially shifts to lower frequencies for the new fault, and larger numbers of higher order faults also grow according to some general reshuffle of the number/length hierarchy (so that the same value of moment is redistributed). The second alternative violates the steady-state assumption, however, upon which the construction is based (see caption of Figure 8) and implies a general increase of fault length with time (see discussion of total fault lengths vs. age in Shaw and others, 1981). Another slant on the possibility for globally invariant fractal conditions is given by including time as a dimension.

Figure 18 attempts to generalize the fractal viewpoint according to the various assumptions about slopes, topological limits, magnitude limits, and time. Figure 18a shows loci of constant fractal dimension plotted against the

Figure 18 near here

coordinates b and c, restricting the range to the topological limit 3 corresponding to Aki's (1981) derivation for length-moment-magnitude scaling (time is considered separately in 18b). The zigzag path of frquency-magnitude data for Japan shown in Figure 7 is mimiced in this plot in terms of either the constant or variable c assumptions. For constant c, the path traced from smaller to larger magnitudes alternates between b-values of about .8 and 1.4. In this mode the fractal dimension correspondingly alternates between about D = 1.6 (lower b-value) and D = 2.8 (higher b-value). This means that when a trend of fault activations (as in Figure 8) jumps from a higher to lower length/number order (i.e., from shorter more numerous to longer less numerous maximum segment lengths) it transiently passes through a regime of maximum fractal dimension nearly equal to the volumetric limit of the topological dimension. Another way of looking at such sequences is to imagine that each fractal object represents a sampling of log N vs log L in the general distribution that satisfies the proportionality D = 3b/c. Sometimes the sampling is fractally tenuous, and at other times it is fractally dense.

That is to say, the progression toward larger, less frequent earthquakes is accompanied by intervals of activity during which faulting and earthquakes are volumetrically disperse before they again focus down to fractally planar to linear distributions. This sort of behavior is somewhat like that described by Mogi (1981). The same general alternation also exists if c-values are allowed to increase to the vicinity of 3 at the highest magnitudes (the nonlinearity of Figure 17c is indicated schematically by the converging dotted boundaries). In this case, however, each zigzag step in the progression toward higher magnitudes is accompanied by a net drift, or sequence of transitions, toward lower fractal dimensions of both the most distributed and most focussed fractal sets (Note: In the dotted trend, this is

offset by the convergence toward the invariant condition of the "Ultimate Event", where the fractal dimension is again maximized). Such alternations appear to fit some of the characteristics of seismic cycles. In these terms, the locked and unlocked portions of the San Andreas fault, and the evidence of disperse to focussed distributions of earthquakes in the partial cycle documented in Northern California (Ellsworth and others, 1981; Kerr, 1984; Wesson and Wallace, 1985), may represent stages of the fractal transitions in the overall cycle. Such a sequence was described earlier in terms of paths in the fractogram (e.g., Figures 8 and 11).

Recognizing that the frequency-magnitude diagram explicitly involves time as a dimension, we can also enquire if there is a fractal scale with a maximum topological dimension of 4 that permits additional generalization of the above observations. This idea is tentatively explored in Figure 18b. In this diagram, we have used the fractogram in Figure 17a, with c = 1.5, to plot the corresponding values of Buildup Times, BT, against the respective ranges of log 1/f (general recurrence times for a given magnitude). We arbitrarily define the dimension D_{MT} as the temporal fractal determined by the slopes in Figure 18b, exactly as we did for spatial fractals in Figure 14. Permissable ranges of values are explored in terms of slopes representing various linear paths in the fractogram; the Inset shows line sets and a schematic path analogous to the zigzag trends of Figures 7, 8, and 18a. Orientation in terms of magnitudes (according to the linear models) is indicated by the large filled circles and numbers; nonlinear modifications, as in Figure 17c, will decrease the magnitude values, but the slope relations in the time plot remain the same. A path at constant fault-segment number, N, has a slope of +1 (= 1 - D_{MT}), defining D_{MT} = 0. At constant Buildup Time, BT, the slope is zero, and D_{MT} = 1.

The consistency of these determinations with the previous spatial definitions and measurements is partially tested by the line of constant magnitude, M = 4.3. If we limit the maximum topological dimension to 4, given by the heavy dashed line, then the fractal sum (D + D_{MT}) can not exceed 4. At M = 4.3, D_{MT} = 2.3, so the consistent spatial fractal does not exceed D = 1.7. This is in agreement with the pairs b = .8, c = 1.4, and b = 1.4, c = 2.5, which also agree with the ranges in Figure 18a and Table 2, depending on where the line of constant magnitude is drawn (M = 4.3 is consistent with the first pair). The fact that there is no requirement that (D + D_{MT}) = 4, means that such a path is not necessarily a globally self-similar set (i.e., in the spatial fractogram, lines of constant magnitude typically would intersect a range of fractal sets defined by combinations of the limiting slopes). Temporally, however, lines of constant magnitude represent fractal self-similarity, by definition, in that D_{MT} is constant.

The bewildering array of dimensions and potential fractal objects in 4 dimensions can be given some perspective by considering possible physical meanings of the extreme cases D_{MT} = 4, and D_{MT} = 0. In the former case, D = 0, so the temporal fractal correlates with a spatial distribution of isolated point sources. That is to say, this object is a spatial fractal dust, which, like the twinkling of stars, has a maximum number of degrees of freedom in time (to be precise in such a description, however, time variables in addition to BT and 1/f would be needed; examples might include duration of slip, longevity of aftershock sequences, etc.). For D_{MT} = 0, on the other hand, events occur at "points" in time, but they have the maximum possible spatial degrees of freedom. There is little wonder that earthquake prediction has proven to be so recalcitrant. Given perfect control on spatial distributions of point sources, the temporal distribution is unpredictable in terms of the variety of time variables needed to describe the behavior. Given

perfect temporal control, the spatial distribution is unpredictable. This appears to be a macroscopic uncertainty principle directly analogous to the Heisenberg Uncertainty principle of particle physics.

The obvious way around this dilemma is a variant of the techniques already being used in seismic studies. Prediction depends on an ability to develop criteria of complex pattern recognition. In this regard, however, methods of fractal classifications, using graphical constructions such as the fractogram, offer new methods of pattern descrimination. If specific sequences, in the sense of characteristic seismic cycles, can be generically recognized, their relations to the extremes of indeterminism may become quantitatively recognizable. A fractal classification analogous to the taxonomic classifications of complex biologic forms may prove useful in making categorical forecasts of navigational locations in seismic space.

It was noticed in the above discussion that many of the paths illustrated in terms of varying b-values and c-values apparently are not fractally self-similar in that they trace out paths of varying D. In view of the added time dimension, however, this is not necessarily the case relative to a maximum topological dimension of 4. That is, both D and D_{MT} can vary while their sum ($D + D_{MT}$) could be a constant equal to or less than 4. Such an object would be self-similar relative to both spatiotemporal and energetic variations of earthquake dynamics. Although we do not have explicit sets of coordinated data to test this idea graphically, it seems to be indicated by the suggestions of seismic cycles characterized by the inverse behaviors of D and D_{MT} described above. If this fractal approach were to prove valid, it could for the first time provide a general framework within which to generate and graphically illustrate forecasts that encompass the entire spectrum of potential faulting and earthquake events at any scale of choice.

Some Implications of the Fractograhic Approach to the Dynamics of Faulting and Earthquakes.

It remains to make a connection between the fractogram and the dynamics of faulting. This is attempted with the help of Figure 19 and a generalized example of the relation between length activation as used so far and actual values of fault slip during earthquake events. A priori, there is no relation

Figure 19 near here

between rupture length rate, RLR, as employed here, and strain rates. Thus, it would not appear to be possible to relate the fractogram directly to stress magnitudes estimated from assumptions about plate motions, etc. Sykes and Quittmeyer (1981), however, give a variety of data relating slip lengths, u, to fault lengths, L, for large earthquakes. For purposes of illustration, we use the simple proportionality $\log u = 10^{-5} \log L$ (1 m slip during a 100 km fault activation event), which they give for strike-slip faults (their Figure 3). Thus, an average slip rate, v, corresponding to a given rupture length rate is approximately $v = 10^{-5}$ RLR. For example, in Table 1 for N = 1, with a fraction of .032 times the total assumed value of RLR for the entire system of branching faults, the inferred slip rate is v = .32 cm/yr or 64 cm in 200 years. The corresponding fault length is 64 km of partial segment length activated in 200 years (magnitude about 7 for the scaling in Table 1). The consistent slip rates agree with the scaling of activation lengths and buildup times, implying that the distribution of cumulative slip is distributed in a manner proportional to the branching distribution. That is, most of the slip occurs on the shorter more numerous fault segments. Using a value of totalstrain of the order 10 cm/yr across the width of the California system in Figure 13 (see Savage 1983, Figure 5), the average strain rate is about 3×10^{-14} sec^{-1}. Thus, these values represent a set of properties dynamically consistent with Plate Tectonics and with the general scale relations of the fractogram.

If we were to view earthquake events as representing a homogeneous flux of strain energy across a seismic zone of prescribed volume and fractal dimension 3, then one would expect there to be a characteristic relationship between shear rate and shear stress that is the same for all sets. This would be analogous to an aseismic continuum flow with some form of rheological "law" (e.g., a power law rheology is often assumed for solid state creeping flow). On the other hand, when the fractal dimension is less than 3, and particularly when it is less than 2, the "flow" is both discontinuous and intermittent. We will attempt to illustrate two extremes of corresponding stress states with the help of a general "plate-scale" stress model similar to that described by Hanks (1977). The essential feature of the model for our purpose is that the sources of crustal stress regimes emanate from the overall tractive balances between the lithosphere and deeper mantle motions. Simplistically, what Hanks (1977) calls the "basal shear stress" represents the areally averaged tractive force couple. Although this stress may be only tens of bars, it is distributed over very large areas. Therefore, if the net work done by the integrated stress is transmitted through the more rigid portions of the crust to zones along plate boundaries, and other regions of finite shear, there is a great focussing or multiplier effect (analogous to the multiplier effects in hydraulic lifts and piston-cylinder pressure devices). Accordingly, local shear stresses across fault zones are potentially much higher than the basal stress.

Figure 19 summarizes the limiting cases of an isolated slip event on a single fault segment in a fault zone of low fractal dimension (a), and

multiple steady-state events in a densely distributed system with fractal dimension near 3 (b). In Figure 19a there are a variety of choices for the dynamic relationships within and across the fault zone. For example, if motion is represernted only by slip on fracture surfaces, then the shear rate depends on the domain of description (the same general situation would apply relative to subtraction of a uniform background creep rate). At the position of section A there is a well-defined shear rate across the local fault zone given by $(du/dt)/w_{fz}$. At position B, however, there is apparently no displacement anywhere within the zone so that $v_{fz}/w_{fz} = 0$, in general. But, if we consider a topological area or volume domain there is some average displacement of one side of the overall zone width relative to the other, which has a magnitude given by the illustrated displacement and displacement rate normalized by the time of observation and the domain size. The shear rate v_{fz}/w_{fz} obviously is large relative to the normalized shear rate v_{avg}/w_{mz} (where the subscript mz refers to "megazone", or plate boundary domains), thus the stress regime also depends on some sort of assumption or measurement that depends on dimensional arguments.

If the shear stress is assumed to be constant (as it might be in an experimental deformation), the local dissipation of work energy is very large compared to the average. If the stress is assumed to be proportional to the shear rate, then the local value is also very large compared to the average. On the other hand, if the dissipation rate given by the product of shear stress and shear rate is assumed to be constant, then the local value of shear stress is very small compared to the average. Since the latter condition comes closest to describing the ambient situation over long times and larger fractal dimensions (i.e., the steady-state continuum limit for a given regime of basal stress and plate motion), it is an appropriate reference for stress states. By this view, the larger the isolated faulting event (notably, excepting the "Ultimate Event" of Figures 17c and 18a, as discussed in the preceding section) the smaller is its "fractal" stress relative to the average state for that general tectonic region (because of the concomitant reduction in D). To some extent, the associated stress drop per event may also tend to decrease, also because of the focussing effect; i.e., the smallest events closest to the ambient stress condition asymptotically approach zero stress drop with vanishing segment and slip lengths. Down to a certain size, however, stress drops may be nearly constant. (Note: An analogy is the potential difference for flooding in a river system with a fixed levee height, relative to the mean flood-plane datum; the difference is nearly the same for large and small events as long as flooding does not inundate the entire region and back up to a hydrostatic level equal to the levee height. When the flooding potential is nearly continuous, however, the latter condition is approached, and the potential difference for individual episodes decreases asymptotically to zero.)

The purpose of this excercise is to comment on the fractal analogies between energy transfer processes in fault dendrites relative to those processes in other branching systems, such as stream dendrites. Both reflect a network that collects energy from topologically large areas and volumes involving large numbers of small dendrites of various characteristic fractal dimensions, and transports that energy to the larger dendrites (usually within the same fractal network, but sometimes also to contiguous networks with different fractal dimensions). In stream systems this represents nearly the total energy transport. In fault systems, on the other hand, only a small fraction of the total energy is transferred to the largest segments for the distributions considered, except in systems where the slope of log N vs log L has an absolute value less than unity (i.e., where the length fraction, X, of

Table 1 is largest for small N, large L), and the fractal dimension is also large. However, judging from the discussions of self-similarity, and the fractal arrays of Table 2 and Figure 18a, such a distribution would be "unnatural" (if it existed, the stress ratio could be constant for faults of different lengths; again, the "Ultimate Event" represents an unusual state where behavior "in-the-large" can fractally resemble the behavior of small-scale distributed events). The analogy between strain energy and hydraulic energy distributions is closer for events of flooding in a river system with a constant long-term average discharge. Once a critical level is exceeded, a large local overflow can occur (large fault activation event), although it is a small part of the total energy transport (i.e., it is well-known that the total work rate of tectonics greatly exceeds the overall rate of seismic energy release). The "Ultimate Event" state in the hydraulic analogy would represent the condition of such wholesale flooding that the flow behavior of the mega-event would return to a distributed mode more akin to the localized description of the original flow field. In the seismic case, it must represent a limit where the scale of fault activation and slip is so large that the motion necessarily would have to engage the entire volumetric scale of Plate Tectonics. In such a limit, either tectonically or hydraulically, the scale of the event itself implies a potentially major reorganization of the system geometries (new and/or redefined fault systems, and/or activation distributions; new and/or redefined river channels, and/or levee regimes)

The above commentary seems consistent with some aspects of discussions of elastic field energy. There is, however, a seeming ambiguity or paradox in different interpretations of the energy sources for small vis a vis large earthquake events. The situation is stated succinctly by Andrews (1978, p 2263), as follows:

> Where does the energy for small earthquakes come from?
> One possible answer is that fault creep, varying in amplitude at all length scales, prepares the fault for small earthquakes. A second possible answer, applicable to a purely brittle seismogenic region, is that larger earthquakes provide energy for smaller earthquakes.

Although Andrews appears to favor the latter possibility based on the analysis of single events, likening it to the energy cascade from larger to smaller scales in fluid turbulence, there would seem to be a need for both types of phenomena. That is to say, there is abundant experimental evidence that the evolution of large failure events is preceded by the hierarchical growth and/or activation of systems of small fractures during progressive deformation imposed at the boundaries of the system (Tchalenko, 1968; Kitagawa and Suzuki, 1975). It also seems evident that large events are sources of strain energy redistribution (in particular, the "Ultimate Event" condition of Figures 17c and 18a). The former regime would appear to derive from the heterogeneities of rheological behaviors related to fractal nonlinearities of the sorts described above. Using the same fluid dynamical analogy, the growth of fluid turbulence also involves an energetic buildup, relative to static and/or laminar modes, wherein there is a dissipative input of vorticity originating from boundary tractions (or other forms of energetic coupling, such as from thermal sources). The cyclic buildups and cascades of dissipative vortical modes resemble the seismic cycles described in the present paper in terms of cyclical paths in the fractogram.

Fractal Concepts and Practical Problems of Earthquake Prediction.

Our view of the dynamics of branching systems of faults has some resemblance to the fractal asperity model of Smalley and others (1985). Their model, however, refers to the distribution of stresses within a fault plane, while our interpretation implies an energy cascade from the smaller to larger segments of a fractally distributed set of fault segments. The implication of our model is that the stress distributions and failure conditions for the smaller sets of distributed fault activations provides an information base for the interpretation of larger events on the more major fault segments (within a given context of fractal dimensions and self-similarity). In this regard there is some parallel with strategies of stream gauging in which information on discharge rates for tributaries is used to forecast potential flood conditions.

These inferences seem consistent with the ideas of seismic cycles in Japan where precursive events occur over large diffuse regions and converge toward the loci of major earthquakes (see Mogi, 1981, Figure 11). The picture of partial seismic cycles in Northern California given by Ellsworth and others (1981) seems to be consistent with the conclusions of this paper (cf., Kerr, 1985; Wesson and Wallace, 1985). The interest of earthquake forecasting would seem to be served by placing even more effort into the documentation of the smaller to intermediate events and fault segments with emphasis on deriving information concerning the domains of coordinated fractal sets; in particular, comparisons of fractal regimes between the vicinities of the so-called locked and unlocked portions of the largest fault systems should be revealing. If characteristic fractal sets within space-time domains with topological limit 4 can be quantified, the earthquake process and the problems of forecasting may have a general solution.

This possibility is put into some perspective by simultaneously viewing combinations of graphical data as navigational aids to the interpretation of seismic patterns. For example, in combination, map patterns (Figure 13), fractal sets in fractograms (Figure 17), fractal sets in b-c space (Figure 18a), and fractal sets in BT-1/f space (Figure 18b) offer an almost complete characterization of the earthquake process (in addition to the derived dynamic information concerning stress and strain states). Alternatively, Figure 18 might be generalized in terms of a 3-dimensional stereographic projection. In a sense, such a diagram would be an analog of a fractal compass and clock. This analogy is not so fanciful, in that Figure 18a gives directions in fractal space, and Figure 18b identifies temporal sequences. In fact, Figure 18b is almost literally a relativistic seimological clock, in that D_{MT} increases in the clockwise direction, while D tends to increase in the counterclokwise direction (although D may have a variety of synchronizations relative to D_{MT}); at the same time (i.e., either at constant BT, or constant 1/f) earthquake magnitudes increase from left to right and from bottom to top.

The term "relativistic" is used in reference to the macroscopic uncertainty principle mentioned in the discussion of temporal fractal dimensions. There is a close parallel here with the problems of predicting trajectories in particle physics, in the sense that, there, the documentation has to choose between specifications of position and momentum (velocity, time, etc.); the Heisenberg Uncertainty Principle states that these parameters (which are analogous to seismic hypocentral location and frequency-magnitude location, where time is meant in the sense of Figure 18b) can not both be determined uniquely at a given "point" in both time and space. In the equivalent seismological quantum dynamics, this principle would suggest that we can not expect to simultaneously predict locations in space and locations in time, except with regard to the similarly analogous approach to

pattern-predictions of alternative futures. That is to say, predictions in both time and space can be made on the basis of the suggested methods of "fractal navigation", but we can't expect them, if the analogy is correct, to "coincide", in the sense of an ability to ever specify both the absolute location and absolute time of an event of given energy.. In a practical sense, this would apparently mean, on the one hand, that it would be possible to predict a spatial fractal sequence without being able to say when any specific point in that sequence would be sampled. And, on the other hand, it would simultaneously be possible to predict a temporal fractal sequence without being able to say exactly where the hypocenter would be located (in combination, the predictive problem would be parallel to predicting particle trajectories in 4-dimensional spacetime).

This interpretation, of course, refers to global predictions in the sense of Figure 18, and the generalized sequences in a fractogram. Prediction in the localized sense is still applicable as it is currently being practiced; i.e., massive information on the behavioral traits of a specific geometrical domain eventually allows pattern recognition with some confidence (a particle physicist who has spent a lot of time studying familiar reactions in a cloud chamber also can say with some confidence what kinds of sequences are likely to appear within given locations and time frames). As was the case in particle quantum dynamics, however, discovery of principles of uncertainty, paradoxically, adds to an entirely new ability for prediction. Before the principle was recognized, many physical phenomena were totally mystifying (zero predictive ability on any terms). Since its advent, entire realms of dynamical regimes previously unknown have been elucidated, from the scales of subatomic particles to the scales of cosmological interactions and force fields. It is hardly surprising, therefore, that these disciplines have in common the same concepts of fractal geometry and scale invariance as a fundamental tool for description and prediction.

Summary.

The maximum moment model of Wesnousky and others (1983) implies that a fault is activated over its total mappable rupture length which is correlative with an earthquake of characteristic maximum magnitude and recurrence time for that length. By comparison, Shaw and others (1981) and Shaw and Gartner (1981) showed that, in general, many possible combinations exist for partitioning of slip among subsets of individual faults of characteristic lengths in a genetically coeval branching system of faults with a hierarchy of lengths spanning many orders of magnitude. This general relation is described in terms of a nomogram they called a paleoseismic parallelogram, which is renamed here a paleoseismic fractogram; the fractogram outlines possible combinations of segment lengths, numbers of segments, and their corresponding recurrence times relative to coordinates of frequency and magnitude. Two types of end-member models on this diagram are arbitrarily defined in terms of: (1) parallel lines of constant Buildup Times which are associated with a characteristic subset of partial to total segment lengths, within a specified range of fault activation rates (segments which, in aggregate, are simultaneously compatible with that buildup time and with a specified overall rate of length activation called the Rupture Length Rate, RLR; this rate refers to the cumulative summation of fault length that can be activated in a specified system of faults, and not to the slip diplacements during earthquakes), and (2) parallel lines of constant branch-length number, N, called Orders, each of which is associated with a constant, but generally different, value of RLR that is characteristic of the branching order (i.e., Order refers to the set of fault branches associated with a given average length, depending on how a hierarchy of lengths is defined).

These models represent an idealized system of fault branches in which the numbers of segments of a given average length decrease in some proportion to increasing segment length; the proportionality used was chosen from a range of values determined statistically by Shaw and others (1981). According to a statistical counting of measured fault lengths of different ages, the value of RLR increases with the degree of segmentation; this is because the proportioning of lengths increases at the shorter lengths, and in the steady state this means that the rupture lengths are similarly proportioned for a given overall rate of strain (implicitly, volumetric as well as areal). Frequency-magnitude data for a well-documented 400-yr history of earthquake and faulting actvity in Japan, as given by Wesnousky and others (1983), plot as a zigzag trend that approximately bisects the acute angle between the above two end-member models; the trend alternates between intervals roughly parallel to one or the other end-member relation. Interpreted in terms of the maximum moment model, this pattern suggests that each branch-length order defines a characteristic maximum earthquake and recurrence time each of which increases at the next lower order (longer fault branches of fewer number) according to a stepwise hierarchy: activation of a given length-set engages more and more segment-length per event, with a corresponding increase in Buildup Time, until that set reaches a limit; activity is then expressed in terms of a shift, at constant Buildup Time, to a longer set containing fewer segments. In each step, the maximum earthquake increases but the frequency decreases relative to what it would have been if the shorter branch sets had not reached saturation at a characteristic maximum moment. Different portions of this sequence may evolve in systematic progressions or in more haphazard patterns of partial event sequences with mixed chronologies. This general pattern appears to describe paleoseismic data in the U. S., although the resolution is not adequate to identify step-like intervals at the scale of fault regions documented in Shaw and others (1981). Comparisons of paleoseismic fractograms

for these faulting regions with frequency-magnitude data for the seismic regions of Algermissen and Perkins (1976) reveals mismatches which suggest the existence of unrecognized active fault systems. Recent discoveries of sand-blows and other evidence of faulting events in the midwest and southeast (Kerr, 1985; Obermeier and others, 1985) are consistent with generalized predictions of unrecognized young fault activity made by Shaw and others (1981).

Although the fractogram provides a convenient form of description that can be used as an independent method of geometrical construction, it is shown to be equivalent to descriptions based on concepts of fractal geometry. Fractally self-similar sets imply special paths in the fractogram. Observed paths imply changing fractal dimensions during the seismic cycle when it is described in terms of a maximum topological dimension of 3. Expansion to 4 dimensions (including time) suggests that fractal variability in space may become fractally invariant or self-similar in spatiotemporal dimensions. If so, the faulting and earthquake process is, in principle, universally describable in terms of a common system of geometrodynamics. Data are given to illustrate how the fractal dimensions of fault systems can be measured, how they relate to dynamical conditions of tectonic stress and strain states, and how they can be applied to problems of prediction, with special reference to fault patterns in California.

References Cited

Aki, Keiiti, 1981, A probabilistic synthesis of precursory phenomena: in D.W. Simpson and P.G. Richards, eds. Earthquake Predictions Washington D. C., American Geophysical Union, p. 566-574.

Algermissen, S.T., 1969, Seismic risk studies in the United States: World Conference on Earthquake Engineering, 4th, Chilean Association for Seismology and Earthquake Engineering, Santiago, Chile, Proceedings, v. 1, p. 1-10.

Algermissen S.T. and Perkins, D. M., 1976, A probabilistic estimate of maximum acceleration in rock in the contiguous United States: U. S. Geological Survey Open-File Report 76-416, p. 1-45.

Algermissen, S.T., Perkins, D. M., Thenhaus, P. C., Hanson, S. L. and Bender, B. L., 1982, Probabilistic estimates of maximum acceleration and velocity in rock in the contiguous United States: U. S. Geological Survey, Open-File Report 82-1033, p. 1-99.

Allen, C.R., 1968, The tectonic environments of seismically active and inactive areas along the San Andreas fault system: in Proceedings of Conference on Geologic Problems of San Andreas fault system, Stanford, CA, Stanford University Press, p. 70-82.

Andrews, D.J., 1978, Coupling of energy between tectonic processes and earthquakes: Journal Geophysical Research, v. 83, p. 2259-2264.

Ellsworth, W.L., Lindh, A.G., Prescott, W.H., and Herd, D.G., 1981, The 1906 San Francisco earthquake and the seismic cycle: in D. W. Simpson and P. G. Richards, eds. Earthquake Prediction, Washington D. C., American Geophysical Union, p. 126-140.

Gutenberg, B. and Richter, C.F., 1944, Frequency of earthquakes in California: Bulletin Seismological Society of America, v. 34, p. 185-188.

Hanks, T.C., 1977, Earthquake stress drops, ambient stresses and stresses that drive plate motions: Pageoph., v. 115, p. 441-458.

Hanks, T.C. and Kanamori, H., 1979, A moment magnitude scale: Journal of Geophysical Research, v. 84, p. 2348-2350.

Hanks, T.C. and Boore, D.M., 1984, Moment-magnitude relations in theory and practice: Journal of Geophysical Research, v. 89, p. 6229-6235.

Howard, K.A., Aaron, J.M., Brabb, E.E., Brock, M.R., and others, 1978, Preliminary map of young faults in the United States as a guide to possible fault activity: U. S. Geological Survey, Miscellaneous Field Studies Map MF-916.

Ishimoto, M. and Iida, K., 1939, Observations sur les seism enregistre par le microseismograph construite dernierment (I): Bulletin Earthquake Research Institute, University Tokyo, v. 17, p. 443-478.

Kerr, R.A, 1984, An encouraging long-term quake "forecast": Science, v. 225, p. 300-301.

Kerr, R.A., 1985, Unexpected young fault found in Oklahoma: Science, v. 227, p. 1187-1188.

Kitigawa ,H. and Suzuki, I., 1975, Reliability approaches in fracture mechanics,: in A. M. Freudenthal (ed.) Reliability Approaches in Structural Engineering, Tokyo, Maruzen, p. 217-233.

Mandelbrot, B.B., 1975, Les Objets Fractals: Paris, Flammarion, p.

Mandelbrot, B.B., 1977, Fractals; Form, Chance and Dimension, NY, Freeman, p.

Mandelbrot, B.B., 1982, The Fractal Geometry of Nature, NY, Freeman, p.

Mandelbrot, B.B., Passoja, D.E., and Paullay, A.J., 1984, Fractal character of fracture surfaces of metals. Nature, v. 308, p. 721-722.

Mogi, Kiyoo, 1981a, Seismicity in Western Japan and long-term earthquake forecasting: in D. W. Simpson and P. G. Richards, Earthquake Prediction, Washington D. C., American Geophysical Union, p. 43-51.

Mogi, Kiyoo, 1981b, Earthquake prediction program in Japan: in D. W. Simpson and P. G. Richards, Earthquake Prediction, Washington D. C., American Geophysical Union, p. 635-666.

Nittmann, J., Daccord, G. and Stanley, H.E., 1985, Fractal growth of viscous fingers: quantitative characterization of a fluid instability phenomenon: Nature, v. 314, p. 141-144.

Obermeier, S.F., Gohn, G.S., Weems, R.E., Gelinas R.L. and Rubin, M., 1985, Geologic evidence for recurrent moderate to large earthquakes near Charleston, South Carolina: Science, v. 227, p. 408-410.

Richardson, L.F., 1961, The Statistics of Deadly Quarrels: Pittsburgh, PA, Boxwood Press (Pacific Grove Press), p.

Savage, J.C., 1983, Strain accumulation in Western United States: Annual Review Earth and Planetary Science, v. 11, p. 11-43.

Shaw, H.R. and Gartner, A.E., 1981, Statistical data on faulting rates in the United States and deduced seismicity: Geological Society of America, Abstract with Programs, v. 13, p. 552.

Shaw, H.R. and Gartner, A.E., 1984, Empirical laws of order among rivers, faults, and earthquakes: U. S. Geological Survey Open-file Report 84-356, 51 p.

Shaw, H.R. and Gartner, A.E., and Lusso ,F., 1981, Statistical data for movements on young faults of the conterminous U. S.: Paleoseismic implications and regional earthquake forecasting: U. S. Geological Survey Open-file Report 81-946, 353 p.

Sieh, K.E., 1981, A review of geological evidence for recurrece times of large earthquakes: in D.W. Simpson and P.G. Richards, eds. Earthquake Predictions, Washington D.C., American Geophysical Union, p. 181-208.

Smalley, R.F., Jr., Turcotte, D.L. and Solla, S.A., 1985, A renormalization group approach to the stick-slip behavior of faults. Journal of Geophysical Research, v. 90, p 1894-1900.

Sykes, L.R. and Quittmeyer, R.C., 1981, Repeat times of great earthquakes along simple plate boundaries: in D.W. Simpson and P.G. Richards, eds. Earthquake Predictions, Washington D. C., American Geophysical Union, p. 217-247.

Tchalenko, J.S., 1968) The evolution of kink-bands and the development of compression textures in sheared clays: Tectonophysics, v. 6, p. 159-174.

Tchalenko, J.S., 1970, Similarities between shear zones of different magnitudes: Geological Society of American, Bulletin, v. 81, p. 1625-1640.

Tchalenko, J.S., and Ambraseys, N.N., 1970, Structural analysis of the Dasht-e Bayaz (Iran) earthquake fractures: Geological Society of America, Bulletin, v. 81, p. 41-60.

Tchalenko, J.S., and Berberian, M., 1975, Dasht-e Bayaz fault, Iran: Earthquake and earlier related structures in bed rock: Geological Society of America, Bulletin, v. 86, p. 703-709.

Turcotte, D.L., Smalley, R.F., Jr., and Solla, S.A., 1985, Collapse of loaded fractal trees: Nature, v. 313, p. 671-672.

Wallace, R.E., 1981, Active faults, paleoseismology, and earthquake hazards in the Western United States: in D.W. Simpsons and P.G. Richards, eds. Earthquake Predictions, Washington D.C., American Geophysical Union, p. 209-216.

Weldon, R.J. II and Sieh, K.E., 1985, Holocene rate of slip and tentative recurrence interval for large earthquakes on the San Andreas fault, Cajon Pass, southern California: Geological Society of America, Bulletin, v. 96, p. 793-812.

Wesnousky, S.G. and Scholz, C.H., 1982, Deformation of an island arc: Rates of moment release and crustal shortening in intraplate Japan determined from seismicity and Quaternary fault data: Journal of Geophysical Research, v. 87, p. 6829-6852.

Wesnousky, S.G. and Scholz, C.H., Shimazaki, K. and Matsuda, T., 1983, Earthquake frequency distribution and the mechanics of faulting: Journal of Geophysical Research, v. 88, p. 9331-9346.

Wesson, R.L. and Wallace, R.E., 1985, Predicting the next great earthquake in California: Scientific American, v. 252, p. 35-43.

Ziony, J.I., Wentworth, C.M., Buchanan-Banks, J.M. and Wagner, H.C., 1974, Preliminary map showing recency of faulting in coastal southern California: U. S. Geological Survey, Miscellaneous Field Studies Map MF-585, 3 pl., Scale 1 : 250,000.

Teble 1: Conversions of Length Distributions to Frequency-Magnitude Relations.

A. Equations for Length Distributions:

(1) log N = 1.12 - 1.76 log L — Constant linear increment;
(2) log N = 2.81 - 2.21 log L — DELX = X.

Note: Equations are for L in cm, for map scale 1 : 5,000,000 (1cm = 50 km).

B. Length fractions per order; Arbitrary orders to base 10:

	N	log N	log L	L (cm)	L (km)	N L (km)	X (X = NL/ΣNL)
(1)	1	0	.64	4.37	219	219	.032
(2)			1.27	18.7	933	933	.016
(1)	10	1	.07	1.17	59	590	.085
(2)			.82	6.60	330	3300	.058
(1)	100	2	-.50	.32	16	1600	.232
(2)			.37	2.33	116	11600	.204
(1)	1000	3	-1.07	.09	4.5	4500	.651
(2)			-.085	.822	41.1	41100	.723
					Totals: (1)	6909	1.000
					(2)	56933	1.001

C. Maximum events per average segment lengths per order (Total RLR = 10 km/yr); SATURATION values:

	(1)				(2)			
Number, N	1	10	100	1000	1	10	100	1000
Segment L (km)	219	59	16	4.5	933	330	116	41.1
FRLR = X (RLR) (km/yr)	.32	.85	2.32	6.51	.16	.58	2.04	7.23
SRT = L/FRLR (yr)	684	69	6.7	.69	5831	569	57	5.7
Frequency, f (yr^{-1})	.0015	.014	.145	1.45	$1.7x10^{-4}$	.0018	.018	.18
log f	-2.84	-1.84	-.84	+.16	-3.77	-2.74	-1.74	-.76
Magnitude, M	7.87	7.16	6.46	5.77	8.66	8.09	7.53	6.97

Note: Magnitude, M, calculated from equation (see text):
M = 1.235 + 1.243 log L (L in meters). Table 1.

D. Uniformly distributed buildup of potential length activation per order, and Buildup Time, BT, where : Delta L = (FRLR) BT; each event is calculated from the normalized increment (Delta L)/N.

BT (yr)	N		Delta L (m)	(Delta L)/N (m)	Freq. (yr^{-1})	M
1	1	(1)	$3.2x10^2$	$3.2x10^2$	1	4.35
		(2)	$1.6x10^2$	$1.6x10^2$		3.97
	10	(1)	$8.5x10^2$	$8.5x10^1$	10	3.63
		(2)	$5.8x10^2$	$5.8x10^1$		3.43
	100	(1)	$2.3x10^3$	$2.3x10^1$	100	2.93
		(2)	$2.0x10^3$	$2.0x10^1$		2.85
	1000	(1)	$6.5x10^3$	$6.5x10^0$	1000	2.24
		(2)	$7.2x10^3$	$7.2x10^0$		2.30
10	1	(1)	$3.2x10^3$	$3.2x10^3$	.1	5.59
		(2)	$1.6x10^3$	$1.6x10^3$		5.22
	10	(1)	$8.5x10^3$	$8.5x10^2$	1	4.88
		(2)	$5.8x10^3$	$5.8x10^2$		4.67
	100	(1)	$2.3x10^4$	$2.3x10^2$	10	4.19
		(2)	$2.0x10^4$	$2.0x10^2$		4.10
	1000	(1)	$6.5x10^4$	$6.5x10^1$	100	3.61
		(2)	$7.2x10^4$	$7.2x10^1$		3.54
100	1	(1)	$3.2x10^4$	$3.2x10^4$	.01	6.83
		(2)	$1.6x10^4$	$1.6x10^4$		6.46
	10	(1)	$8.5x10^4$	$8.5x10^3$	.1	6.12
		(2)	$5.8x10^4$	$5.8x10^3$		5.91
	100	(1)	$2.3x10^5$	$2.3x10^3$	1	5.42
		(2)	$2.0x10^5$	$2.0x10^3$		5.34
	1000	(1)	$6.5x10^5$	$6.5x10^2$	10	4.73
		(2)	$7.2x10^5$	$7.2x10^2$		4.79
1000	1	(1)	$3.2x10^5$	$3.2x10^5$	.001	8.08
		(2)	$1.6x10^5$	$1.6x10^5$		7.70
	10	(1)	$8.5x10^5$	$8.5x10^4$	.01	7.36
		(2)	$5.8x10^5$	$5.8x10^4$		7.16
	100	(1)	$2.3x10^6$	$2.3x10^4$	.1	6.66
		(2)	$2.0x10^6$	$2.0x10^4$		6.58
	1000	(1)	$6.5x10^6$	$6.5x10^3$	1	5.98
		(2)	$7.2x10^6$	$7.2x10^3$		6.03

Explanation:

FRLR is Fractional Rupture Length Rate, which is the total Rupture Length Rate, RLR, multiplied by the fraction, X, of the total length (all orders) per order (i.e., X is defined as the aggregate length of all segments in a given order, N = i, divided by the summation of lengths in all orders); see B and C (the value of RLR used, 10 km/yr, is based on a conservative estimate of the overall rate in the U.S. given in Shaw and others, 1981; they point out that this estimate is probably low, and we have also illustrated results in Figure 7b for a value of about 40 km/yr).

SRT is the Segment Recurrence Time, which is the time for the potential activation of one complete segment length (Figure 1) in a given order at the fractional rate of length activation FRLR (statistically, the length L is equal to the average segment length in a specified order; i.e., there is a distribution of lengths within an order, as well as the general dendritic distribution over all orders); i.e., SRT = L / FRLR.

BT is the Buildup Time, defined as the time for the potential activation of any arbitrarily chosen length increment, Delta L, at the fractional rate FRLR. The number of potential partial events summing up to this measure of intra-order length is given by the number of possible subdivisions within the order, N. Thus, the smallest uniform distribution of averaged partial lengths within the order is given by the potential length activated at the rate FRLR, for that order, divided into N parts, (Delta L)/N; see D.

Table 2. Fractal Dimensions Consistent With Slopes of Frequency-Magnitude (b) and Moment-Magnitude (c) Plots.

(Note: Values in parentheses exceed the topological limit 3 for the volume-filling set, but time adds 1 to the potential fractal dimension in a topology of 4 dimensions; see Figure 18 and text. Also, observe that if c can assume the value 3, then the slope, -b, of the frequency-magnitude plot is identically equal to the fractal dimension of that data set; whether or not this dimension is associated with a fractally self-similar branching distribution of faults, however, depends on considerations such as those represented by the fractogram. That is to say, a self-consistent set of seismic data, such as sets identified with the seismic zones of Algermissen and Perkins, 1976, and Algermissen and others, 1982, does not necessarily relate to a single self-similar branching distribution of faults, because of intersecting trends, overprinting, etc.)

	c		
	1.0	1.5	3.0
b = .75	2.3	1.5	.75
b = 1.0	3.0	2.0	1.0
b = 1.5	(4.5)	3.0	1.5
b = 2.0	(6.0)	(4.0)	2.0
b = 3.0	(9.0)	(6.0)	3.0

Figure 1. Scale relations and the definition of fault segments:

(a) Total segment length equivalent to a complete activation event relative to two different length scales. At the larger scale, the segment is one of the two longest fault traces, representing the order N = 2. At the smaller scale, this trace may be one of a higher order set (N greater than 2), or the length shown may relate to a longer segment at the left as the first order fault, in which case the count of numbers per length may also require some revision.

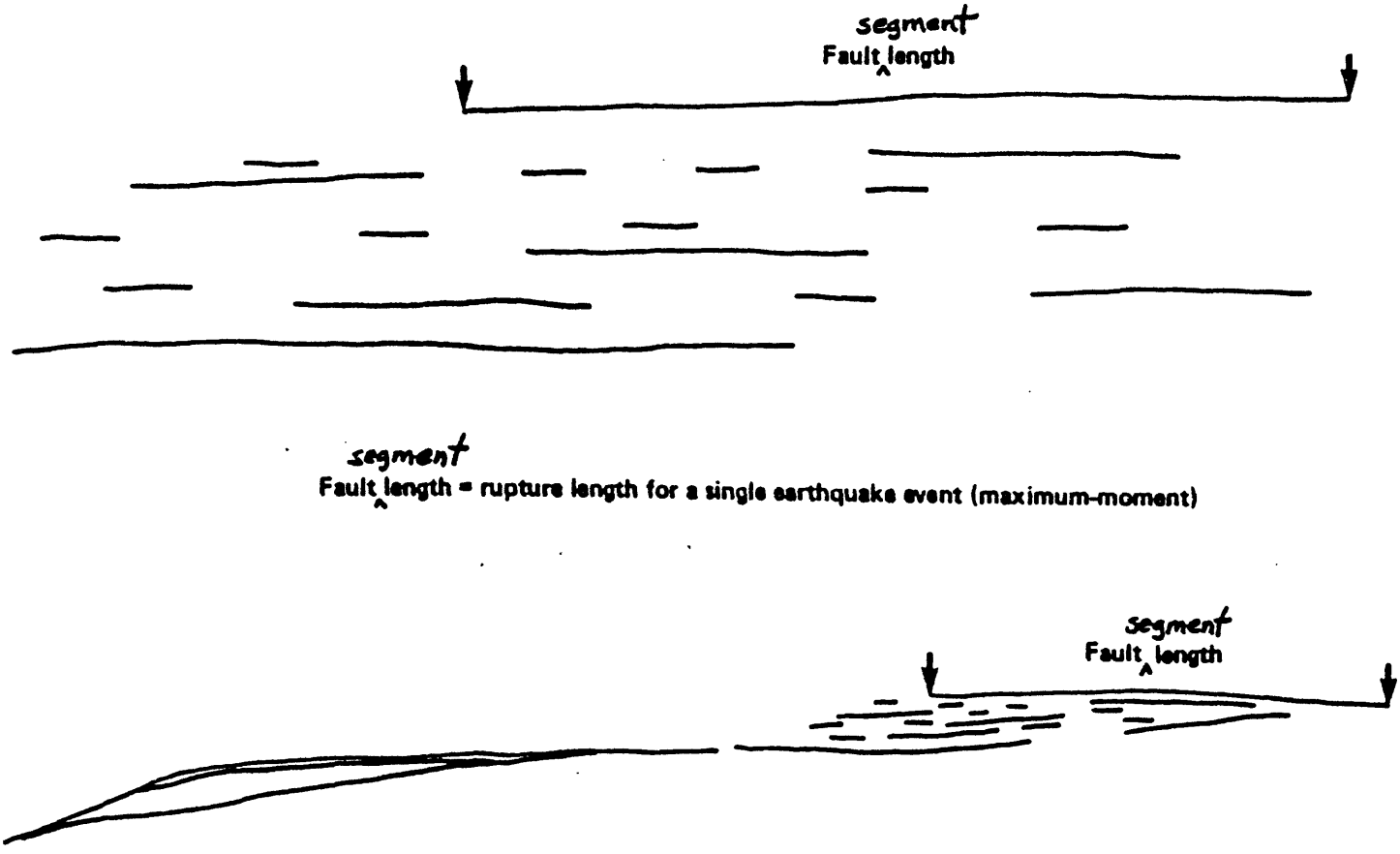

Figure 1. Scale relations and the definition of fault segments:

(b) Scale relations for partial segment lengths. If each demarked interval represents an earthquake event, then there is a more continuous spread of frequencies and magnitudes than there is if the segment represents only one discrete event of maximum magnitude.

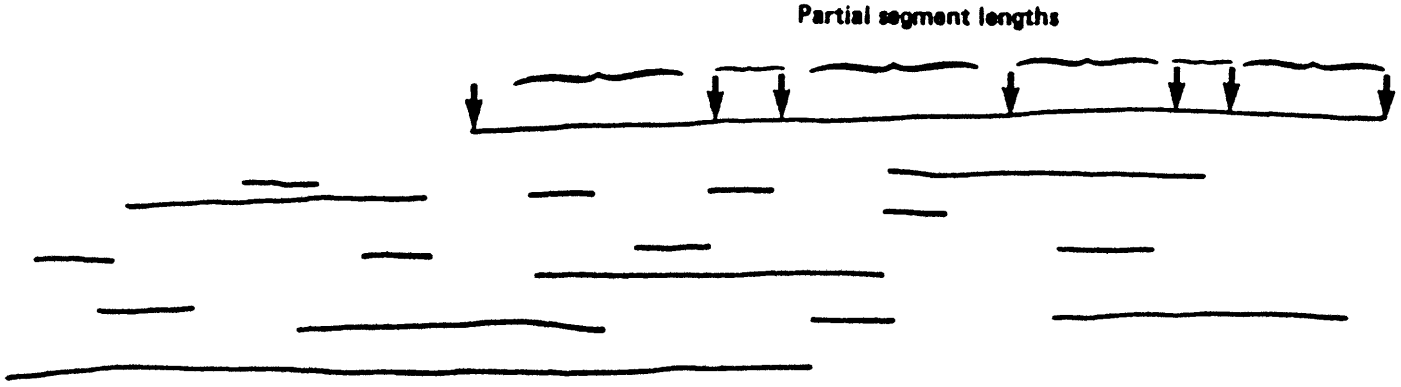

Partial segment lengths summing to segment length in Fig. 1a.

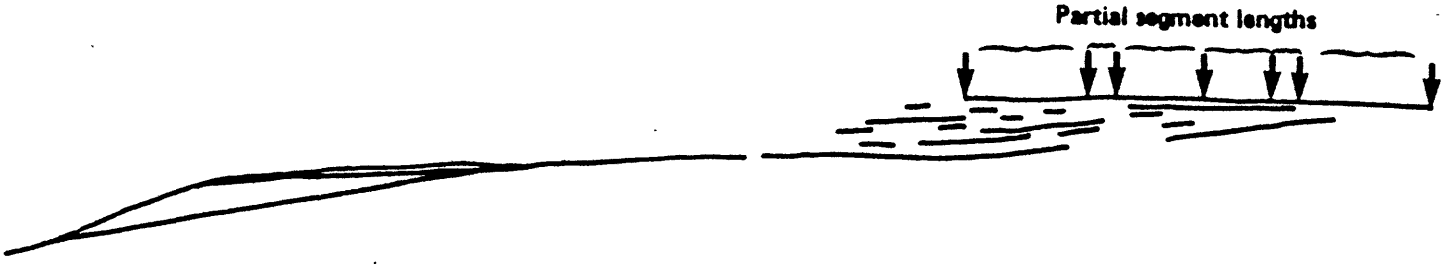

Figure 2. Illustration of the difference between the frequency-magnitude relations for "b-value" and "maximum-moment" type events (redrawn from Wesnousky and others, 1983). Essentially, one of the latter types of events is equivalent to the summation of several distributed events. If the total moment rate is the same, then it takes longer in the b-value mode to produce an event of the same magnitude as in the maximum-moment mode (see Figure 3 and discussion in text).

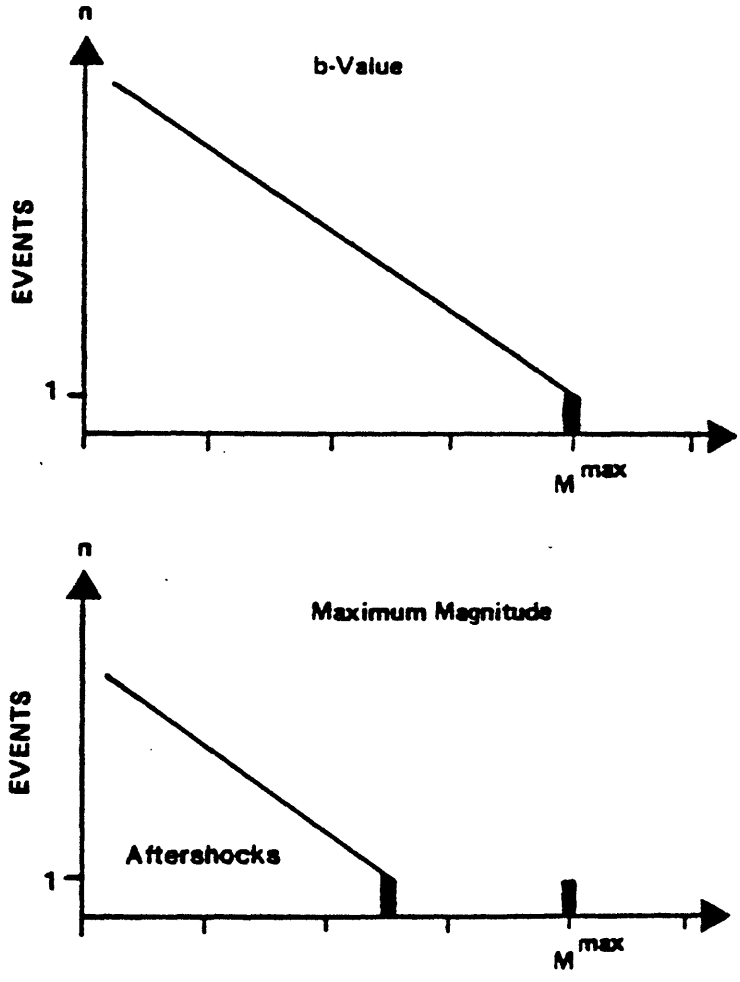

Figure 3. Illustration of the b-value and maximum-moment modes in terms of schematic distributions of fault activation lengths:

(a) The series of x's demark fault length that is activated in a single earthquake of maximum-moment type (ignoring local foreshock-aftershock events). This event would also be the largest possible event in a region limited to the larger scale. At the smaller scale, this event may be small relative to longer fault segments of lower number/length order in a more regional set.

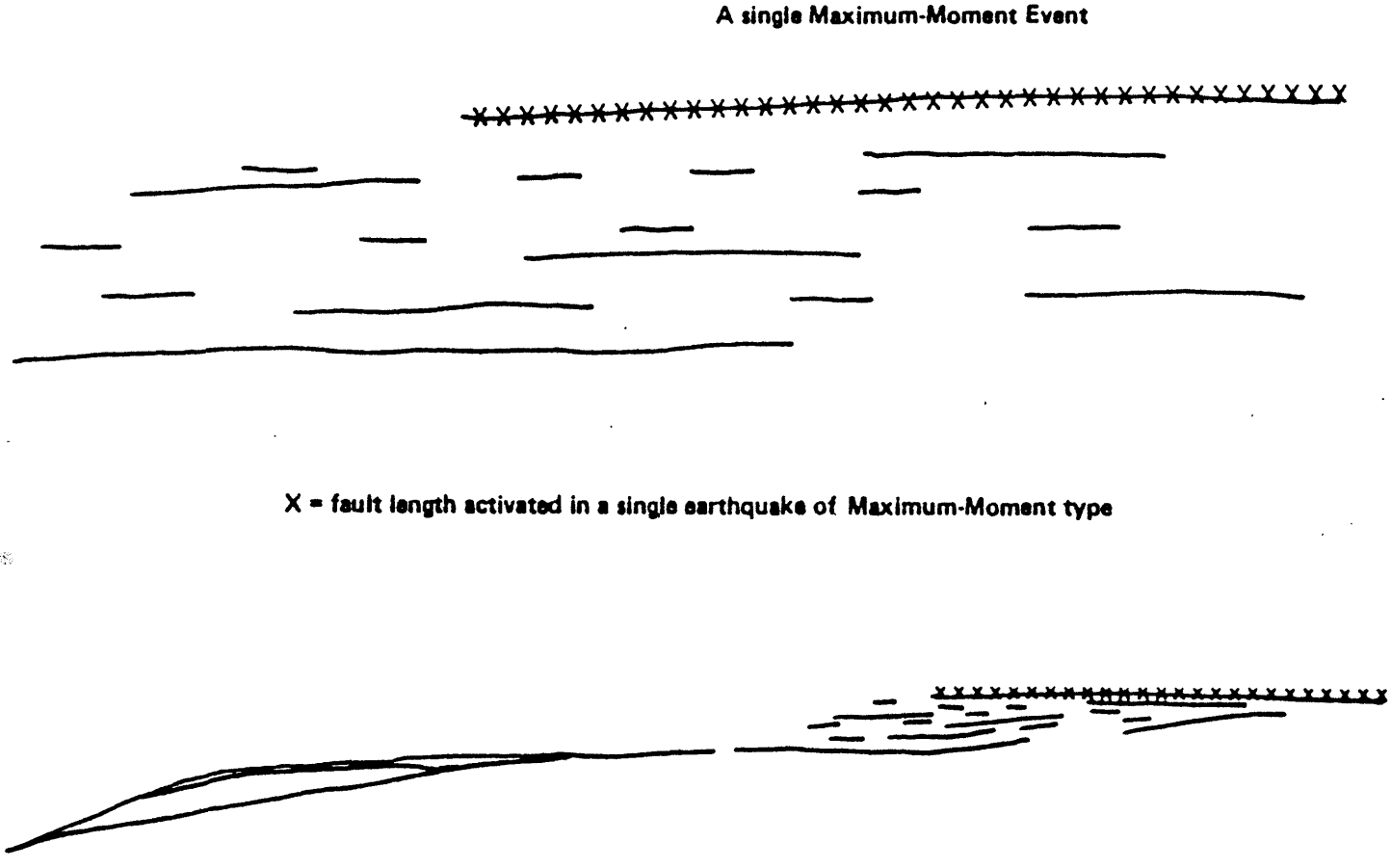

Figure 3. Illustration of the b-value and maximum-moment modes in terms of schematic distributions of fault activation lengths:

(b) Partial events along several segments in different number/length orders during the same amount of time for the buildup to the event in (a) at the same rate of energy accumulation. In this mode, events equivalent to (a) require longer to build up to the same magnitude because of the more continual energy consumption in the partial activation events. If the scale were made even smaller, it would be difficult to distinguish a partial activation from a total activation of a given segment length. The difference in frequency-magnitude plots, however, is still preserved (i.e., relatively lower frequencies, perhaps by as much as a factor of two, that are spurious if the Maximum Moment model is a more accurate description of length activations); see Wesnousky and others (1983) for numerical examples and discussion.

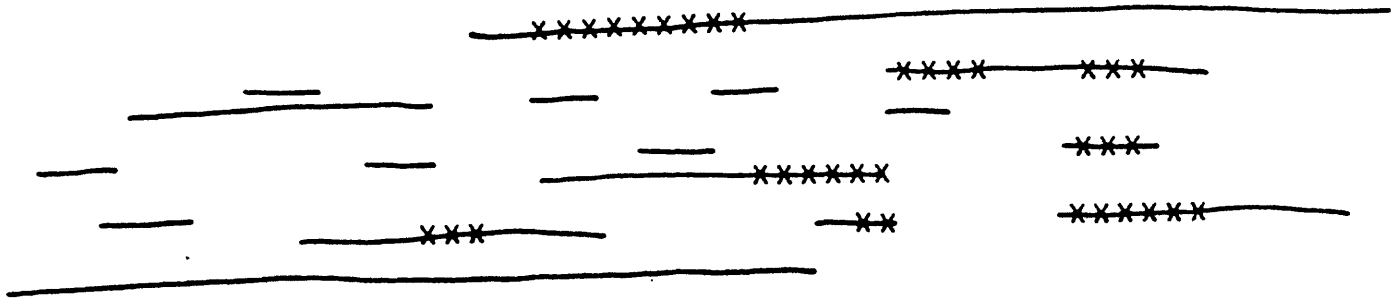

Partial events along several faults making up the same total moment as in Fig. 3a.

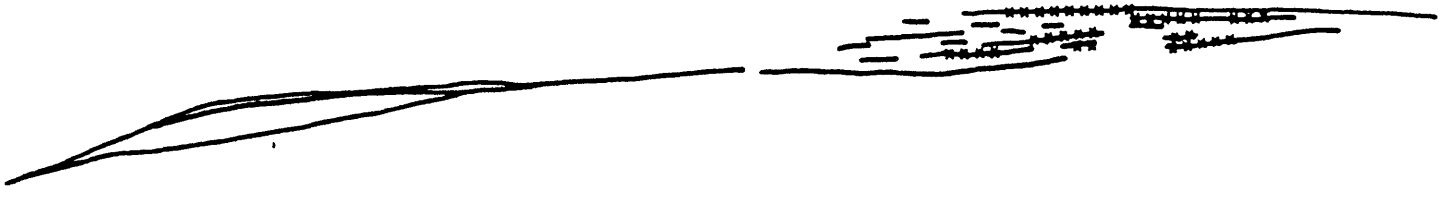

Figure 4. Histograms of fault-length measurements from Shaw and others (1981) based on the map of young faults in the U. S. by Howard and others (1978) at a scale of 1 : 5,000,000, and in the Los Angeles area by Ziony and others (1974) at a scale of 250,000 but plotted at the same scale as the U.S. data (i.e., at the scale 1 cm = 50 km). Both sets of data represent a time span of roughly 15 m.y.; see Shaw and others, 1981, for histograms broken down into 30 Faulting Regions and five age groups. Data for the Los Angeles vicinity are shown as a test of the effect of map scale on length cutoff, and as evidence of scale invariance of the general form of the distributions (see Figures 5 and 13, and discussions of self-similarity in text):

(a) Counts based on constant linear increments of about 1 km (minimum readability at 1 cm = 50 km was about .2 mm).

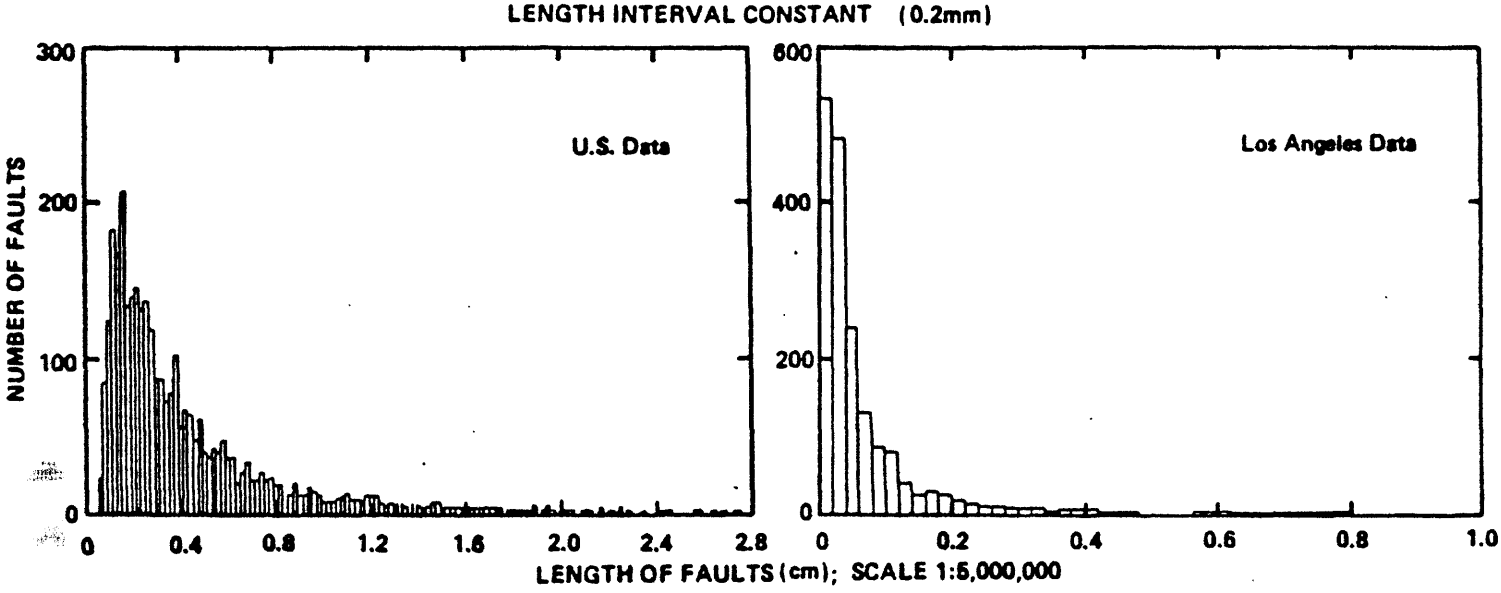

Figure 4. Histograms of fault-length measurements from Shaw and others (1981) based on the map of young faults in the U. S. by Howard and others (1978) at a scale of 1 : 5,000,000, and in the Los Angeles area by Ziony and others (1974) at a scale of 250,000 but plotted at the same scale as the U.S. data (i.e., at the scale 1 cm = 50 km). Both sets of data represent a time span of roughly 15 m.y.; see Shaw and others, 1981, for histograms broken down into 30 Faulting Regions and five age groups. Data for the Los Angeles vicinity are shown as a test of the effect of map scale on length cutoff, and as evidence of scale invariance of the general form of the distributions (see Figures 5 and 13, and discussions of self-similarity in text):

(b) Counts based on the convention DELX = X, where the length interval is increased geometrically so that no gaps occur in the length data.

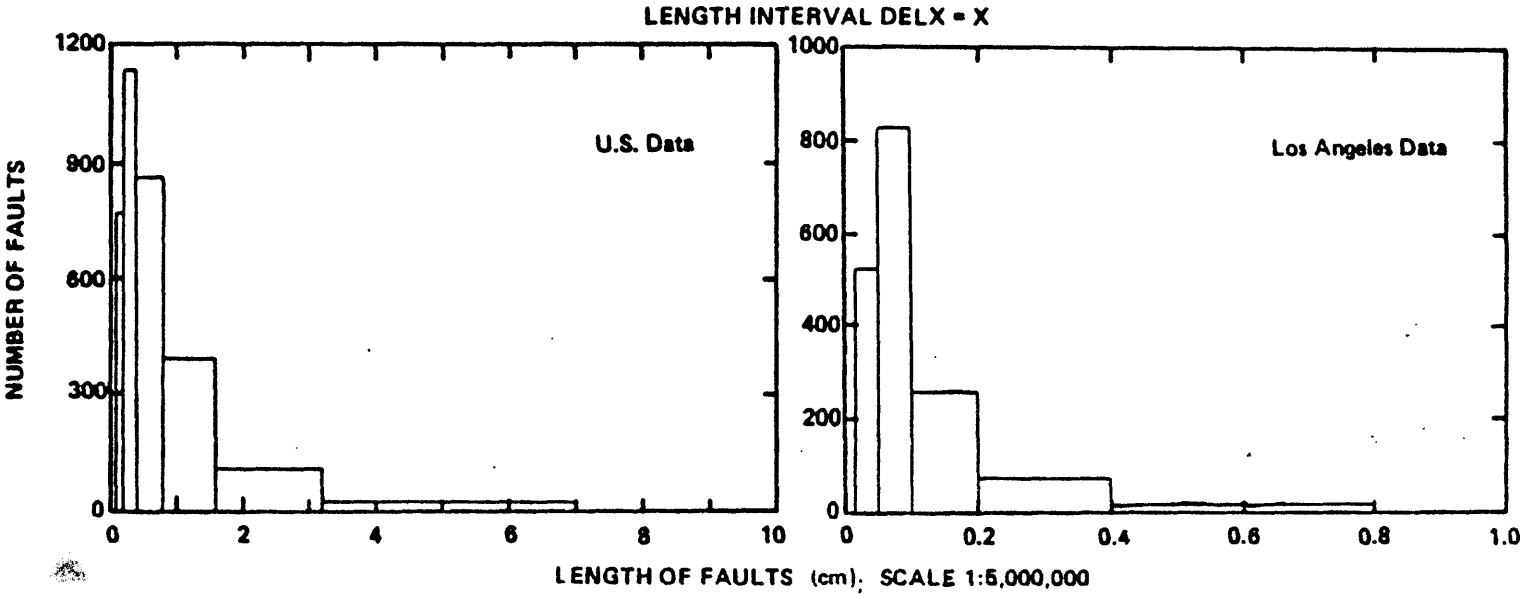

Figure 5 Plots of log N vs log L based on the sets of data in Figure 4; the Los Angeles data are shown to illustrate scale invariance (regression equations are for L in cm at map scale 1 cm = 50 km):

(a) Constant linear increments; in this mode the intermediate lengths dominate the regression slopes, and the longest fault lengths are not adequately represented.

NOTE: Fractal geometric analysis described later (Figures 13-18) shows that the fractal dimension is given by the relation Slope = (1 - D) in a plot of log (NL) vs. log L, where N is the number of units of length L associated with all faults individually equal to or longer than L; that is, NL represents all of the fault length for faults of length L and longer. Thus, L becomes the "yardstick" for measurement of length. Furthermore, if the slope, s, in plots of log number vs. log length, as given in this figure, is greater than unity then it provides an approximation to log (NL) vs. log L because most of the length at each L is accounted for by the incremental values. By this approximation the relation between s and D is given by (s + 1) = (1 - D), or D = -s. Accordingly, absolute values of slopes in Shaw and others (1981, Table 2.2.1-1.) indicate approximate variations of D for different faulting regions. Qualifications are: (1) maximum D should not exceed 2 for planar map distributions, therefore absolute values of s greater than 2 should not be observed (larger values occur because long faults are underestimated in some regions due to truncation or lack of recognition; this applies to the LA data of this figure, although the value may approach 2); (2) values near s = -1 underestimate D. The US value of 1.76 may be a true reflection of a "bushier" distribution than exists for long strike-slip fault systems; the value of 1.28 - 1.38 for California Coast agrees with other measurements given later.

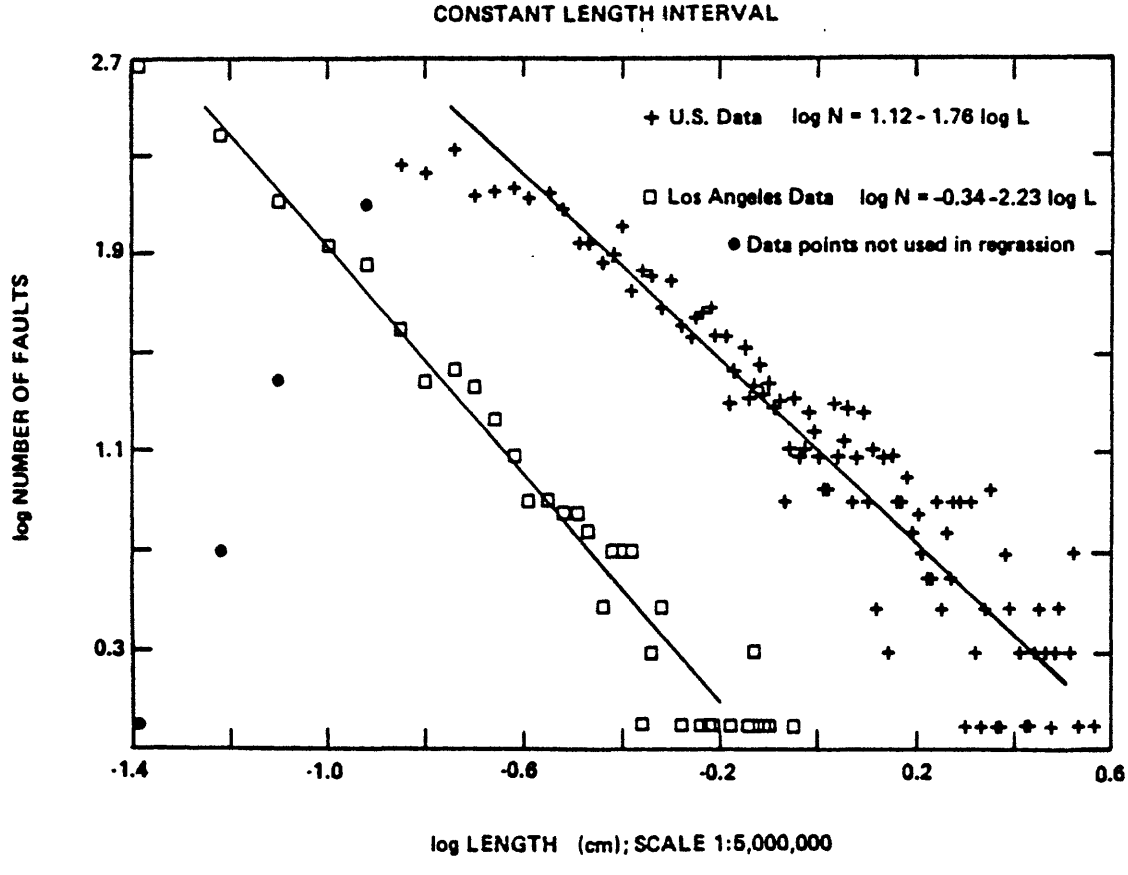

Figure 5 Plots of log N vs log L based on the sets of data in Figure 4; the Los Angeles data are shown to illustrate scale invariance (regression equations are for L in cm at map scale 1 cm = 50 km):

(b) DELX = X convention; in this mode the longer faults dominate the regression equation, and the numbers of short faults are overestimated.

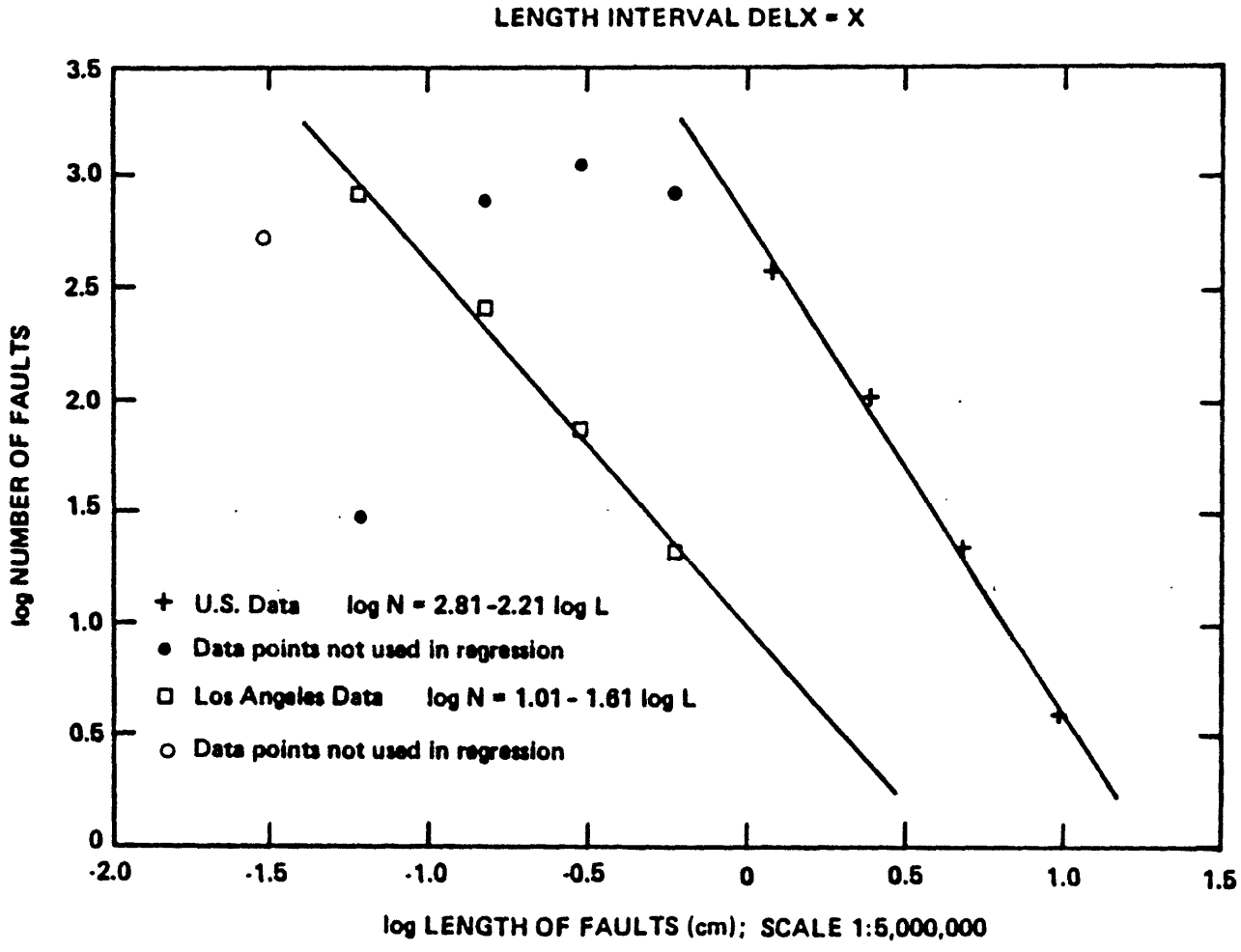

Figure 6. Construction of the fractogram for coordinates of magnitude, M, and the logarithm of frequency, log f, (the "paleoseismic parallelogram" of Shaw and others, 1981) based on the data in Figure 5 and Table 1 (U.S. data, all ages) for a rate of length activation ("rupture length rate" of Shaw and others, 1981) of 10 km/yr. The number of segments is indicated for four arbitrary orders to base 10, N = 1 to N = 1000. Values in parentheses identify the buidup time, BT, for the value of RLR normalized by the fraction of the total length in each order (see Table 1). The crosses and dashed lines indicate the SATURATION condition in Table 1. The heavy dot-dash lines show the composite distribution of historic seismicity for the U. S. from Algermissen (1969); the Roman numerals V and XII designate Modified Mercalli intensities representing his suggested range of validity of the regression (see text for definitions of magnitude derived from length data and from intensities). Fractograms are not constructed at the larger map scale of the Los Angeles data, because regional comparisons with seismicity in the U.S. and Japan are emphasized in this paper. A parallel construction can be made, however, following the same stepwise procedure detailed in Table 1 and tested against seismic data available in the Los Angeles vicinity (see Algermissen and others, 1982). In the regression equations, L is in cm for the scale ratio 1 cm = 50 km.

(a) Constant linear increment, U.S. data: $\log N = 1.12 - 1.76 \log L$.

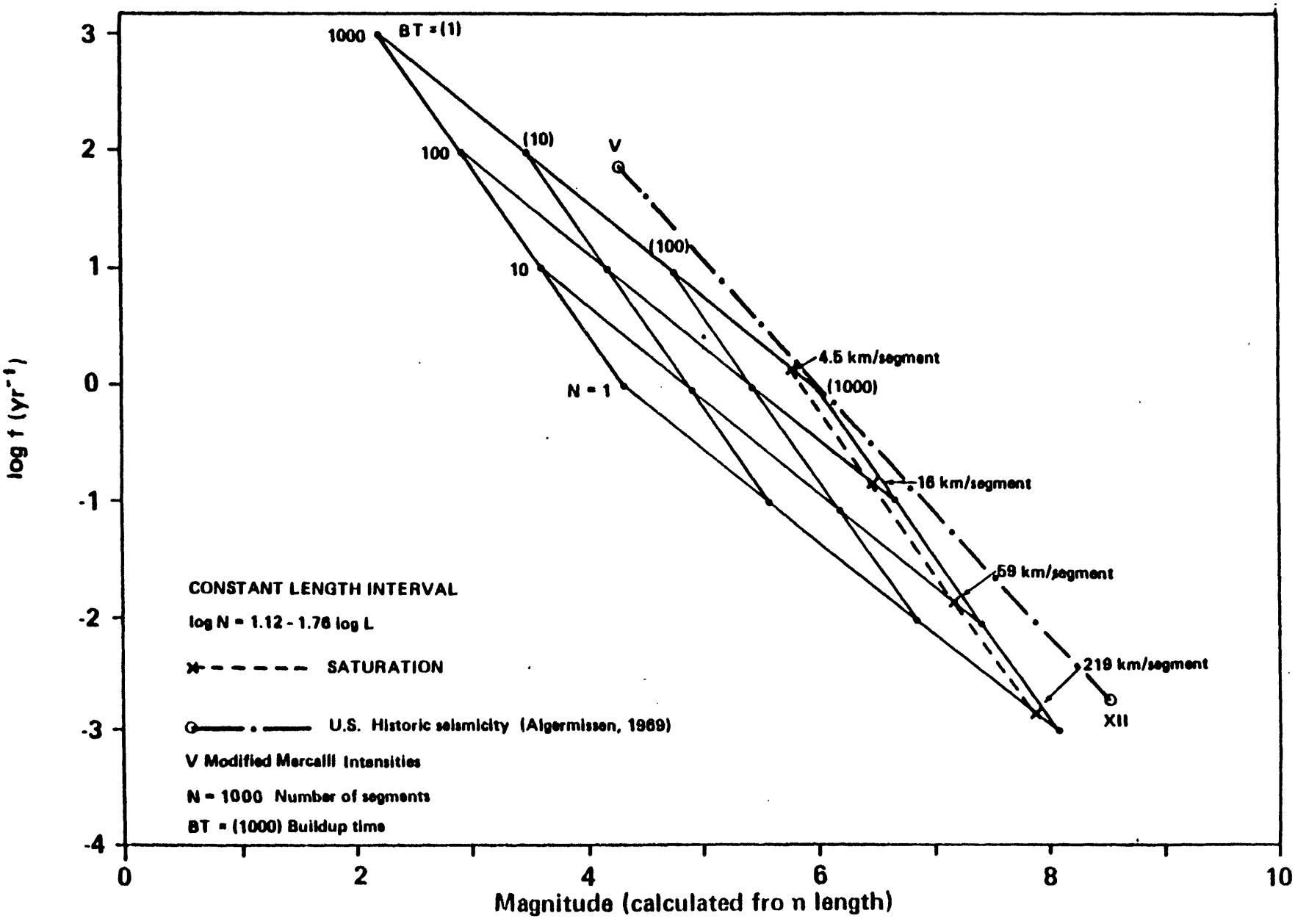
3
2
1
0
-1
-2
-3
-4
0
2
4
6
8
10
log f (yr⁻¹)
Magnitude (calculated fro n length)
1000
BT = (1)
100
(10)
10
N = 1
V
(100)
(1000)
4.5 km/segment
16 km/segment
59 km/segment
219 km/segment
XII
CONSTANT LENGTH INTERVAL
log N = 1.12 - 1.76 log L
SATURATION
U.S. Historic seismicity (Algermissen, 1969)
V Modified Mercalli Intensities
N = 1000 Number of segments
BT = (1000) Buildup time

Figure 6.

(b) DELX = X, U.S. data: log N = 2.81 - 2.21 log L (Note: This equation is a correction of the equation used in Shaw and others, 1981, to illustrate the construction of the fractogram: two data points apparently were misread in the input of the original regression routine, resulting in an erroneously large value of absolute slope.)

The parallelogram in (b) is not drastically different from (a), but notice that the Buildup Time to SATURATION is considerably greater because of the greater segment lengths per order. The maximum length at N = 1 is nearly equal to the length of the San Andreas (see Figures 10 and 11).

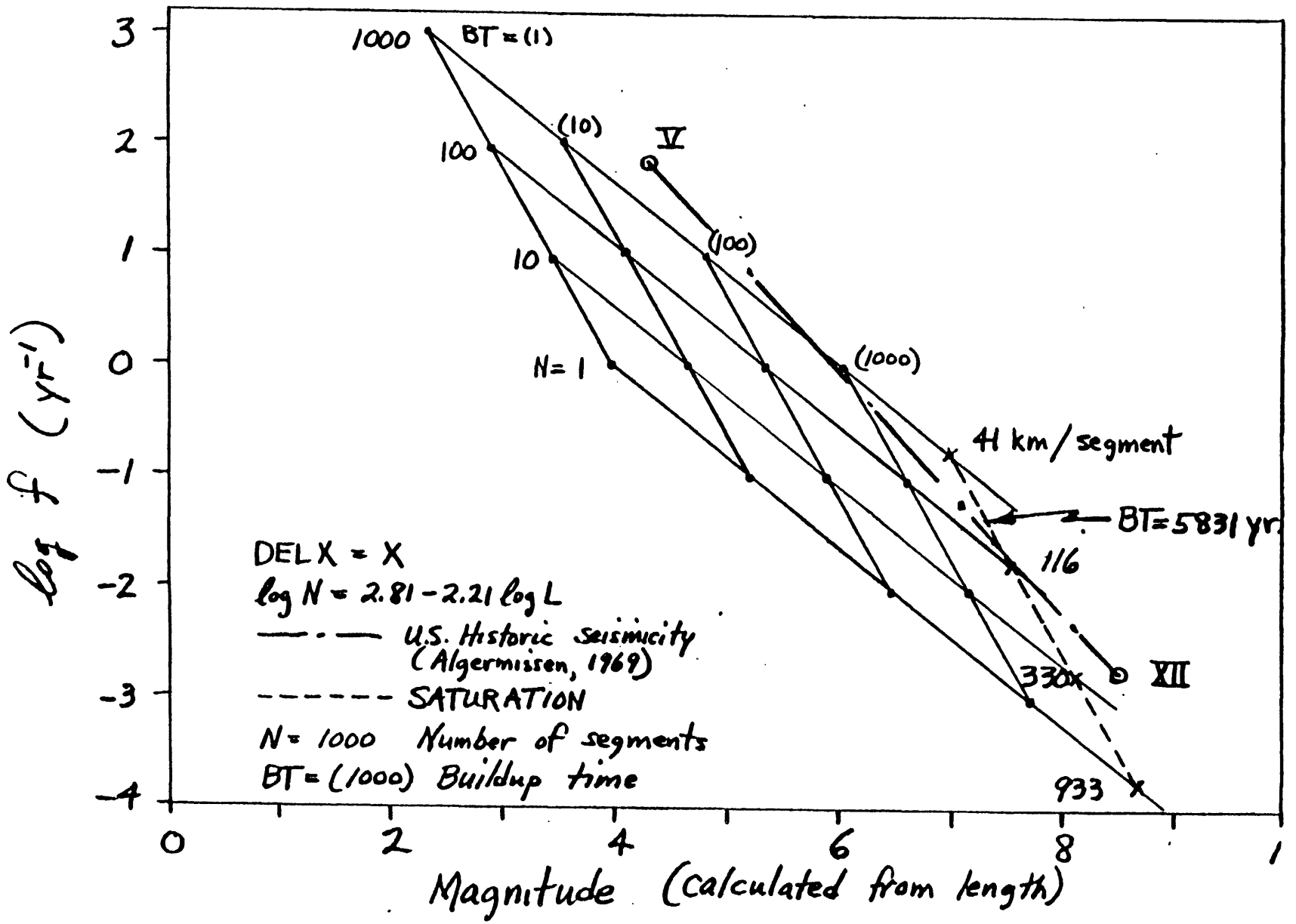
3
2
1
0
-1
-2
-3
-4
log f (yr⁻¹)
1000
BT = (1)
(10)
100
V
(100)
10
N = 1
(1000)
41 km/segment
BT = 5831 yr
116
330
XII
933
DEL X = X
log N = 2.81 - 2.21 log L
U.S. Historic seismicity (Algermissen, 1969)
SATURATION
N = 1000 Number of segments
BT = (1000) Buildup time
0
2
4
6
8
Magnitude (calculated from length)

Figure 7. Frequency-magnitude diagrams showing the relative positions of fractograms, fault activation rates, RLR, and seismic data for Japan and the U. S. In this and later illustrations, the fractogram is scaled as in Figure 6a, unless otherwise stated (see Figure 17); in some cases, however, it is shifted relative to the coordinates to illustrate contrasts in assumed local or overall activation rates (see b below, and Figure 9). Open circles indicate the raw data for historic seismicity in Japan, and the crosses represent the corresponding calculations for the maximum moment model (replotted from Wesnousky and others, 1983, Figure 7; Note: Their data are expressed in terms of cumulative moment, thus the frequencies equivalent to the incremental data based on lengths, or equivalent to the U.S. seismicity, will be somewhat lower, depending on the scales of resolution. These uncertainties, however, are masked by the uncertainties of RLR, and of the moment vs. magnitude relations discussed by Hanks and Boore, 1984, and illustrated in Figure 17c.). The heavy dash-dot line represents the U. S. data from Figure 6. Lines marked RLR represent the loci of frequencies and magnitudes for steady-state production of activated fault length at the rates indicated on the curves, using the same relation for magnitude from length given in the text; e.g., at a rate of 1000 km/yr, the length of activated fault produced in 100 years is 10 km which converts to a magnitude of about 6.2, etc. The potential rate identified by a value of RLR, such as the value 10 km/yr used for the rate of activation of total length in Table 1, is normalized by the fraction of length in each number/length order to give the relative distribution of frequencies and magnitudes for a given branching hierarchy (see stepwise calculations in Table 1):

(a) Position of the fractogram as in Figure 6, based on RLR = 10 km/yr.

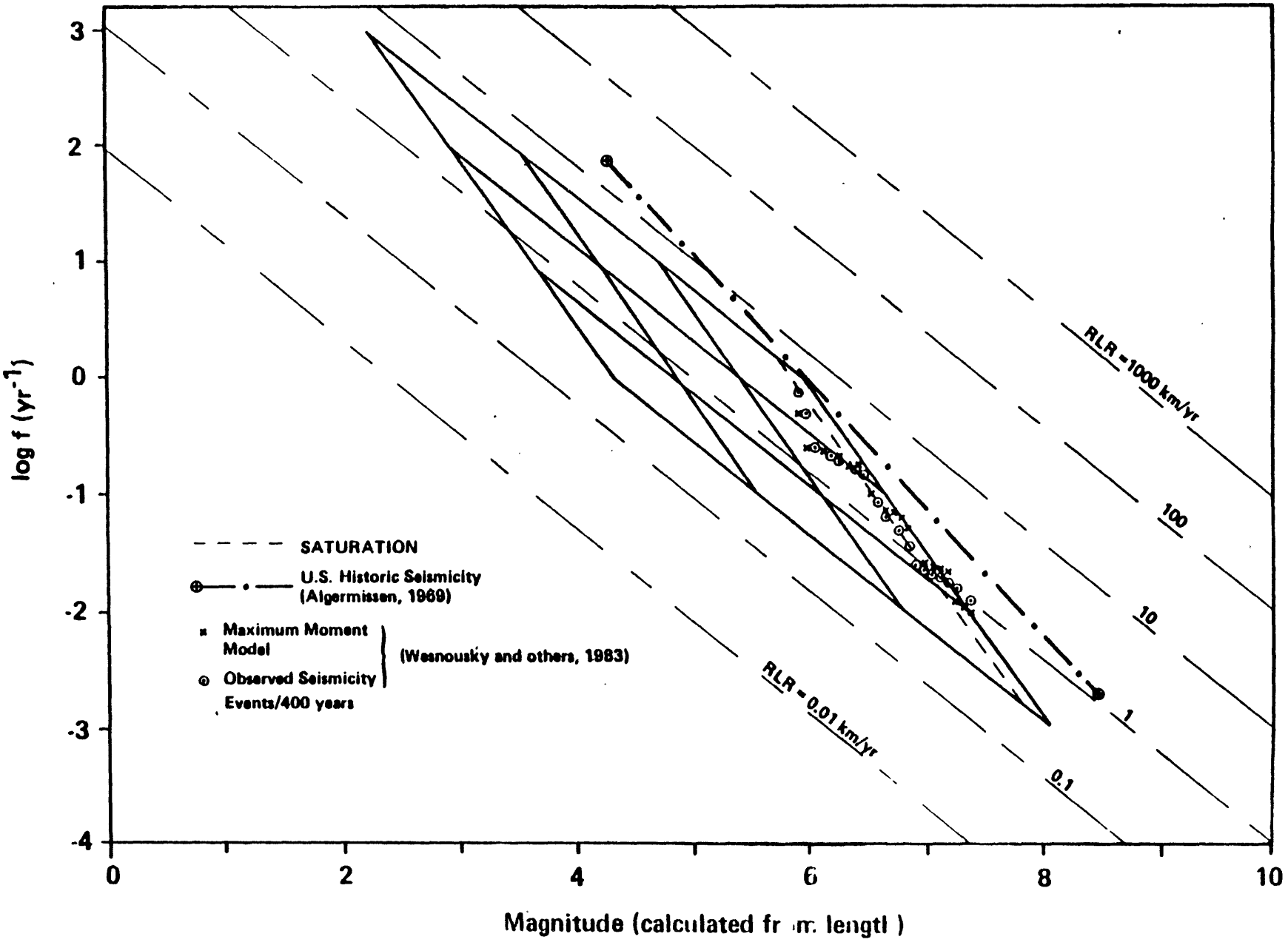
log f (yr^{-1})
3
2
1
0
-1
-2
-3
-4
0
2
4
6
8
10
Magnitude (calculated fr m lengtl)
RLR = 1000 km/yr
100
10
1
0.1
RLR = 0.01 km/yr
SATURATION
U.S. Historic Seismicity
(Algermissen, 1969)
Maximum Moment
Model
Observed Seismicity
Events/400 years
(Wesnousky and others, 1983)

Figure 7. Frequency-magnitude diagrams showing the relative positions of fractograms, fault activation rates, RLR, and seismic data for Japan and the U. S. In this and later illustrations, the fractogram is scaled as in Figure 6a, unless otherwise stated (see Figure 17); in some cases, however, it is shifted relative to the coordinates to illustrate contrasts in assumed local or overall activation rates (see b below, and Figure 9). Open circles indicate the raw data for historic seismicity in Japan, and the crosses represent the corresponding calculations for the maximum moment model (replotted from Wesnousky and others, 1983, Figure 7; Note: Their data are expressed in terms of cumulative moment, thus the frequencies equivalent to the incremental data based on lengths, or equivalent to the U.S. seismicity, will be somewhat lower, depending on the scales of resolution. These uncertainties, however, are masked by the uncertainties of RLR, and of the moment vs. magnitude relations discussed by Hanks and Boore, 1984, and illustrated in Figure 17c.). The heavy dash-dot line represents the U. S. data from Figure 6. Lines marked RLR represent the loci of frequencies and magnitudes for steady-state production of activated fault length at the rates indicated on the curves, using the same relation for magnitude from length given in the text; e.g., at a rate of 1000 km/yr, the length of activated fault produced in 100 years is 10 km which converts to a magnitude of about 6.2, etc. The potential rate identified by a value of RLR, such as the value 10 km/yr used for the rate of activation of total length in Table 1, is normalized by the fraction of length in each number/length order to give the relative distribution of frequencies and magnitudes for a given branching hierarchy (see stepwise calculations in Table 1):

(b) Position of the fractogram on the assumption that the termination of the seismic line for the U. S. identifies the SATURATION value at order N = 1; to fit both this assumption and the number vs length distributions, the value of RLR would have to be about 40 km/yr distributed according to the same fractions as in (a) and Table 1. SATBT indicates the buildup time for SATURATION based on this assumption and its submultiples, as in Figure 6a; here, however, SATBT is identical with the right side of the parallelogram and is slightly smaller (about 600 years instead of 700; dashed line in a). The heavy dashed line shows where the SATURATION limit would be if the longest first-order fault were of length 1000 km; the Buildup Time, BT, in this case would be about 1000 years (compare with Figure 6b, where SATURATION for a comparable length is about 6000 years). Open circles connected by a solid line represent the trend of the observed seismicity in Japan from graph (a). The light dashed lines and numbers in parentheses represent seismic trends within some selected Seismic Zones from Algermissen and Perkins (1976): (2) San Andreas system, CA, (61) vicinity of Mississippi Embayment (New Madrid system, etc.), (65) vicinity of Charleston, SC. We refer to the Seismic Zones of Algermissen and Perkins (1976), rather than Algermissen and others (1982), because the general trends are the same, and the earlier zonations are more readily compared with the Faulting Regions in Shaw and others (1981); see Figure 9.

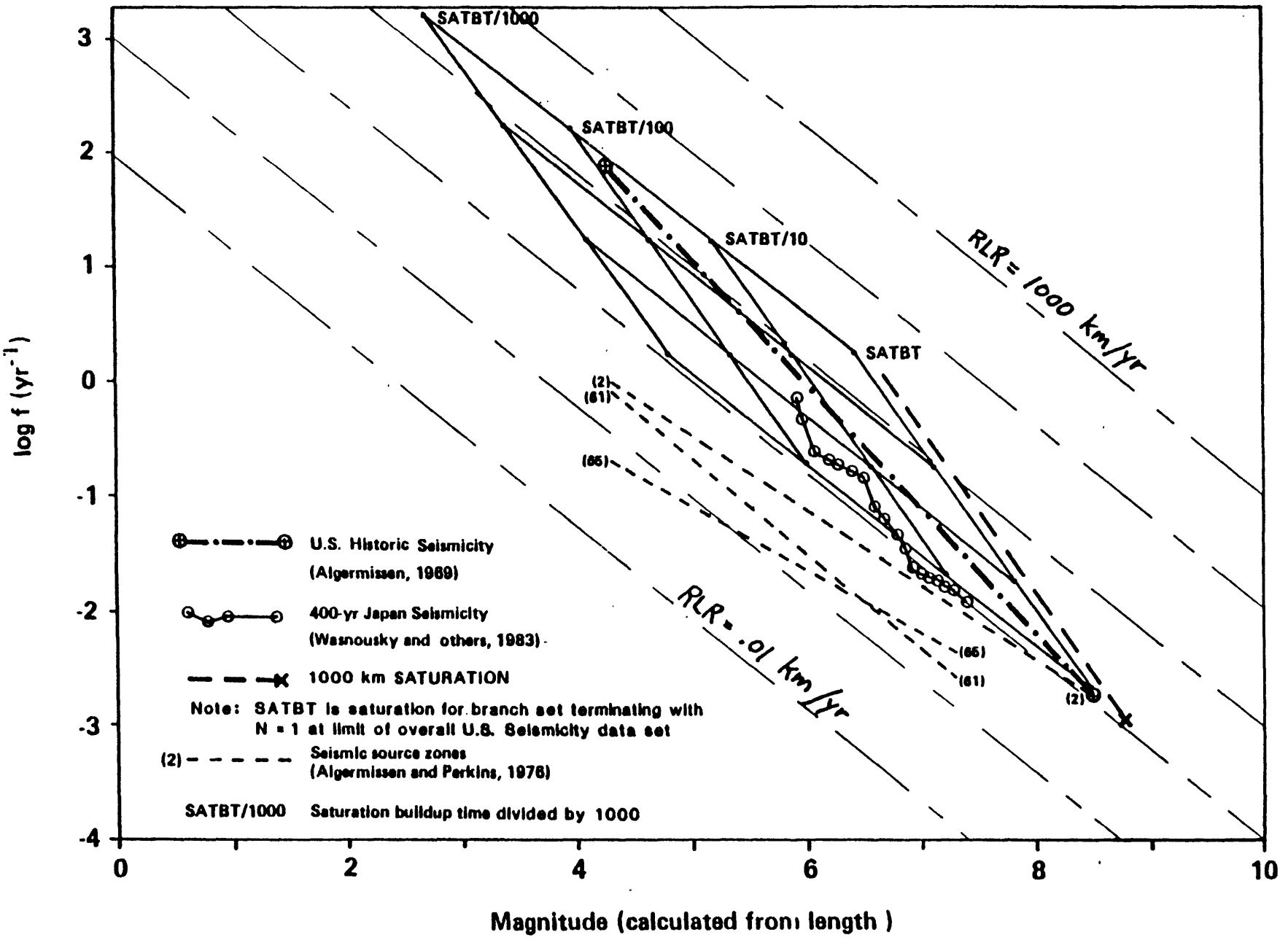
SATBT/1000
SATBT/100
SATBT/10
SATBT
RLR = 1000 km/yr
RLR = .01 km/yr
(2)
(61)
(65)
log f (yr⁻¹)
Magnitude (calculated from length)
U.S. Historic Seismicity
(Algermissen, 1969)
400-yr Japan Seismicity
(Wasnousky and others, 1983)
1000 km SATURATION
Note: SATBT is saturation for branch set terminating with N = 1 at limit of overall U.S. Seismicity data set
Seismic source zones
(Algermissen and Perkins, 1976)
SATBT/1000 Saturation buildup time divided by 1000

Figure 8. Hypothetical regimes of fault-length activation expressed as combinations of order sequences in the fractogram as constructed in Figures 6 and 7 from Table 1:

(a) All number/length orders are uniformly activated in proportion to the fraction of the aggregate fault length (length fraction X in Table 1); in this "diffusive" mode the potential magnitudes and frequencies are given by the same uniform buildup time for which it is assumed earthquakes can occur (this kinematic balance does not consider information on failure conditions). The dashed line schematically indicates the trend of net frequency-magnitude relations.

(b) Each number/length order, beginning with the highest order (large N, small L), is activated in a sequence of partial events which terminate in a SATURATION event ("ultimate" moment for that order) before the next lower order (larger length-subset) begins to show seismic activity. When all orders have been sampled the sequence repeats. The dashed line indicates that the net frequency-magnitude graph would lie above and subparallel to the trends at constant N.

(c) Similar to (b) except that the sequence in each order is terminated at some maximum event charateristic of that order, at a level of potential activation less than SATURATION; the total cycle time in this case is less than in (b). Numbers indicate 6 subregimes of the overall cycle, 3 at constant N, and 3 at constant BT.

(d) SATURATION mode, in which no events occur until every order has built to its ultimate potential moment, and events then occur in proportion to the SATURATION lengths and length fractions of the total activation rates (see Table 1).

Note: The fractogram is based on generally steady-state arguments concerning distributions of activation lengths. The above models, however, imply transient behavior in strain distributions (apart from the obvious transients associated with seismic radiation) over at least some portions of a seismic cycle. In order to reconcile these viewpoints, information on actual rates of change in strain energy distributions is needed (a relationship between RLR and rates of fault slip is considered in a later section; see Figure 19). For a steady-state RLR in these diagrams, the portions of faults for which no events are recorded imply either aseismic slip or storage of strain energy equivalent to a given value of RLR. In the former case, RLR is a potential rate relative to seismicity even though it is an actual measure of fault lengths showing evidence of motion; in the latter case, both motion and seismicity are episodic in the several kinds of possible sequences. The effective values of RLR during the episodes of motion, therefore, are increased in proportion to the times representing storage episodes in each order. This will modify the assumption concerning the constant fractional distribution of RLR; in the storage mode the fractions also will be functions of time which average to the steady state distributions over multiple cycles.

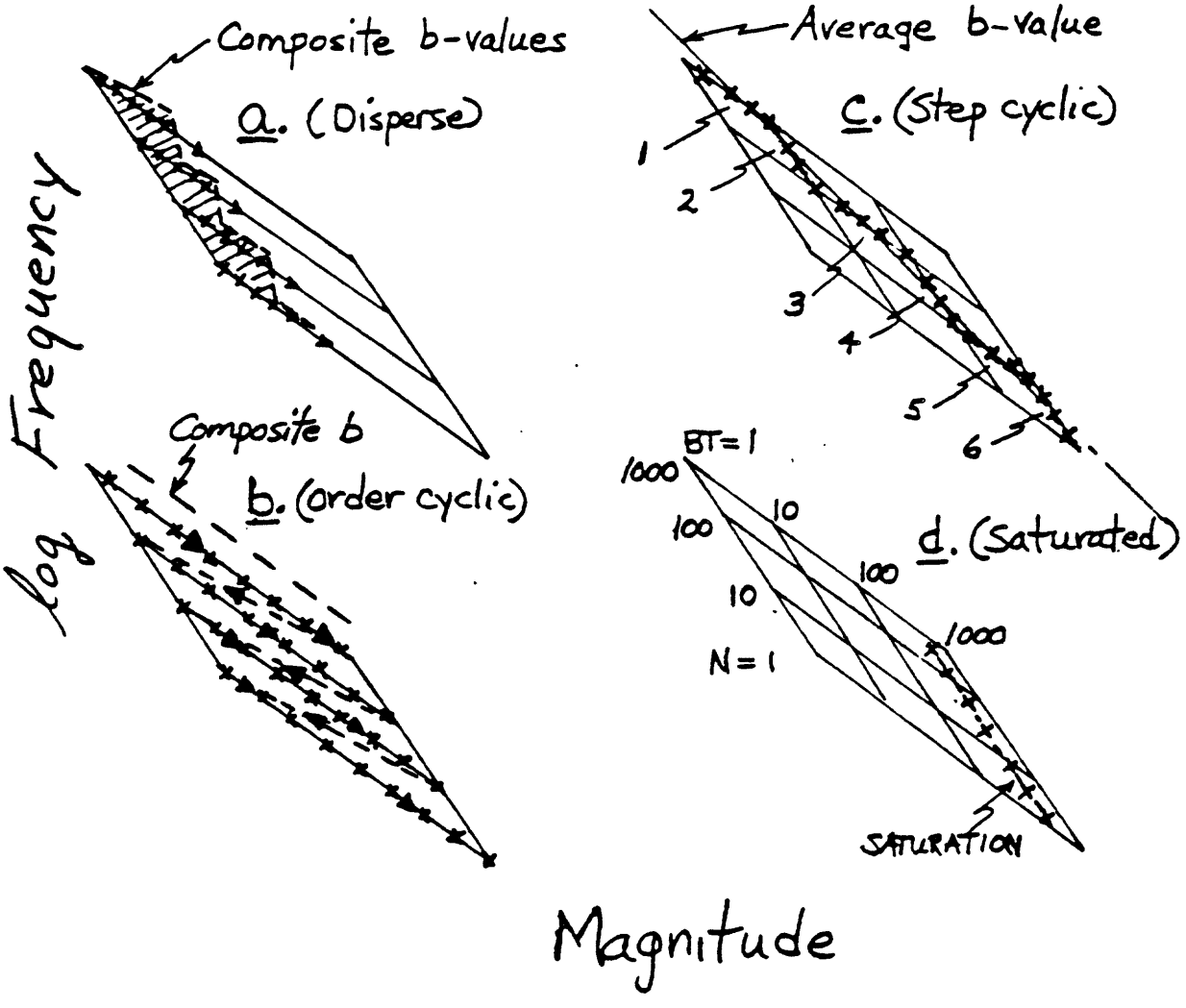
Composite b-values
a. (Disperse)
Composite b
b. (order cyclic)
log Frequency
Average b-value
c. (Step cyclic)
1
2
3
4
5
6
BT=1
1000
100
10
N=1
10
100
1000
d. (Saturated)
SATURATION
Magnitude

Figure 9. Regression distributions of historic seismicity for selected Seismic Zones in California calculated from data in Algermissen and Perkins (1976) and plotted vs the range of values of RLR in earlier diagrams; the dotted outlines show the positions, respectively, of the fractogram in Figure 7b and one that might hypothetically include activity only in zones 3, 4, and 18. The geographic boundaries of Seismic Zones are shown in Figure 10.

Note: Algermissen and others (1982) revised the seismic zoning of Algermissen and Perkins (1976) into many more zones. For present purposes, however, the coarser distribution is more readily compared with the Faulting Regions evaluated by Shaw and others (1981). Ranges and patterns of b-values are generally similar in the newer zonations, but any detailed study of geographic/chronologic correlations will have to consider questions of systematic interactions at the finer resolution.

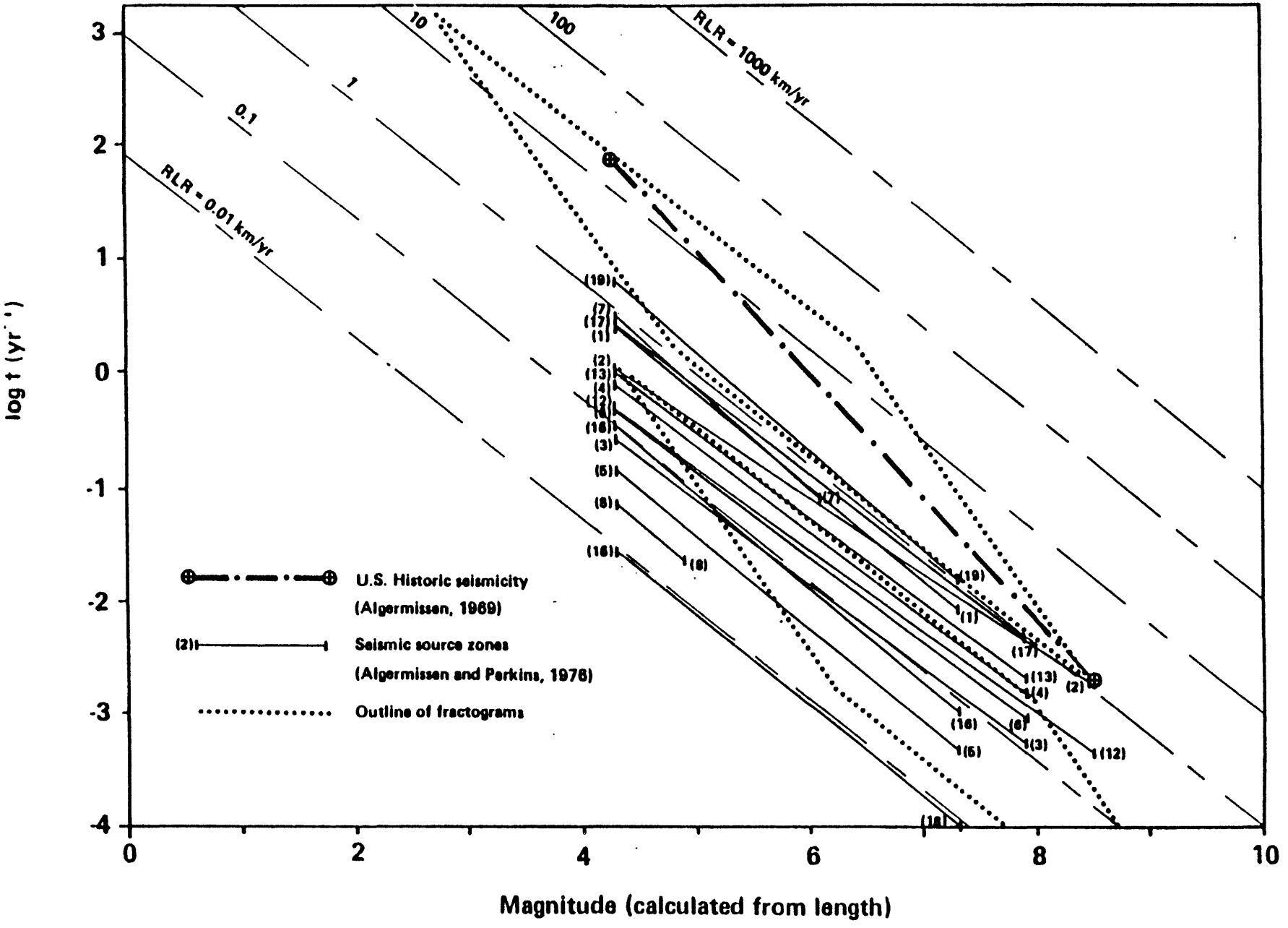
RLR = 0.01 km/yr
0.1
1
10
100
RLR = 1000 km/yr
log t (yr⁻¹)
3
2
1
0
-1
-2
-3
-4
0
2
4
6
8
10
Magnitude (calculated from length)
U.S. Historic seismicity
(Algermissen, 1969)
Seismic source zones
(Algermissen and Perkins, 1976)
Outline of fractograms

Figure 10. Distribution of Seismic Zones in California as defined by Algermissen and Perkins (1976; redrawn from their Figure 2). Seismic Zone 2 essentially refers to a mappably continuous portion of the San Andreas system; solid circles indicate an approximately 1000 km length of the San Andreas system, which is also used as a reference length in Figures 11 and 13. A more detailed map of seismic zones is given by Algermissen and others (1982), but the general distributions of b-values in frequency-magnitude plots remains roughly the same (see Figure 9).

Note: A fractogram constructed from the fault-length distributions for the Los Angeles vicinity shown in Figure 5, following the procedure in Table 1, can be compared with Seismic Zone 4, and with its revised subdivisions in Algermissen and others (1982).

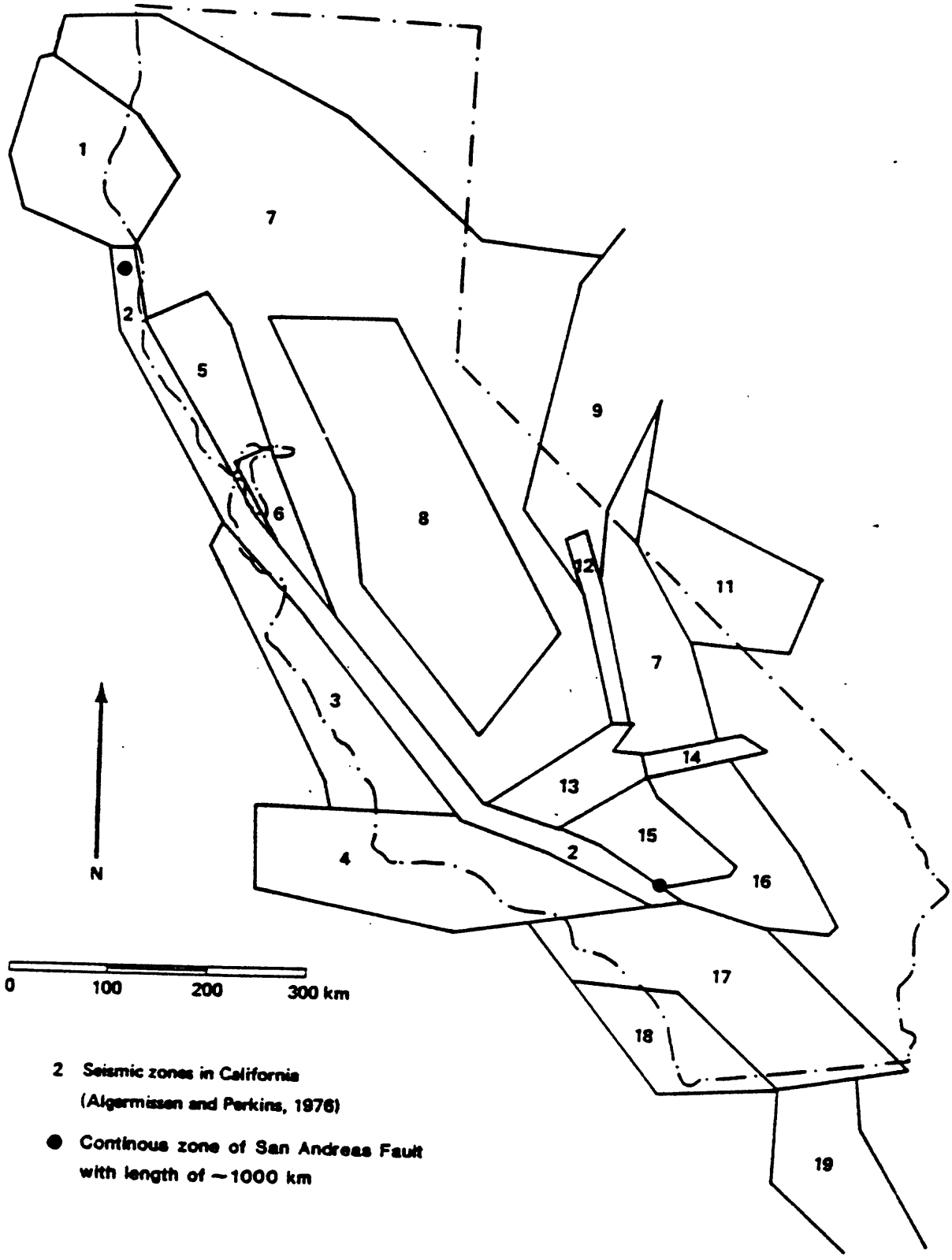

2 Seismic zones in California (Algermissen and Perkins, 1976)

● Continous zone of San Andreas Fault with length of ~1000 km

Figure 11. Sketch map of the San Andreas system (modified from Allen, 1968). Solid circles indicate the approximately continuous zone with a length of about 1000 km as shown in Figures 10 and 13. The Inset shows possible relationships to hypothetical portions of the fractogram as outlined in Figure 8 (see text). If the San Andreas system is viewed in the context of multiple Seismic Zones and Fault Regions (Howard and others, 1978; see Shaw and others, 1981), a multiple hierarchy of fractograms is required to accomodate the implicit ranges of RLR and frequency-magnitude trends. It is noted later (see Figure 17b) that as log N vs log L approaches direct inverse proportionality, the fractogram collapses to a line ("parallelogram of zero width"); the "California Coast" Fault Region, which largely includes the San Andreas system has the following regression equations: log N = .13 - 1.28 log L (linear increments), and log N = 1.31 - 1.26 log L (DELX = X), for cm at scale 1 cm = 50 km. In such a case the distributions of activation lengths and seismic events are nearly superimposed on the same trend, making it difficult to distinguish between partial and maximum events in the absence of direct correlations of activation lengths with specific earthquakes. As noted in Figure 3, however, the distinctions between b-value and maximum moment interpretations are nonetheless real and important. Also, the linearity of the fractogram does not imply restriction of fault activations to a linear zone, as is usually assumed for the San Andreas system. Therefore, the same general implications hold concerning the importance of establishing characteristic number/length hiearchies over a "dendritic" region (see later discussion of fractal dimensions in text, and compare with Figures 8, 17, and 18). The Inset schematically indicates subregimes of the fractogram, as in Figure 8, that might apply to different portions of the San Andreas system; smaller events are distributed over a range of number/length orders and higher frequencies during a characteristic portion of a seismic cycle, as in Figure 8, whereas another portion of the cycle experiences partial activations of larger events and lower frequencies within a restricted number/length order (e.g., N = 1). At present, these would correspond roughly to the unlocked and locked portions, respectively, of the fault. Such distributions would show seismic gaps, both in terms of the frequency-magnitude plots, and in terms of geographic locations.

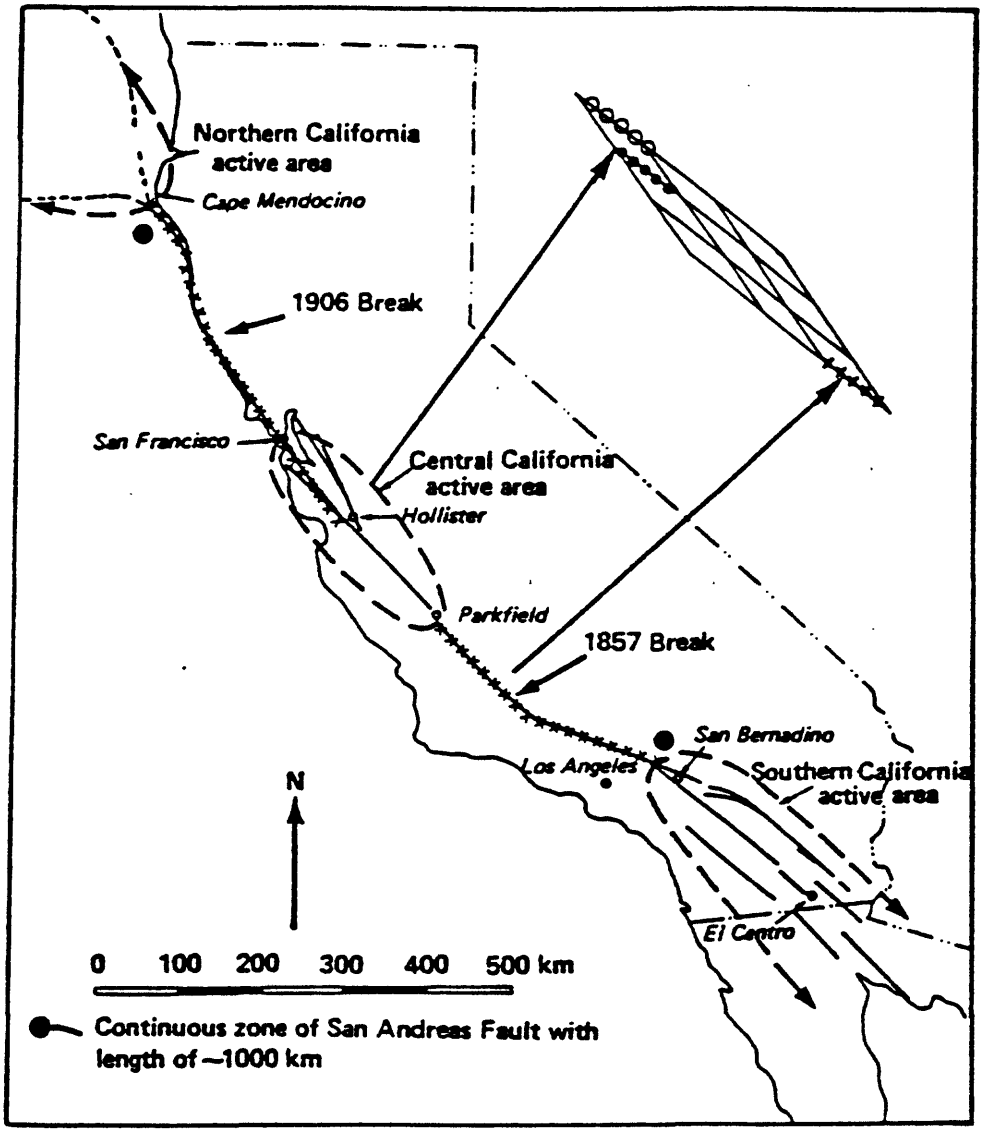
Northern California
active area
Cape Mendocino
1906 Break
San Francisco
Central California
active area
Hollister
Parkfield
1857 Break
San Bernadino
Los Angeles
Southern California
active area
El Centro
N
0 100 200 300 400 500 km
Continuous zone of San Andreas Fault with
length of ~1000 km

Figure 12. Comparison of fault-length distributions implied by record of historic seismicity in Japan with data for U. S. based on measurements for different age classes from Shaw and others (1981). Lengths for the Japanese data were inverted from moment distributions (Wesnousky and others, 1983, Figure 7) using the relation in the text (Eq. 2): log M_o = 23.50 + 1.94 log L, for L in km. The trend for Japan therefore represents the number of equivalent lengths greater than or equal to the length L; this overestimates the number relative to the incremental data for the U. S. by about a factor of 2 (.3 log unit). The step-like distribution of crosses is partly an artifact of the assumption that each event represents the activation of an entire fault segment; if some partial activations exist , as is inferred from Figure 7, and if incremental data were used, the steps would be less conspicuous. It is evident, however, that the seismically inferred numbers of active faults in Japan are much greater than are the measured numbers in the U. S. over a comparable time-span of activity, relative to the more similar comparative levels of seismicity as shown in Figure 7 (see discussion in text). By inference, many active faults exist in the U. S. that are not included in the catalog of direct measurements compiled by Shaw and others (1981); that reference draws the same conclusion on the basis of comparing levels of implicit fault activation for each Seismic Zone of Algermissen and Perkins (1976) with measured levels of faulting in each of the Fault Regions of Howard and others (1978).

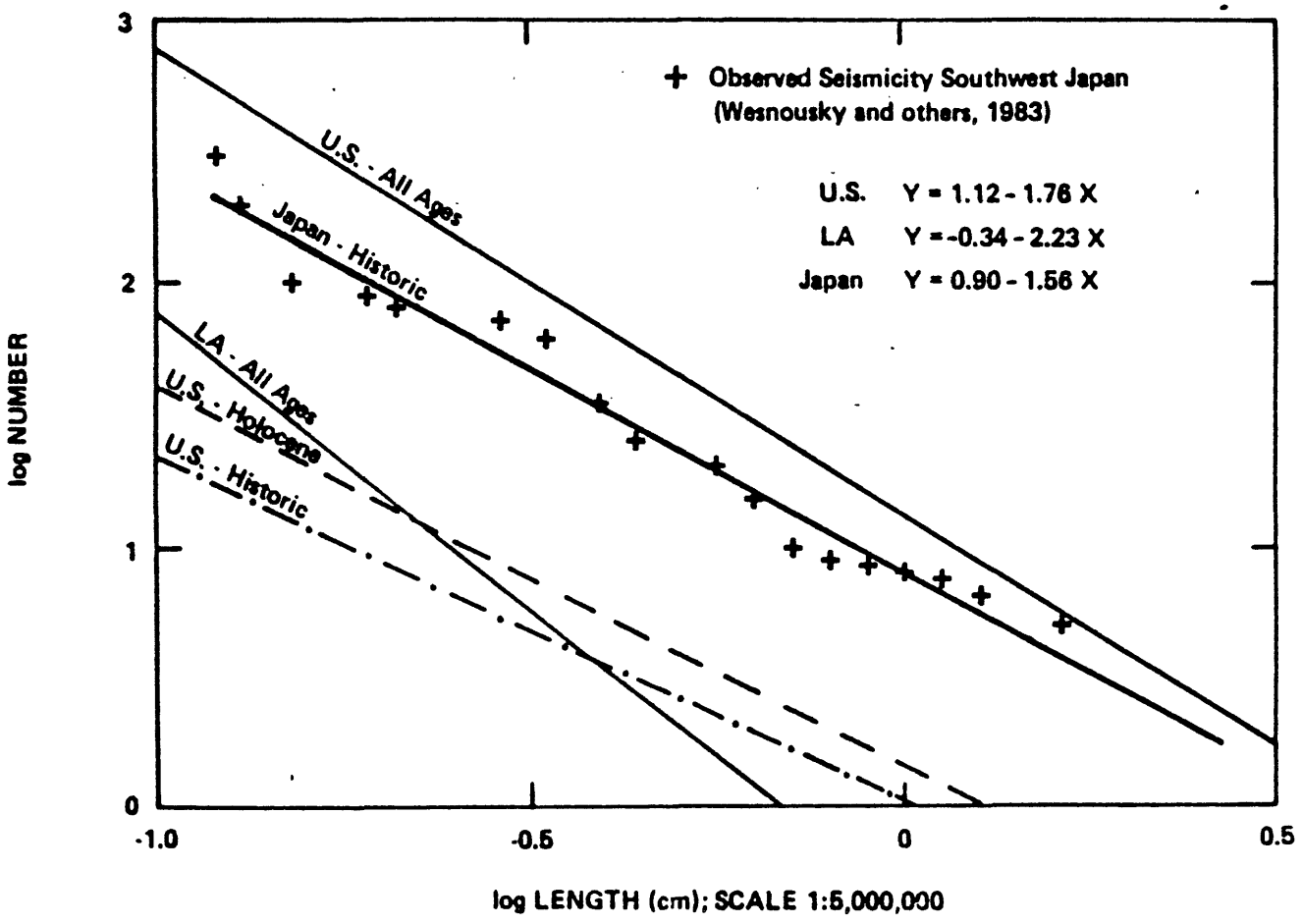

Figure 13. Geometric comparison of fracture patterns as a function of scale without regard to either kinematic or dynamic histories of growth: (a) California faults showing evidence of activity in the latest 15 my, redrawn from Howard and others (1978; see maps in Shaw and others, 1981); (b) through (d) were redrawn from Tchalenko (1970, Figure 11): (b) Dasht-e Bayaz earthquake fault, Iran, (c) clay deformation in a Reidel shear experiment, (d) detail of shear box experiment. The solid circles in (a) mark the approximate 1000 km interval of the San Andreas fault zone shown in Figures 10 and 11.

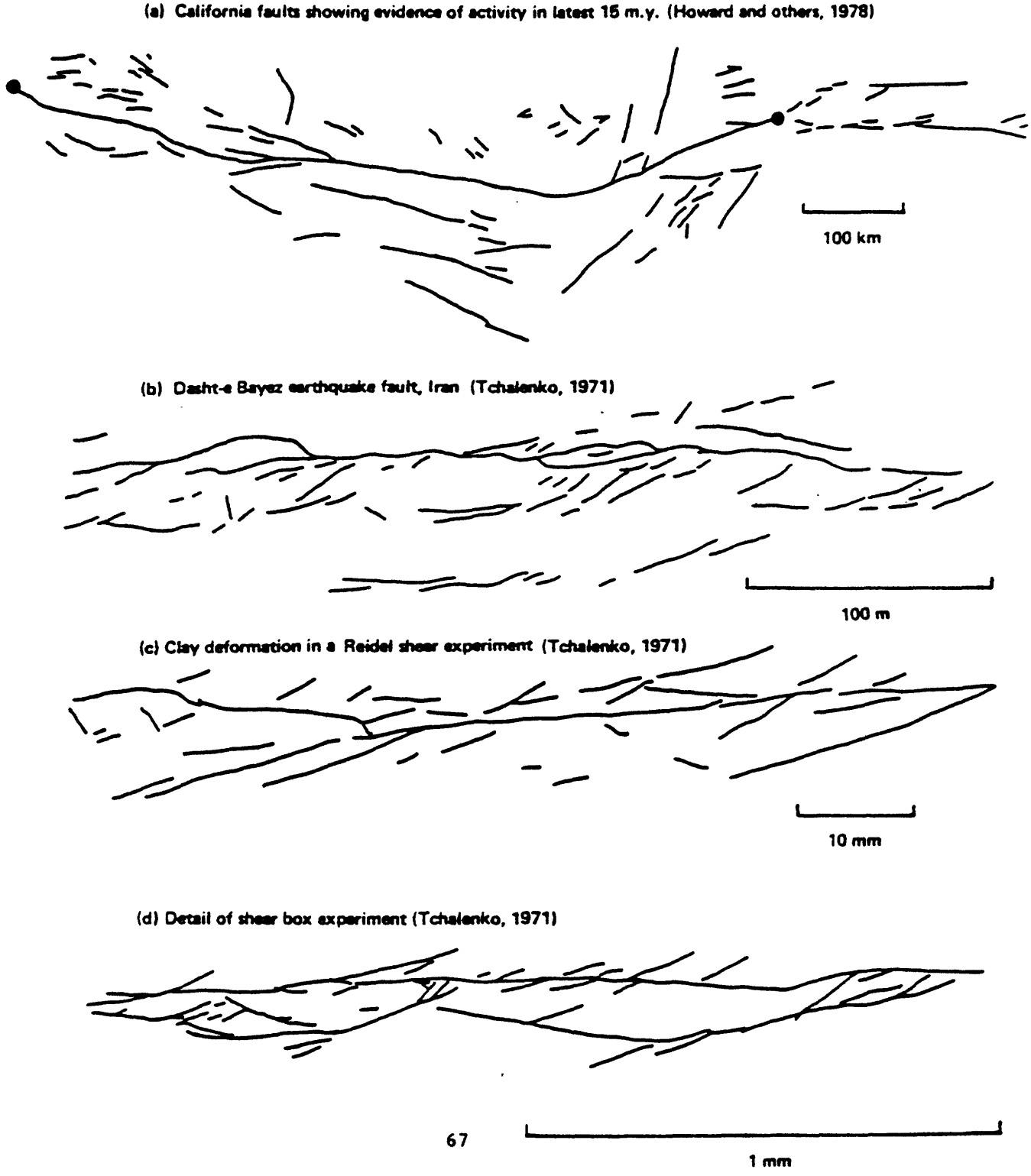

Figure 14. Estimates of fractal dimensions, D, for the fracture patterns of Figure 13 taken to represent a potentially self-similar set:

(a) Measurements of log N vs log L for each of the patterns subdivided into 4 or 5 number/length orders; the mean slope is about -1, and the distribution is given approximately by: log N = 1 - log L, for L given by the scale of the drawing (slope -2 is shown for reference).

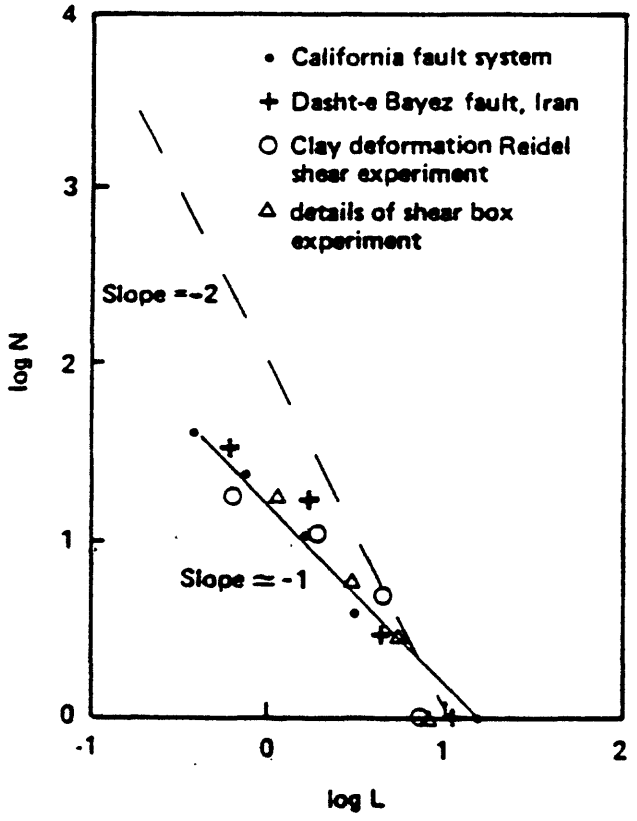

Figure 14. Estimates of fractal dimensions, D, for the fracture patterns of Figure 13 taken to represent a potentially self-similar set:

(b) Total length of fracture at each scale based on multiples of the total measured length in (a) plotted vs the ruler length, R, characteristic of the individual measurements; that is, each scale is considered to contain additional fractures as shown at the higher magnifications, so that the total number and length of fractures of all sets in (a) is a product of the series of proportions. The slope of about -.25 is for the distribution log N = 1 - log L, and the slope about -.4 is for log N = 2 - 2 log L; this denser distribution is considered because the steeper slope is more typical for fault measurements. The fractal dimensions are determined from the relation (Eq. 7) that equates the slope with the quantity (1-D), where D is the fractal dimension; the respective values are D = 1.25 and D = 1.4 (see discussion in text)

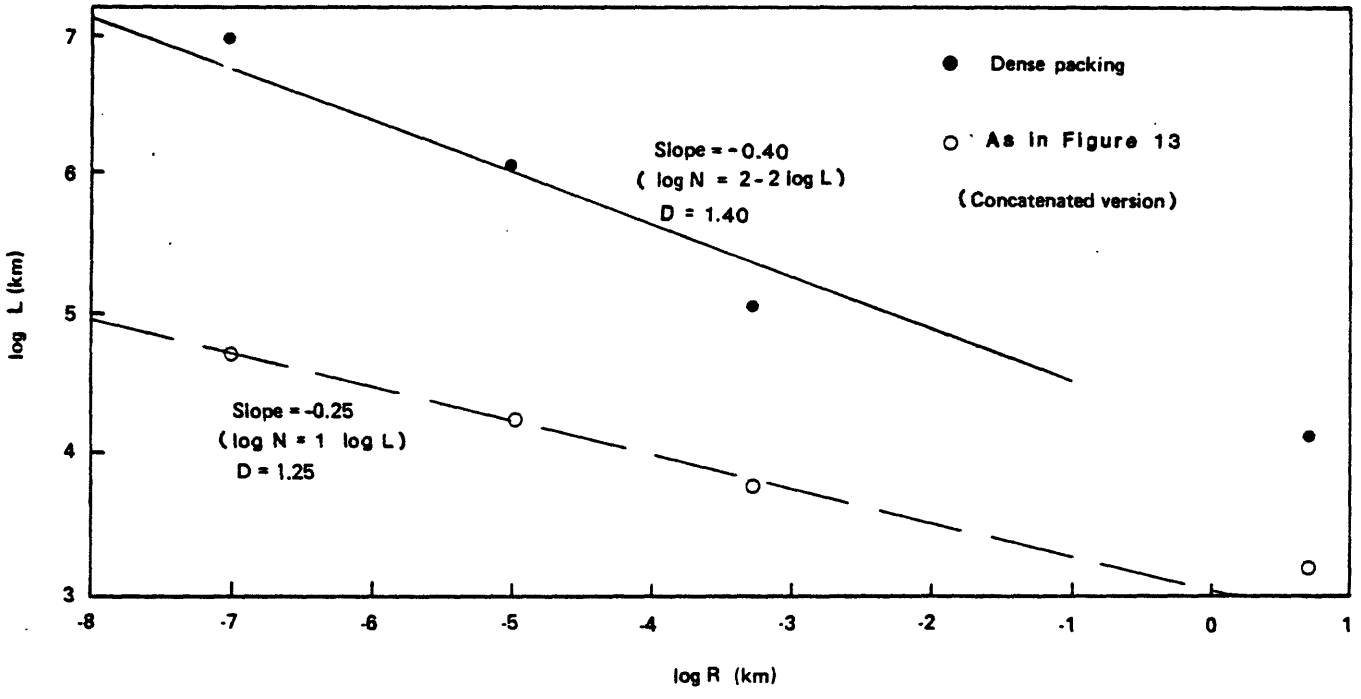

Figure 14. Estimates of fractal dimensions, D, for the fracture patterns of Figure 13 taken to represent a potentially self-similar set:

(c) Total length of fractures on the assumption that gaps (areas, and implicitly volumes) between the faults in (a) contain fractures at all the larger scales. The slope is about -1, giving a fractal dimension D = 2 in agreement with an area-filling distribution (this would be D = 3 for a volume-filling distribution, if the same ratios applied to patterns in cross section).

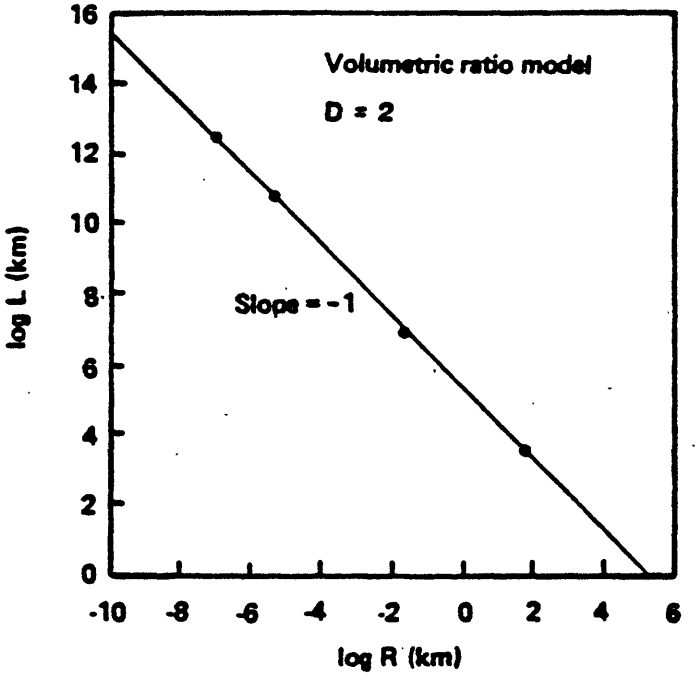

Figure 14. Estimates of fractal dimensions, D, for the fracture patterns of Figure 13 taken to represent a potentially self-similar set:

(d) Density of fracture pattern for a number-length relation approximating the distribution log N = 2 - 2 log L. If the sets at different scales have systematically steeper slopes than -1, the fractal dimensions will vary from those in (b), but the distribution in (c) remains the same if the ratios of areas are constant (i.e., the area-filling, and volume-filling, modes are the fractal limits for topological dimensions 2 and 3, respectively).

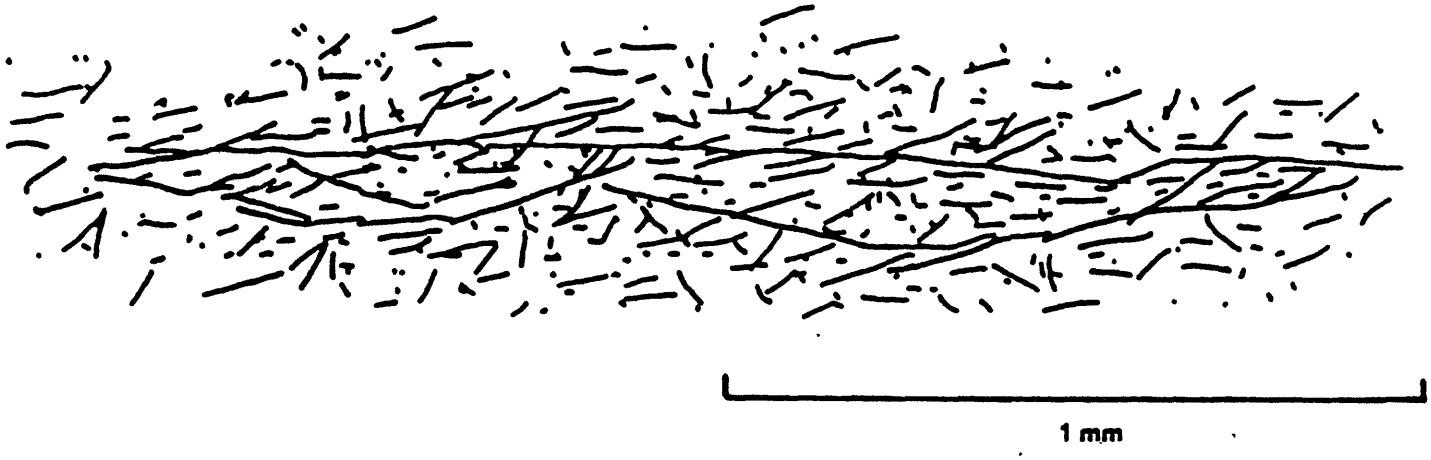

Figure 14. Estimates of fractal dimensions, D, for the fracture patterns of Figure 13 taken to represent a potentially self-similar set:

(e) Fractal dimension of a fracture surface in metal (300-Grade Maraging steel), as measured by Mandelbrot and others (1984) using the technique called "slit island analysis". The ratio of area to perimeter, measured with different ruler lengths, defines the fractal dimension. A linear regression fit of the data defines the constant fractal proportionality, D = 1.28, showing that the data are fractally self-similar (within the statistical accuracy of the measurements). The drawing is modified from Mandelbrot and others (1984, Figure 1); the line D = 1 was added. Note: In that reference, there is an ambiguity between the definition of fractal dimension and "fractal dimensional increment" (which may be a missprint). It is clear from the context, and the definition in their text (p. 722), that the dimension D' is the slope in the graph of log (area) vs. log (length), which is about 6/4.7 = 1.28, where D' refers to a maximum topological dimension 2 (giving D = 2.28 for their specimen as a whole). In the figure caption, however, 1.28 is said to be the fractal dimensional increment. We prefer to use the single symbol D, referring in each case to the appropriate topological limit.

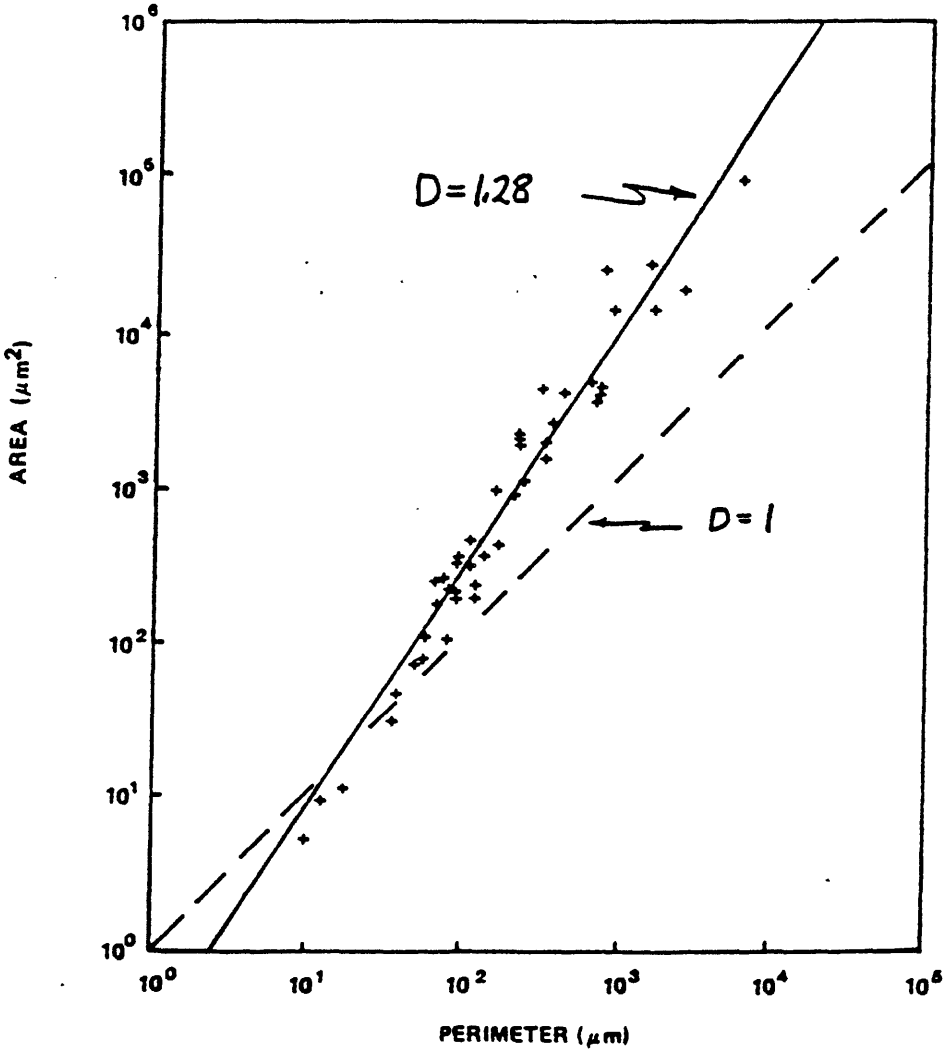

Figure 15. Illustration of "dissected" line sets:

(a) The Cantor set in which the central 1/3 is cut out in successive stages of dissection (see Mandelbrot, 1977, p 98 ff.); the fractal dimension is about D ≐ .63, a value that is "less-than-linear".

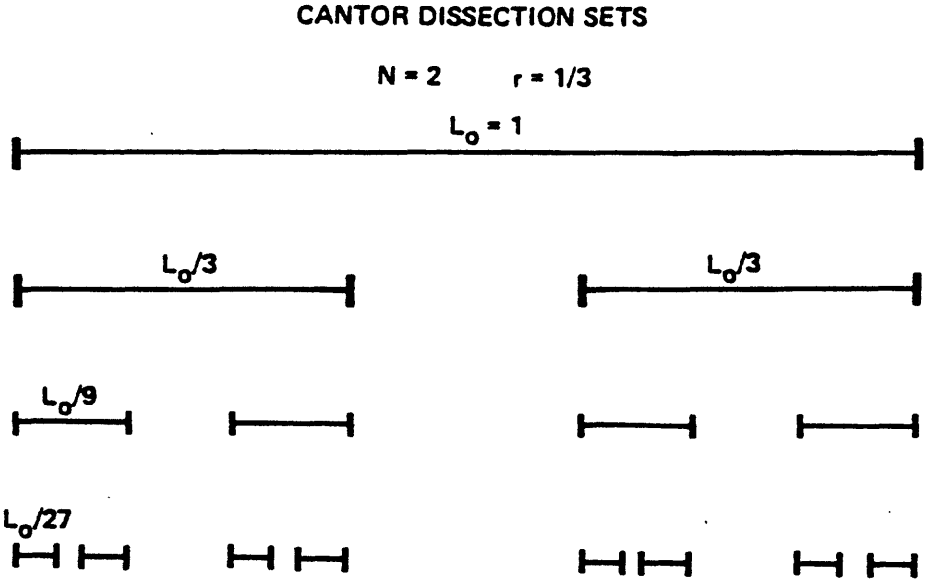

$$\sum L = \sum_{0}^{n} \left[\frac{N}{(1/r)}\right]^{n} L_o$$

Figure 15. Illustration of "dissected" line sets:

(b) An "inverse Cantor set" as invented in this paper to illustrate a dissection sequence in which the central third doubles in every successive cutout; D = 1.26 based on formula D = log N / log (1/r), where N is the number of "solid" segments and r is the ratio of the cutout length to the unit length (1/3 in the Cantor set). Any other ratio of cutout length and degree of subdivision is possible, making the variety of possible fractal sets created in this manner unlimited. If the cutout lengths are included (dashed lines), as though they represented the fossil traces of previous segment lengths, the fractal dimension increases to about D = 1.47. This set is a geometric object with a similar fractal structure to the fracture patterns in Figure 13 as measured in Figure 14; as discussed in the text, however, there are implicit regimes of fault activation where the fractal dimension implies a degree of dissection resembling the Cantor set proper (D less than 1).

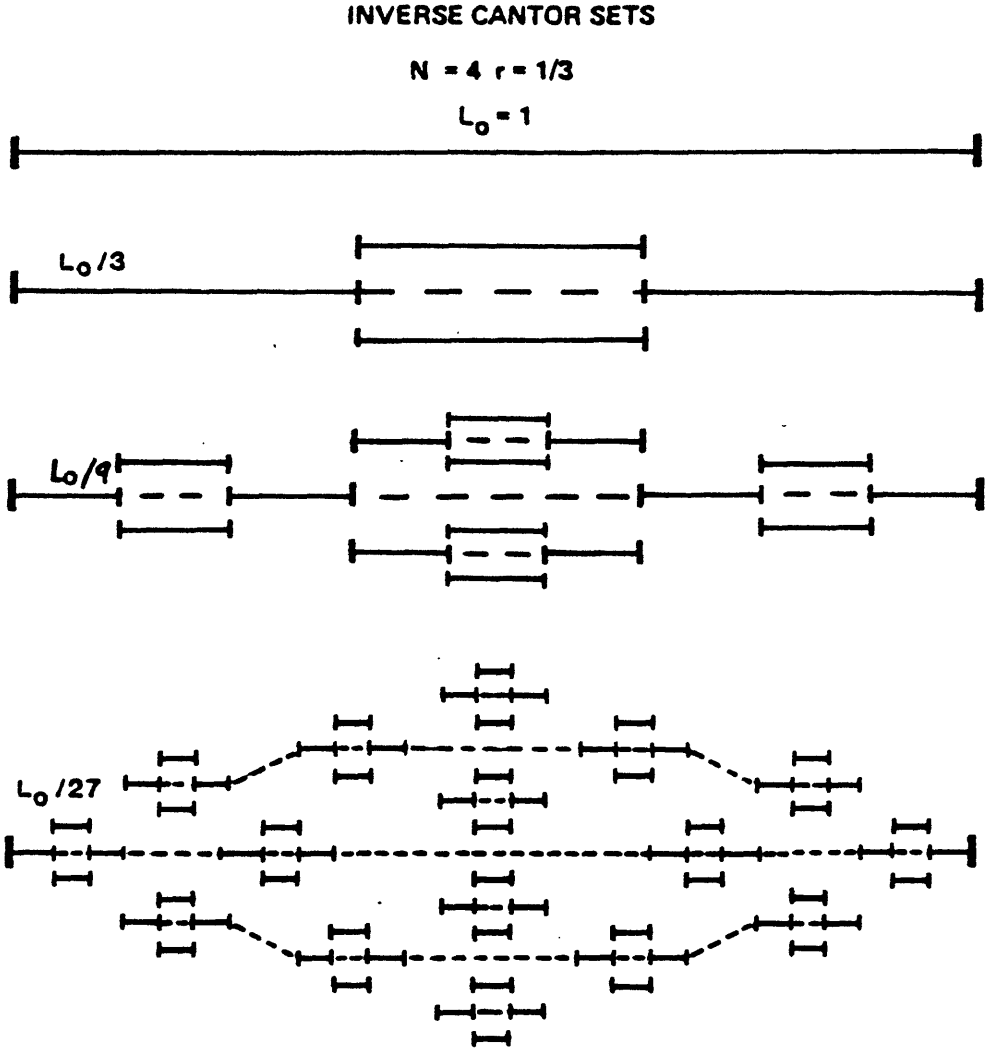

$$\sum L = \sum_{0}^{n} \left[\frac{N}{(1/r)} \right]^{n} L_o$$

Figure 15. Illustration of "dissected" line sets:

(c) Plot of Total Length vs. segment length as Ruler Length, normalized to the value L_o = 1000 (as in a maximum fault length of 1000 km). Slopes measured from direct plotting of cumulative segment lengths agree with Eq. 8, D = Log N / log (1/r). The horizontal dashed line demarks the transition from less-than-linear to greater-than-linear fractal sets.

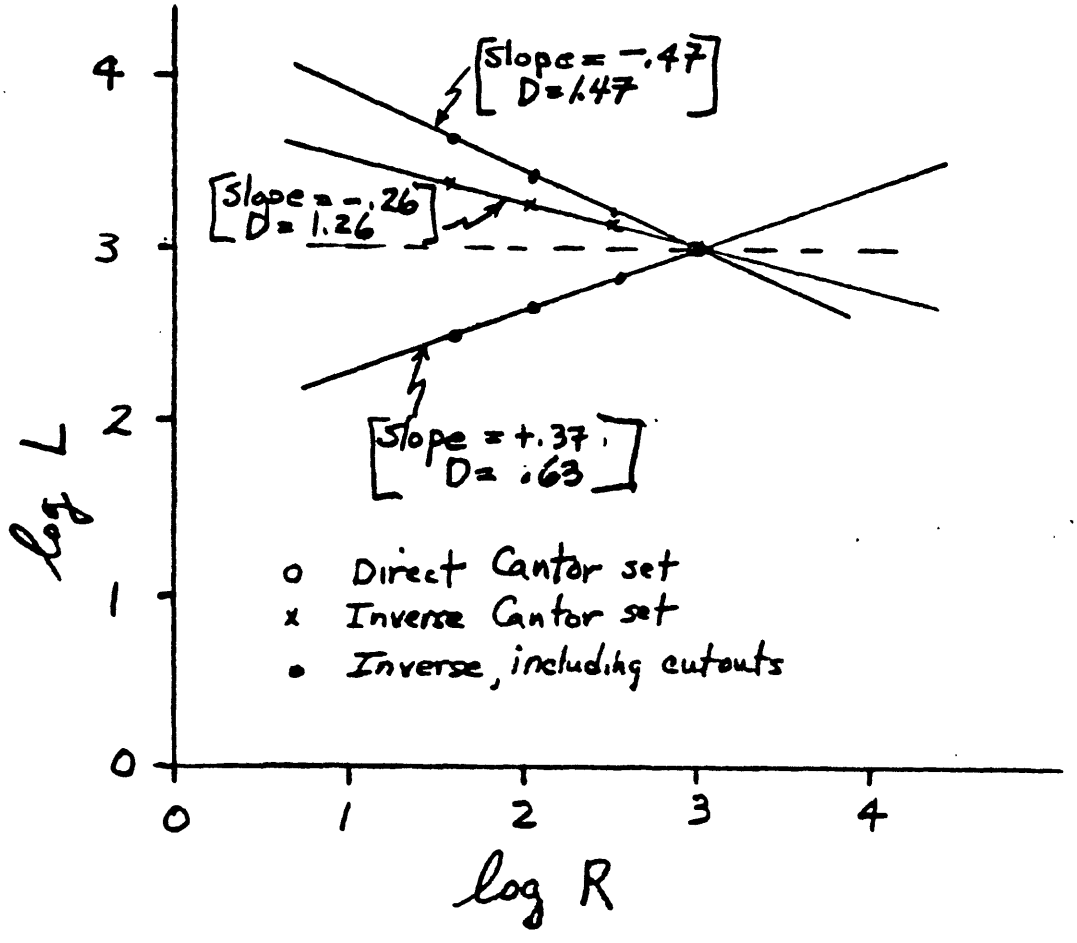

Figure 16. Illustration of the measurement of fractal dimension for dendritic patterns, by analogy with the fingering flow of a viscous fluid:

(a) Published example of fractal dimension (D = 1.38) as measured for flow in a Hele-Shaw experiment (redrawn from Nittmann and others, 1985); the ruler length, R, defines different lengths of perimeter which are plotted as in Figure 14, except that here the total number, N, rather than total length of measurement is plotted (N is to be multiplied by R to get the total length).

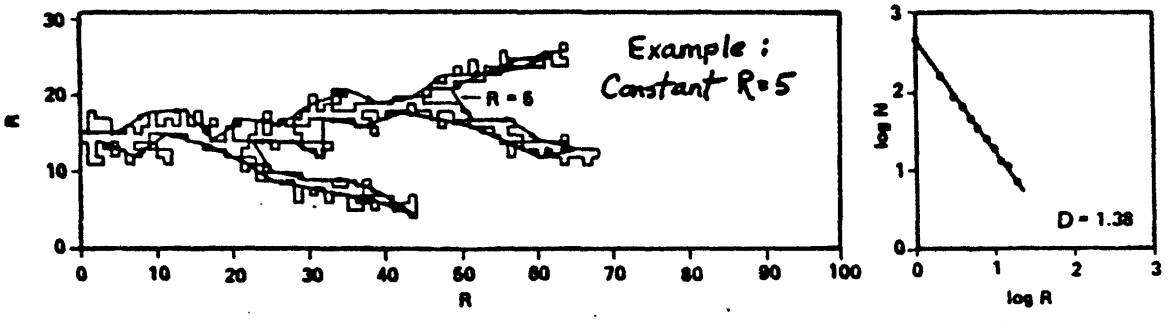

Figure 16. Illustration of the measurement of fractal dimension for dendritic patterns, by analogy with the fingering flow of a viscous fluid:

(b) Fracture pattern from Figure 13a enclosed by a subjective perimeter, as though the overall pattern represented an irregular valley eroded by prehistoric stream action that left only traces of channels. Measurement by various ways with different ruler lengths gives a fractal dimension of about D = 1.4, in reasonable agreement with (a), in that this is a more closed rather than open dendrite. The fractal dimension also resembles the value of about D = 1.4 for dense "dendritic" packing illustrated in Figures 14b and 14d.

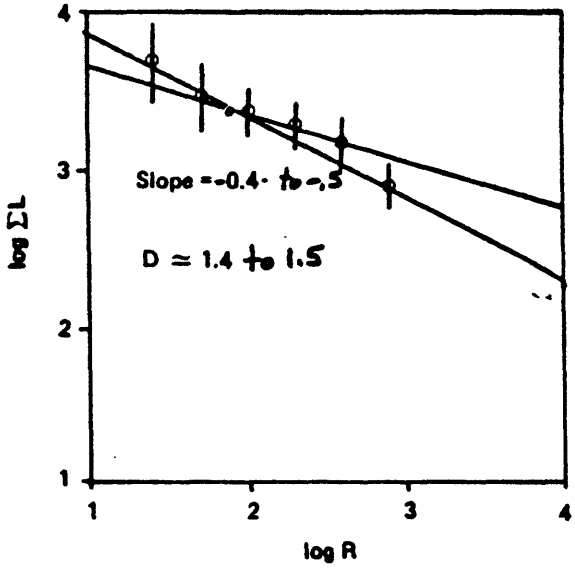

Figure 17. Fractal sets implied by slopes in the fractogram based on the relation D = 3b/c, for the volumetric topologic limit D = 3, where b is the slope and c is the coefficient in the moment-magnitude equation (e.g., Eq. 3): log M_0 = Const. + c M, (Aki, 1981):

(a) Values of b and D along the limiting slopes of the fractogram, and along the overall trend of U.S. historic seismicity, for constant c = 1.5. The transition slopes at constant BT (D = 2.83) are nearly volume-filling at c = 1.5, the overall seismic trend is a little more than area-filling (D = 2.1), and the base of the fractogram, which corresponds approximately in b-value to many of the seismic zones in California (see Figure 9), is about halfway between a line-filling and area-filling fractal (D = 1.6). All these values of D are larger than the measured values in Figures 14 through 16. This is because those values are based on planar measurements (i.e., they are relative to the maximum topologic dimension 2). For comparative purposes, we can either add 1 to the previous values, or subtract 1 from the present values. The latter gives the respective values: D = 1.83, D = 1.1, and D = .6, which is essentially the same range as the measurements (the highest value approximates the area-filling mode in Figure 14c, and the smallest is essentially that of the direct Cantor Set in Figure 15).

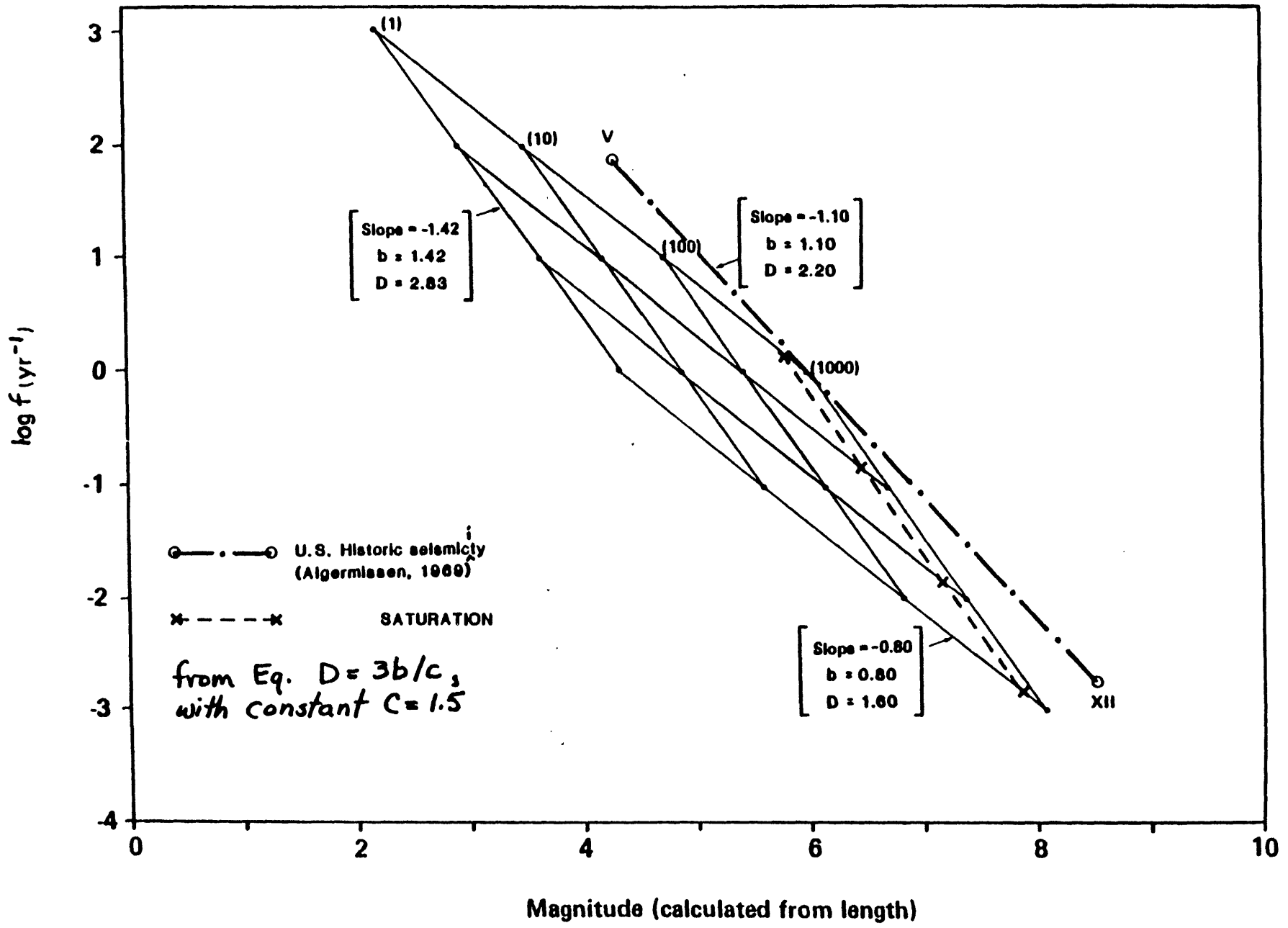
log f (yr⁻¹)
3
2
1
0
-1
-2
-3
-4
0
2
4
6
8
10
Magnitude (calculated from length)
(1)
(10)
V
(100)
(1000)
XII
Slope = -1.42
b = 1.42
D = 2.83
Slope = -1.10
b = 1.10
D = 2.20
Slope = -0.80
b = 0.80
D = 1.60
U.S. Historic seismicity
(Algermissen, 1969)
SATURATION
from Eq. D = 3b/c,
with constant C = 1.5

Figure 17. Fractal sets implied by slopes in the fractogram based on the relation D = 3b/c, for the volumetric topologic limit D = 3, where b is the slope and c is the coefficient in the moment-magnitude equation (e.g., Eq. 3): log M_o = Const. + c M, (Aki, 1981):

(b) Degenerate fractogram for the relation log N = 1 - log L. Whereas there is only one limiting slope, with a single value of D = 1.6 (b = .80) for constant c = 1.5, there is a series of possible partial and total activation lengths, ranging from the set marked by open circles (BT = 1 year, and N = 1 to 1000) to the SATURATION values indicated by solid circles (BT much less than before, about 200 years, and N = 1 to 1000). The distribution, however, is still "dendritic" within some topological volume. Also, the fractal dimension varies with variable c (see caption of c below; also see Figure 18, Table 2, and text for discussion of ranges of coefficient c). These considerations may apply to interpretations of the San Andreas system (e.g., compare this diagram with Figures 9, 11, and 18). Coincidently, the SATURATION value of BT resembles the recurrence time for large events on the San Andreas fault proper, according to trenching studies by Sieh (1981) and Weldon and Sieh (1985). According to this interpretaion, the various Seismic Zones in Figure 9 would apparently represent subsystems each of which is fractally self-similar with the overall distribution (i.e., the single trend would be the sum of the subtrends). Because, the slopes of log N vs. log L for the Faulting Regions of California (Shaw and others, 1981), however, are significantly steeper than -1, the degenerate model does not totally resolve the sorting problems implied by seismic cycles that must be consistent, simultaneously, with the various views of Figures 8, 9, and 11.

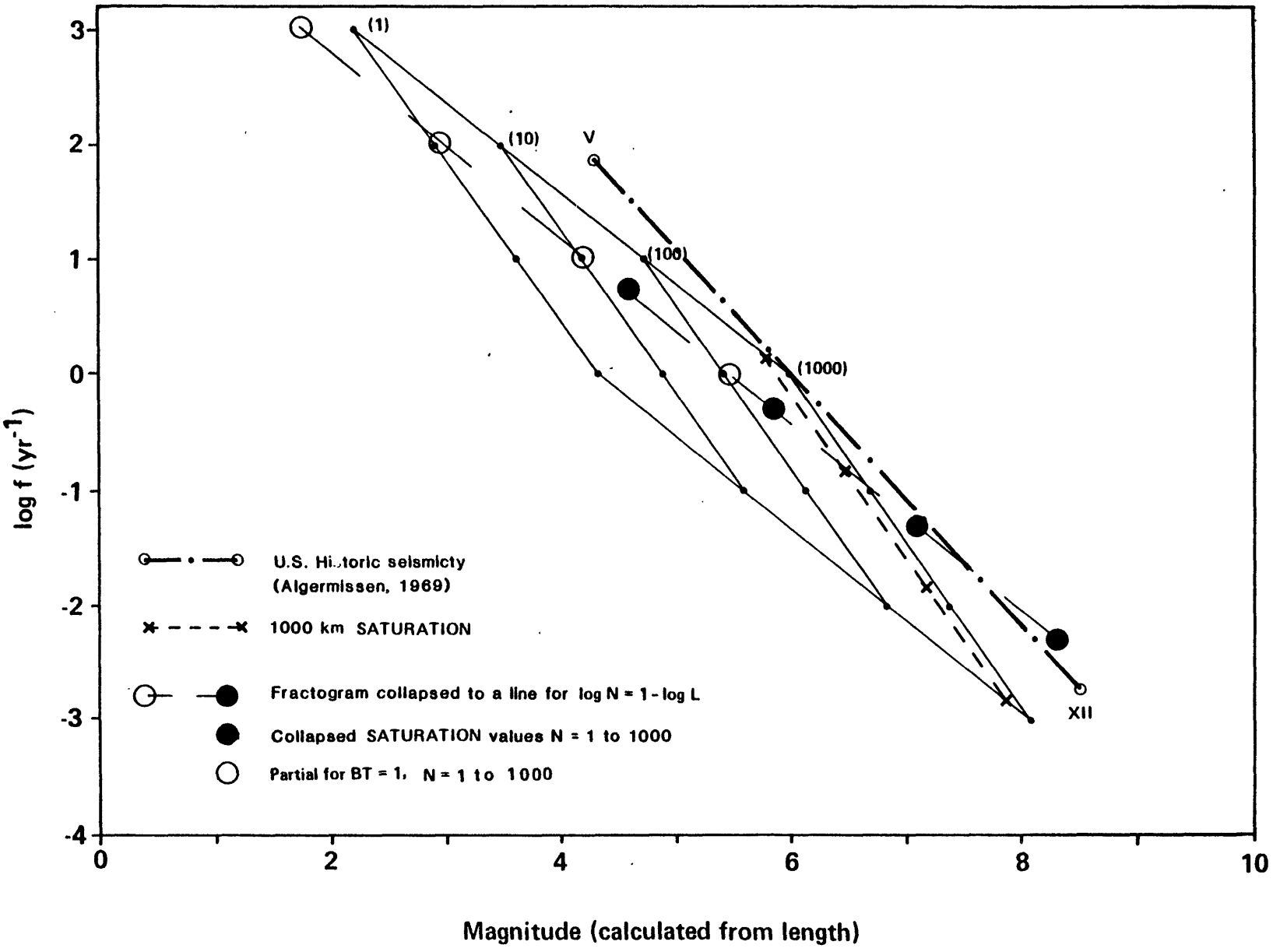
log f (yr^{-1})
Magnitude (calculated from length)
(1)
(10)
V
(100)
(1000)
XII
U.S. Historic seismicty
(Algermissen, 1969)
1000 km SATURATION
Fractogram collapsed to a line for log N = 1 - log L
Collapsed SATURATION values N = 1 to 1000
Partial for BT = 1, N = 1 to 1000

Figure 17. Fractal sets implied by slopes in the fractogram based on the relation D = 3b/c, for the volumetric topologic limit D = 3, where b is the slope and c is the coefficient in the moment-magnitude equation (e.g., Eq. 3): log M_o = Const. + c M, (Aki, 1981):

(c) Fractogram modified schematically to account for the variable slopes (c-values) of the moment-magnitude relation of Hanks and Boore (1984) at large magnitudes; relations at small magnitudes have not been adjusted. The result is to systematically and progressively increase both b-values and fractal dimensions, D, near the SATURATION limit in the fractogram (i.e., magnitudes are smaller for the same values of moment, hence they are smaller for the same distributions of fault-length segments for the largest partial or total activation events). In the limit, a condition is reached where the b-values for the base and the sides of the fractogram tend toward the same value (heavy dashed lines at lower right). If these slopes attain the common value b = 3, at c = 3, the lower right apex of the fractogram becomes globally invariant at a fractal dimension D = 3 (from the relation D = 3b/c). This would mean that changes either at constant number, N, or at constant buildup time, BT (but variable N), both represent a topological volume-filling mode of behavior under conditions of the ultimate earthquake event implied by the analysis of Hanks and Boore (1984). This would also imply a condition in which no distinction could be drawn between multiple activations within a constant number/length order (e.g., for N = 1), or activations engaging a sequence of orders of decreasing numbers of maximum moment events, as in the SATURATION condition (cf., Figure 8). Whether or not this is physically plausible is not resolved by these dimensional considerations. Qualitatively, however, it is evident that when fault activation reaches a length-scale comparable to the scale of Plate Tectonics, it is difficult to avoid implications of volumetric modes of deformation. This issue compounds the ambiguities mentioned in (b) above concerning interpretations of California earthquakes.

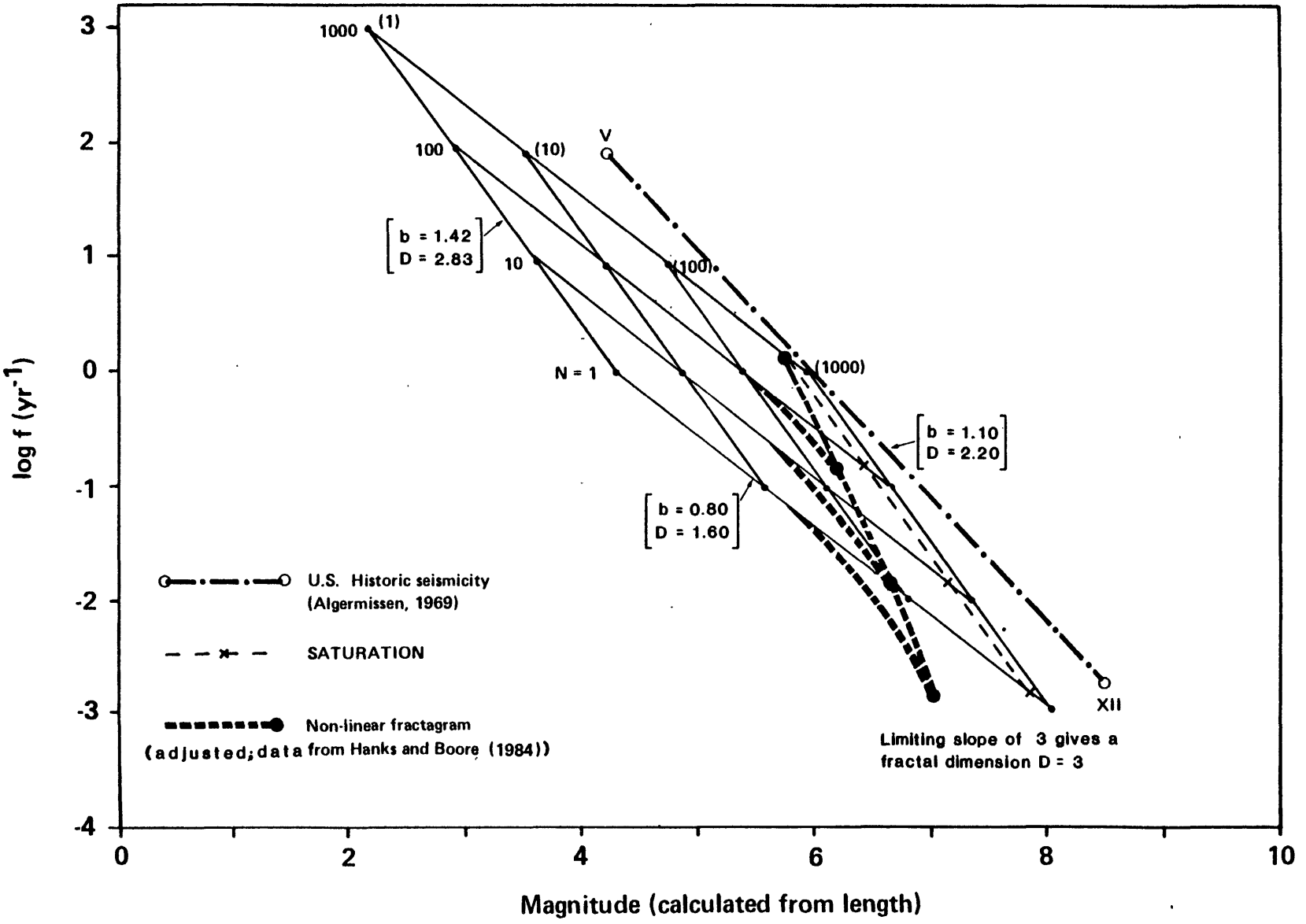
log f (yr^{-1})
Magnitude (calculated from length)
1000
(1)
100
(10)
10
N = 1
V
(100)
(1000)
XII
[b = 1.42 D = 2.83]
[b = 1.10 D = 2.20]
[b = 0.80 D = 1.60]
U.S. Historic seismicity (Algermissen, 1969)
SATURATION
Non-linear fractagram (adjusted; data from Hanks and Boore (1984))
Limiting slope of 3 gives a fractal dimension D = 3

Figure 18. Fractal dimensions in space and time:

(a) Lines of constant fractal dimension, limited to topological dimension 3, plotted vs variable values of b and c as defined in Figure 17 (see text). The solid lines with arrows schematically indicate the paths of fractal dimensions for two different assumptions concerning stepwise progressions of seismic frequency-magnitude data, as in Japan (see Figures 7 and 8): (1) the heavy horizontal line with arrows indicates the alternations of D corresponding to alternations of b between the limiting slopes of the fractogram in Figure 7a for a constant value of c = 1.5, and (2) the orthogonal zigzag line with arrows indicates the same alternations, but with c increasing in the larger events according to the correlation of Hanks and Boore (1984). There are two important qualifications of these idealized sequences: (i) when c increases, the equations relating fault length, moment, and magnitude are also modified, so that b also increases; in the extreme limit, b might also approach the value 3 for the ultimate magnitudes shown in Figure 17c, so that the upper part of the zigzag path is skewed to the right toward the fractal limit D = 3, as indicated by the dotted lines (see discussion in text, and caption b), and (ii) if the log number-length relation has a slope near -1, the fractogram degenerates to a more nearly single-valued slope, so that the range of b-values shrinks toward zero difference for different paths of number/order activations (see Figure 17b, and discussion in text; qualification (i), of course, still holds. The stippled area represents the range of conditions, for small to intermediate earthquakes, where volume-filling activations are possible (i.e., D = 3); however, there is another possible volume-filling limit corresponding to the Hanks-Boore ultimate magnitudes mentioned above, where the dotted curves converge at the value D = 3 (cf., caption b).

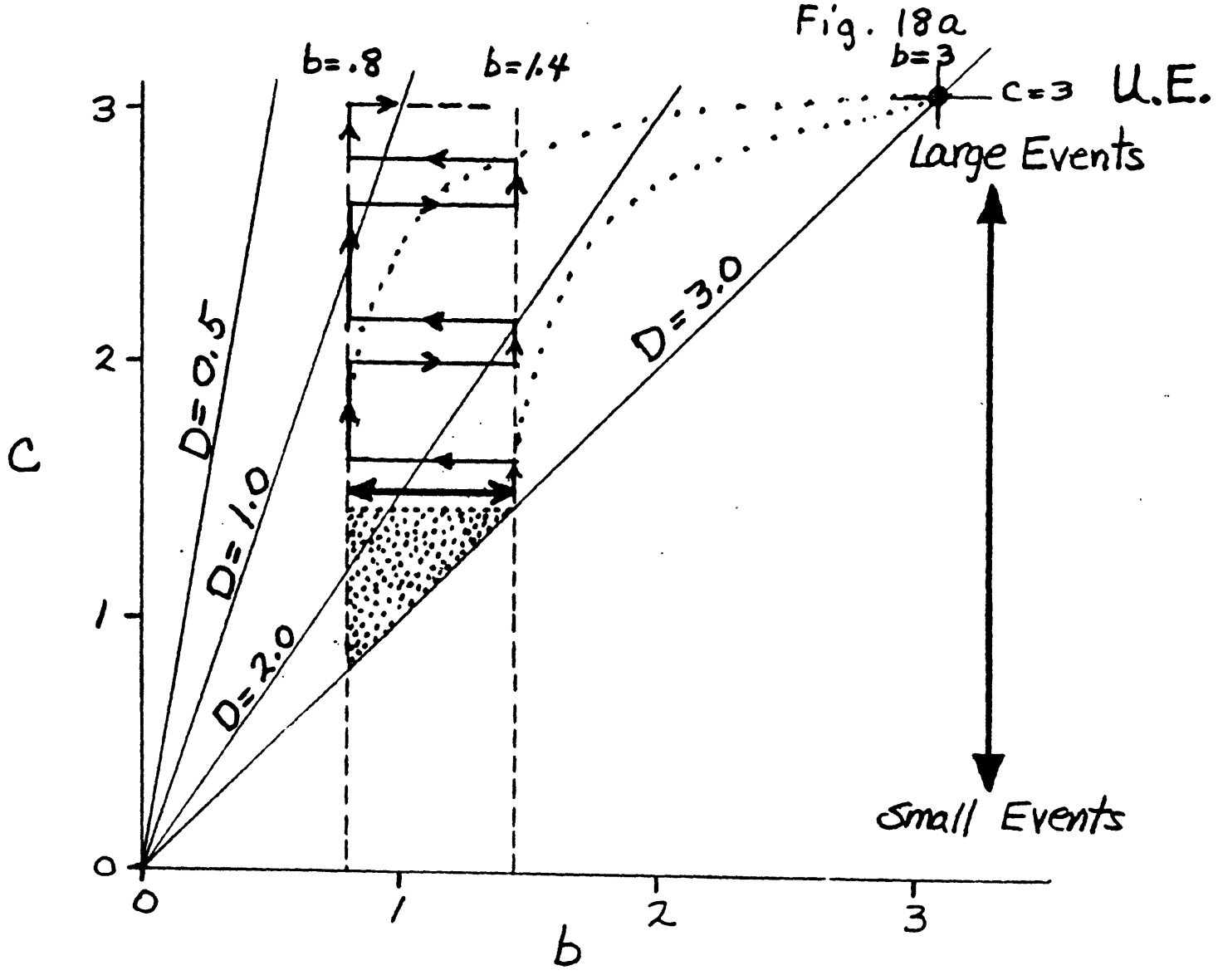
Fig. 18a
b=.8
b=1.4
b=3
c=3
U.E.
Large Events
Small Events
D=0.5
D=1.0
D=2.0
D=3.0
C
b
0
1
2
3

Figure 18. Fractal dimensions in space and time:

(b) Temporal fractal dimension implied by the relation of Buildup Time, BT, in the fractogram to recurrence time, 1/f, as the "ruler length" for time. Examples ot temporal fractal, D_{MT} (the subscript is a reminder that the definition refers to magnitude-time, or energy-time, space) are shown for different assumptions about paths in the fractogram (actually this is a grid of parallel lines, shown in the Inset, representing arbitrary choices of the parameters); none of the fractal slopes illustrated is necessarily unique, because each specific earthquake sequence may have a different fractal signature, both spatially and temporally (see text concerning possibility of a characteristic spatiotemporal fractal relative to a maximum topological dimension of 4). The roman numerals indicate fractal regimes (angular sectors of slope regimes), increasing in the clockwise direction, according to the same rule used for spatial fractals (Slope = 1 - D). Thus, in I the slope exceeds +1, and the fractal dimension is negative (or imaginary). In II, D_{MT} has the range 0 to 1, and in III it has the range 1 to the maximum topological limit, whatever that may be. This limit depends on dimensional context, which may be unlimited (the vertical line for "constant time" implies an "infinite fractal", which is qualitatively explained by the fact that this imaginary condition implies that "all magnitudes", hence energies, are simultaneosly present. The dashed line indicates an assigned topological limit of 4. If it is assumed that in real spacetime the fractal dimension is equal to or less than the sum, $D + D_{MT} = 4$, then the line at $D_{MT} = 4$ is associated with a spatial fractal dimension zero; i.e., this is a spatial distribution of point sources of maximal temporal degrees of freedom, a "fractal dust of earthquakes in spacetime", presumably representing the extreme of randomized distributions of spatially unique events. Any set of lines with slope zero ($D_{MT} = 1$), meaning at constant BT, implies that the spatial fractal, D, is less than or equal to 3, indicating, as mentioned before, that such conditions have the higher b-values and are the more volume-filling regimes (see a above, Figure 17c, and discussion in text). Notice that $D + D_{MT}$ does not have to sum to the limit 4. The set of lines for constant numbers of fault segments, N, have $D_{MT} = 0$, hence D implicitly can range up to 4; i.e., 3 is volume-filling, and values between 3 and 4 are spatially imaginary. This limit is of interest relative to the implicit conditions of the "ultimate earthquake" according to the discussion of a, and of Figure 17c, in that it occurs at a unique "point in time" and is volumetrically maximizing. This is, however, a different sort of spatiotemporal fractal from $D_{MT} = 1$, which also tends to be volume-filling, in that the latter is, presumably, a linear sequence in time (i.e., a fractal "time-line" analogous to a spatial fractal of D = 1); see discussion of Figure 17c. The special case for constant magnitude, M = 4.3, is shown because it gives an indication of internal consistency of the various fractal definitions: the slope is -1.3, giving $D_{MT} = 2.3$, and a maximum value D = 1.7 for topological limit 4. This implies a self-consistent value of c = 1.4, which is a reasonable value at this magnitude; a completely consistent value for constant c = 1.5, and the definition D = 3b/c, gives D = 1.6 for b = .80, as in the base of the fractogram in Figure 17a. Apparently, this also implies that there is a fractal distribution of earthquakes in space and time occurring along all the number/length orders (distributed mode of Figure 8), which is consistent with earlier interpretations (cf., Figures 8 and 11). The large filled circles with numbers indicate respective magnitude values, as in Figure 6a and Table 1; these values would be decreased according to the moment magnitude relations of Hanks and Boore (1984), but the general slope regimes remain the same.

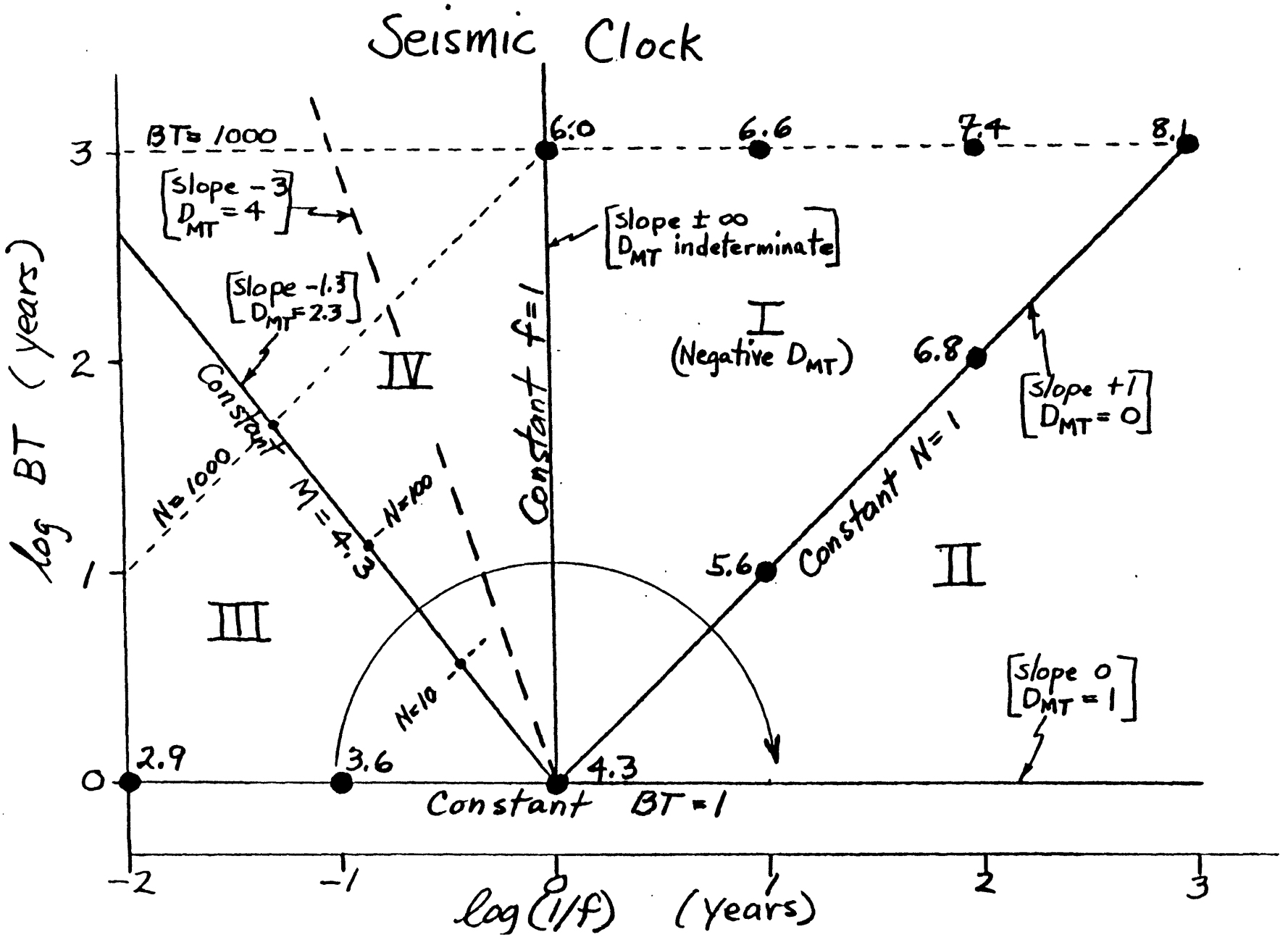
Seismic Clock
BT = 1000
6.0
6.6
7.4
8.1
3
2
1
0
log BT (years)
[Slope −3
D_{MT} = 4]
[Slope −1.3
D_{MT} = 2.3]
[Slope ± ∞
D_{MT} indeterminate]
Constant f = 1
I
(Negative D_{MT})
IV
6.8
[Slope +1
D_{MT} = 0]
Constant N = 1
Constant N = 1000
N = 100
N = 10
5.6
II
III
[Slope 0
D_{MT} = 1]
2.9
3.6
4.3
Constant BT = 1
−2
−1
0
1
2
3
log (1/f) (Years)

Figure 18. Fractal dimensions in space and time:

The Inset shows a schematic sequence of earthquake events resembling the relations in Figure 7 for Japanese earthquakes. Although the path tends to alternate between $D_{MT} = 0$, and $D_{MT} = 1$, transition intervals of higher temporal fractal dimensions may exist (intervals of negative slopes). Such a distribution is not a unique self-similar fractal object, but it could be viewed as a "self-similar set" of subintervals each of which is more strictly a self-similar fractal (see Figure 17b, caption, and discussion in text).

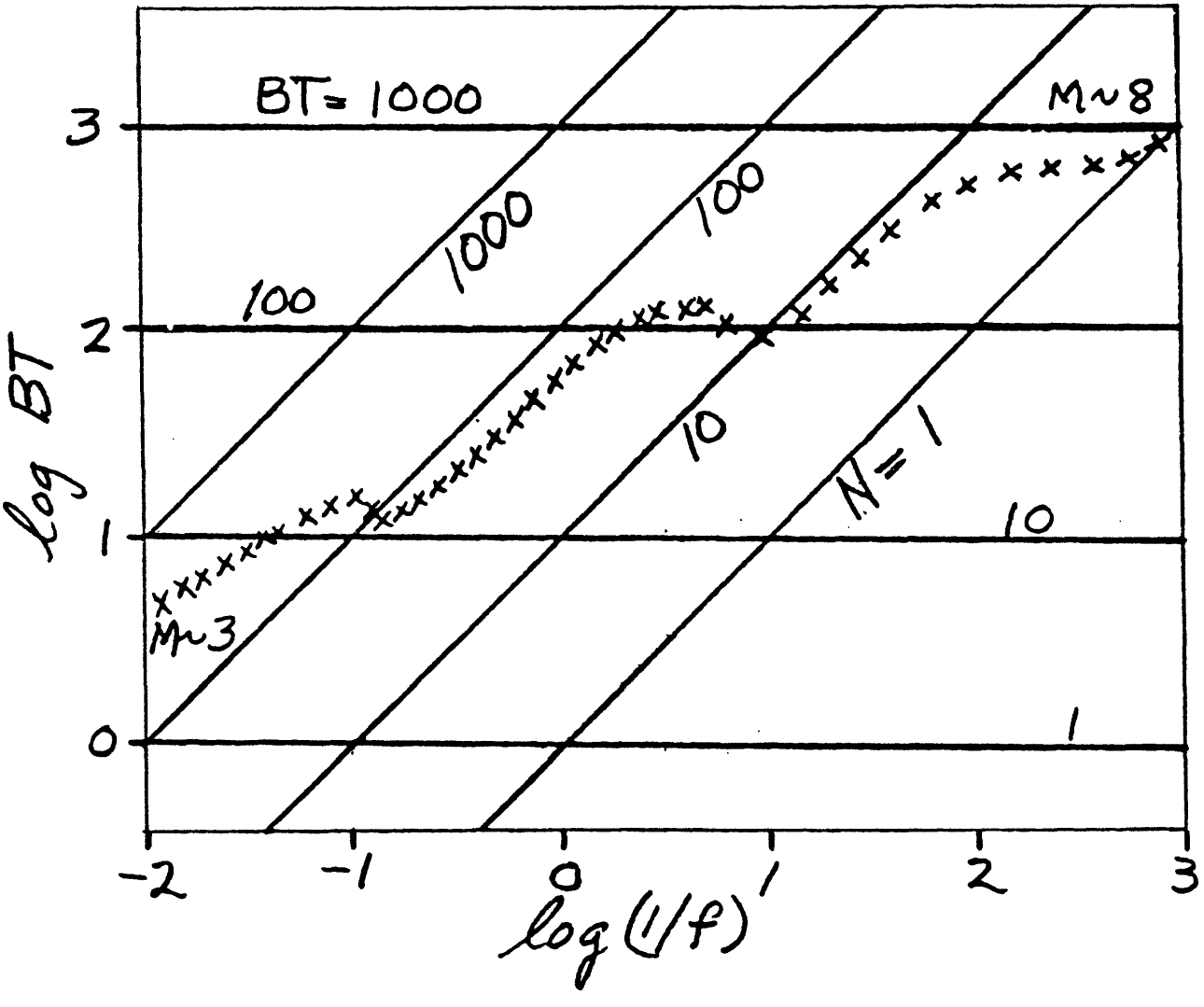

Figure 19. Schematic illustration of transient and steady-state slip and shear rates relative to spatial distribution and duration of activation events:

(a) Single maximum moment event relative to scale of a major "subzone" and a "megazone" (plate-boundary scale) shear system. The Inset defines relations of fault zone width, w_{fz}, megazone width, w_{mz}, slip, u, activation length, L, and slip velocity, v. In this transient case the definition of shear rate is extremely structure-dependent as compared to continuum models of deformation (see text for discussion of relation to fractal dimensions).

TRANSIENT STAGE - SUBZONE

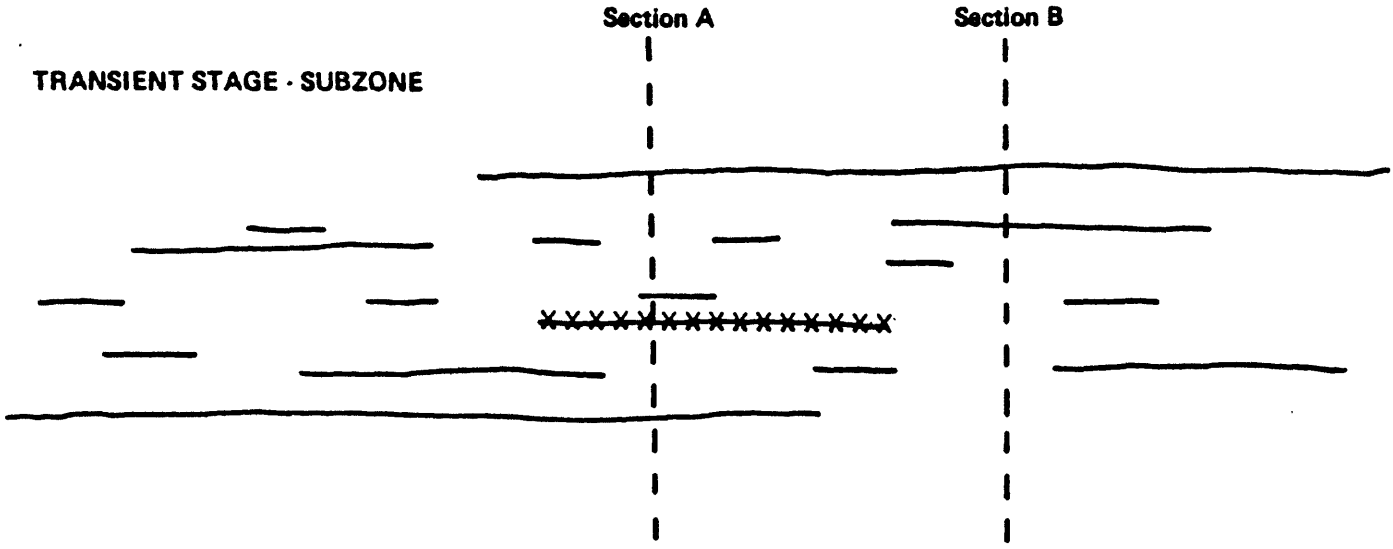

TRANSIENT STAGE - MEGAZONE

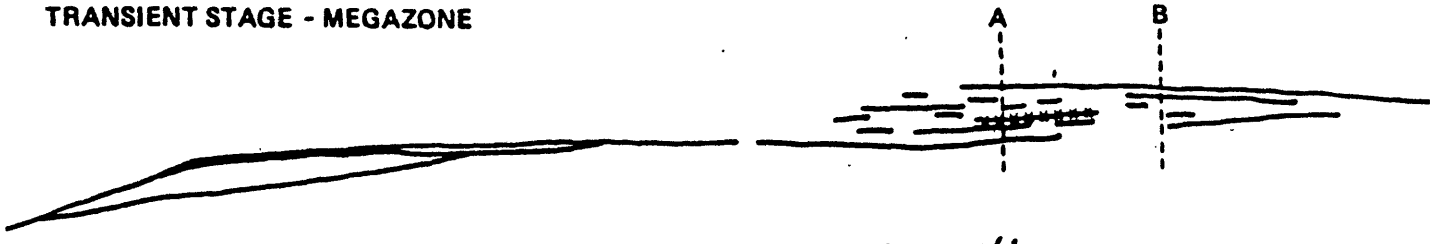

DEFINITIONS:

L = (Activated length)

u = (Slip length)

Σu_{mz} = (Net slip length across megazone)

$v = \Delta u/\Delta t$ (Slip rate on a fault)

$v/W_{fz} = (\Delta u/\Delta t)/W_{fz}$ (Fault zone shear rate)

$\overline{v}_{mz} = \Sigma u/\Delta t$ (Net slip rate across megazone)

$\overline{v}_{mz}/W_{mz} = (\Sigma u/\Delta t)/W_{mz}$ (Net megazone shear rate)

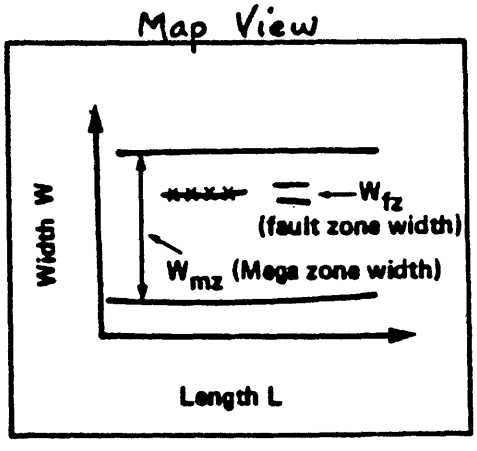

Figure 19. Schematic illustration of transient and steady-state slip and shear rates relative to spatial distribution and duration of activation events:

(b) Quasi-steady and nearly area-filling (and possibly volume-filling) mode of shear for zones in (a) averaged over times long compared to the overall buildup times for the seismic cycle (see text for discussion of average shear rate relative to stress models and fractal structure).

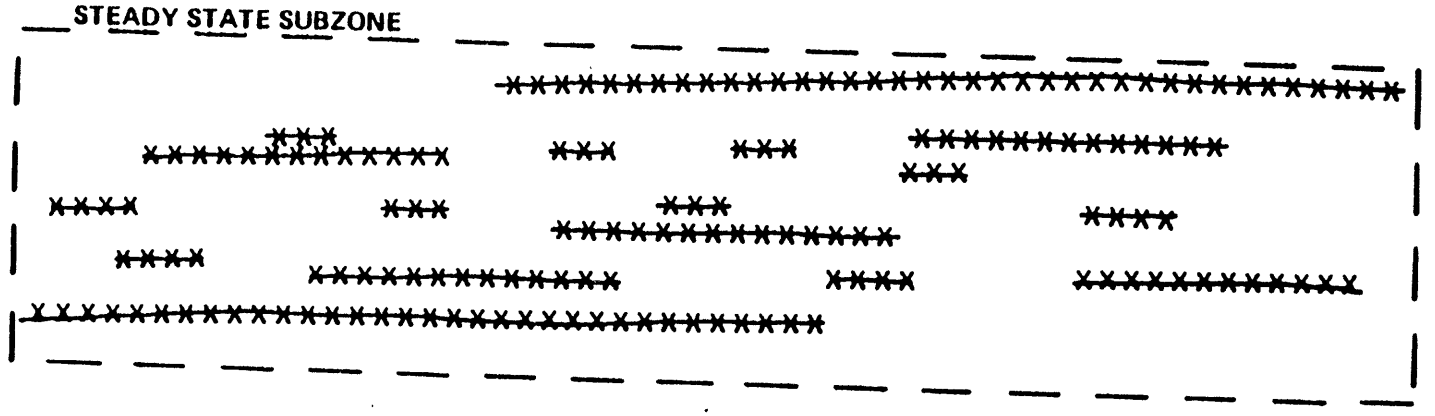
STEADY STATE SUBZONE

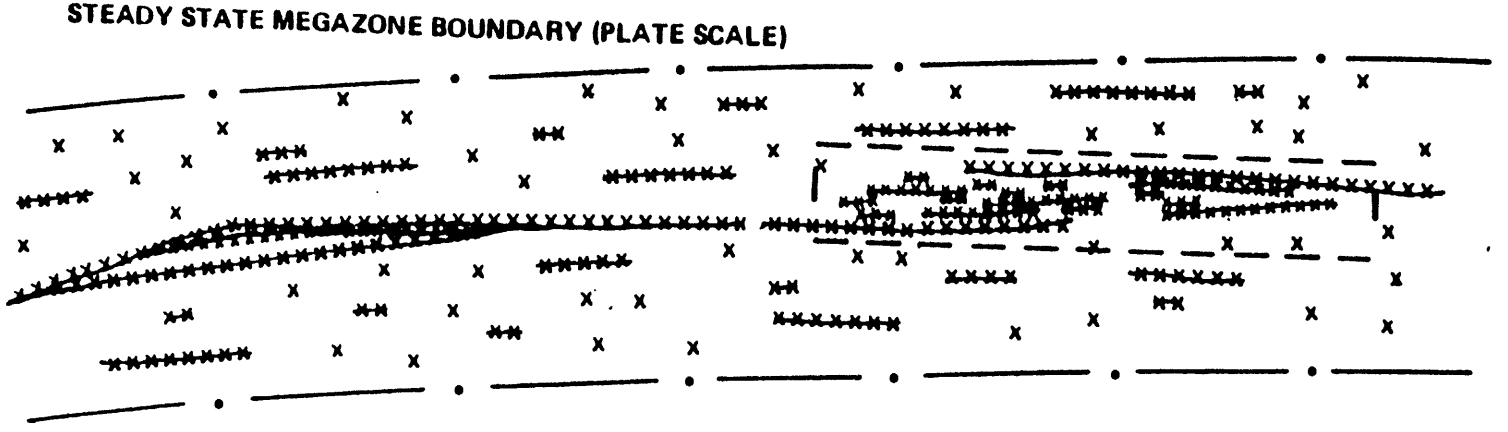
STEADY STATE MEGAZONE BOUNDARY (PLATE SCALE)